Site U1336[1]

Expedition 320/321 Scientists[2]

Chapter contents

Background and objectives

Integrated Ocean Drilling Program Site U1336 (site survey PEAT-5C; 7°42.067′N, 128°15.253′W; 4286 meters below sea level [mbsl]) (Fig. F1; Table T1) is in the central area drilled during the Pacific Equatorial Age Transect (PEAT) program (Expedition 320/321). Site U1336 (~32 Ma crust) is between Site U1334 ~410 km to the west and Site U1335 ~330 km to the southeast and ~100 km to the west of Deep Sea Drilling Project (DSDP) Site 78. Site U1336 is also ~30 km north of the center of the Clipperton Fracture Zone. The site survey data (Lyle et al., 2006; Pälike et al., 2008) show that Site U1336 is on abyssal hill topography draped with thick sediment (Fig. F2). The fabric of the abyssal hills is oriented slightly west of due north.

Water depth in the vicinity of Site U1336 is relatively shallow for the age of the crust, between 4200 and 4400 m. Surprisingly, the crust south of the Clipperton Fracture Zone is only 100 m deeper than the crust north of the zone, despite a water depth of nearly 5 km in the middle of the fracture zone trace. A few oblique ridges and depressed topography occur in the south of the survey area, showing some interaction between the fracture zone and the Site U1336 region. The site is thickly covered with sediment (300–400 ms two-way traveltime [TWT]) (Fig. F2) and has a very thin layer of recent to middle Miocene sediment, with frequent sediment erosion on flanks of abyssal hills. Based on correlation to the Neogene central equatorial Pacific seismic stratigraphy of Mayer et al. (1985) and the Paleogene equatorial Pacific stratigraphy of Lyle et al. (2002), we estimated ~120 m of Oligocene sediment for an average Oligocene sedimentation rate of 13 m/m.y., assuming a crustal age of 32 Ma. The total sediment thickness, using the velocity-depth conversion for DSDP Site 574 (Mayer et al., 1985) was estimated as 253 m prior to drilling.

Based on stage-pole reconstructions of Pacific plate motion, observations of basement age from previous drilling sites, and magnetic anomaly maps (Cande et al., 1989), we estimated that Site U1336 is on 32 Ma crust. The best control on age is information from Site 78, ~100 km east of Site U1336. The base of Site 78 reaches the lower Oligocene.

Site U1336 targets the Oligocene and is on lower Oligocene crust. This interval of time is noted by heavy oxygen isotopes and a relatively deep calcium carbonate compensation depth (CCD) (Zachos et al., 2001a, 2001b; Pälike et al., 2006a, 2006b; Lyle, 2003).

[1] Expedition 320/321 Scientists, 2010. *In* Pälike, H., Lyle, M., Nishi, H., Raffi, I., Gamage, K., Klaus, A., and the Expedition 320/321 Scientists, *Proc. IODP,* 320/321: Tokyo (Integrated Ocean Drilling Program Management International, Inc.). doi:10.2204/iodp.proc.320321.108.2010
[2] Expedition 320/321 Scientists' addresses.

doi:10.2204/iodp.proc.320321.108.2010

There was probably ice on Antarctica during this interval, but not the large ice sheets found there in the middle Miocene. There is no compelling evidence for ice sheets in the Northern Hemisphere during the Oligocene and early Miocene. Thus, there was apparently a relatively low global ice volume, relatively cold bottom waters, a relatively cold South Pole, and a relatively warm North Pole. This scenario of a "one cold pole" world has given rise to speculation on the impact of interhemispheric temperature imbalance on pole to Equator temperature gradients and on the symmetry of the global wind systems. The extent to which such an imbalance may have affected trade winds, the position of the intertropical convergence zone, and seasonal shifts in this zone should be seen in the wind-driven currents of the equatorial region.

Older low-resolution DSDP data (Hays et al., 1972) indicate relatively high but variable sediment accumulation rates during the Oligocene and better carbonate preservation south of the Equator (van Andel, 1975). In the Ocean Drilling Program (ODP) Leg 199 equatorial transect (Lyle, Wilson, Janecek, et al., 2002), the highest accumulation rates encountered (>15 m/m.y.) occurred in the lower part of the Oligocene, but these were in sites north of the Oligocene Equator or on relatively old (and therefore deep) crust. Thus we expected better fossil preservation and a thicker carbonate section at the Oligocene Equator.

Studies of Oligocene sections from Leg 199 (Lyle, Wilson, Janecek, et al., 2002) and from other ODP sites (e.g., Paul et al., 2000; Zachos et al., 2001b) indicate the presence of strong eccentricity and obliquity cycles in carbonate preservation and suggest a strong (southern) high-latitude influence on the carbonate record. These cycles are leading to the development of an orbitally tuned timescale that reaches to the base of the Oligocene (Pälike et al., 2006b). Such a timescale makes it possible to develop a very detailed picture of equatorial geochemical fluxes and of the degree of variability in the equatorial system of the Oligocene.

Site U1336 also targets paleoceanographic events in the late Oligocene and into the early Miocene, including the climatically significant Oligocene–Miocene transition and the recovery from the Mi-1 glaciation event. In conjunction with Sites U1335 and U1337, it was also sited to provide a latitudinal transect for early Miocene age slices. At the end of the Oligocene there is a significant multimillion year long rise in the oxygen isotope record (supplementary material in Pälike et al., 2006b), which is closely followed by a relatively short, sharp increase in oxygen isotope values that has been interpreted as a major glacial episode (Mi-1) (Zachos et al., 1997, 2001a, 2001b; Pälike et al., 2006a, 2006b) and correlated to a pronounced drop in sea level (Miller et al., 1991). This event is very close to the Oligocene/Miocene boundary and has now been astronomically age calibrated in several ocean basins (Shackleton et al., 2000; Billups et al., 2004; Pälike et al., 2006a). Although there are clear periodic isotopic signals indicating major changes in ice volume, ocean temperatures, and/or ocean structure, this biostratigraphic boundary has always been somewhat of an enigma. Unlike the major changes in the isotopic stratigraphy, the biostratigraphies of planktonic microfossils show very little change at all. In fact it is one of the most difficult epoch boundaries to pick using only microfossil biostratigraphies.

Given the Clipperton Fracture Zone geographical constraint, we positioned Site U1336 as close as possible to the estimated paleoequatorial position at the target age in order to maximize the time that the drill site remains within the equatorial zone (i.e., ±2° of the Equator), to allow for some southward bias of the equatorial sediment mound relative to the hotspot frame of reference (Knappenberger, 2000) and to place the interval of maximum interest above the basal hydrothermal sediments. We located the site using the digital age grid of seafloor age from Müller et al. (1997), heavily modified and improved with additional magnetic anomaly picks from Petronotis (1991) and Petronotis et al. (1994) and DSDP/ODP basement ages. For this grid, each point is then backrotated in time to zero age, using the fixed-hotspot stage-poles from Koppers et al. (2001) and Engebretson et al. (1985) and the paleopole data from Sager and Pringle (1988). From the backtracked latitudes for each grid point we then obtained the paleoequator at the crustal age by contouring of latitudes.

One of the common objectives of the PEAT program for all sites is to provide a limited depth transect for several Cenozoic key horizons, such as the Oligocene–Miocene transition (Shackleton et al., 2000; Pälike et al., 2006a; Zachos et al., 2001b). For the Oligocene–Miocene transition objective, Sites U1334–U1337 will form a combined depth transect for Oligocene–Miocene time. Site U1336 has an estimated crustal paleodepth of ~3.7 km during the Oligocene–Miocene transition, ~300 m deeper than Site U1335 and ~500 m shallower than Site U1334.

Expedition 320/321 drill sites all have in common the objective to improve and extend the extensive intercalibrated bio-, magneto-, chemo-, and astronomical stratigraphies for the Cenozoic (e.g., Shackleton et al., 2000; Pälike et al., 2006b).

Seismic reflection data (Fig. F2) (Pälike et al., 2008; Lyle et al., 2006) allowed us to optimize the Site

U1336 position on seismic Line PEAT-5C-sl-6, west of the intersection with the north–south Cross-line PEAT-5C-sl-1, to better image basement and obtain a more expanded lower sediment section. We estimated sediment thickness using interval velocities published for Site 574 by Mayer et al. (1985), which drilling determined later to underestimate the basal interval velocities and therefore total sediment thickness. Based upon correlation to the central equatorial Pacific seismic stratigraphy of Mayer et al. (1985), middle Miocene sediment has been exposed.

Site survey piston Core RR0603-7JC was taken east of Site U1336 (Fig. F1B). The cores recovered mottled brown to light brown alternating carbonates and siliceous biogenic sediments. The age at the base of this core is ~13 Ma, based on radiolarian biostratigrapy.

Science summary

Two holes were cored at Site U1336 (proposed Site PEAT-5C; 7°42.067′N, 128°15.253′W; 4286 mbsl) (Fig. F1; Table T1) targeting paleoceanographic events in the late Oligocene and into the Miocene, including a focus on the Oligocene–Miocene transition and the recovery of the Mi-1 glaciation event (Zachos et al., 2001b; Pälike et al., 2006b). In conjunction with Sites U1335 and U1337, Site U1336 was also designed to provide a latitudinal transect for early Miocene age slices. Site U1336 provides data toward a depth transect across the late Oligocene and Miocene that allow us to verify and apply a previous astronomical age calibration from Site 1218 (Pälike et al., 2006a).

At Site U1336, advanced piston corer (APC) cores were taken from the seafloor to 184.8 m (Cores 320-U1336A-1H through 21H) and 173.6 m (Cores 320-U1336B-1H through 20H). Nonmagnetic core barrels were used for Cores 320-U1336A-1H through 16H and Cores 320-U1336B-1H through 16H and steel barrels were used for all other cores. Two hard layers, one at ~121 m core depth below seafloor (CSF) (Cores 320-U1336A-14H and 320-U1336B-14H) and one at ~135 m CSF (Core 320-U1336B-16H) caused core loss and prevented the development of a continuous sediment section. Extended core barrel (XCB) cores (320-U1336A-22X through 35X) were taken from 184.8 to 302.9 m CSF in Hole U1336A. We stopped coring before reaching the basement objective because of decreasing rates of penetration, relatively low recovery, and the possibility of obtaining a stratigraphically complete Miocene section by allocating the remaining operational time during Expedition 320 to Hole U1336B.

At Site U1336, ~300 m of pelagic sediments are divided into three major lithologic units (Fig. F3). The sediments are composed mainly of nannofossil oozes, nannofossil chalks, and chert. The lower to middle Miocene sedimentary sequence of Unit I (0–74.54 m CSF) contains more radiolarians, clay, foraminifers, and diatoms relative to the lower Miocene to lower Oligocene sediments below ~70 m CSF. Subtle changes in the relative proportions of these minor components produce meter-scale dark–light color cycles and two diatom-rich layers. Numerous rounded fragments of pumice occur throughout this unit.

Unit II (74.50–189.50 m CSF) is dominated by nannofossil ooze. Sediment color changes downhole from pale yellow to light greenish gray at 92 m CSF. Below this boundary, the color of Unit II alternates between light greenish gray and white to 184.80 m CSF. Oxidation-reduction reactions are responsible for the observed vivid colors and pore water chemistry changes, likely fueled by varied availability of organic carbon. Occasional thin chert layers were encountered below 120 m CSF in Unit II. Mainly broken chert fragments were recovered, except for a small in situ chert fragment at 159.6 m CSF in Section 320-U1336B-18H-4, 106 cm. More abundant chert layers are common in the lower third of the recovered sequence.

Unit III (189.5–299.6 m CSF) was only recovered in Hole U1336A. The dominant lithologies of this unit are light greenish gray and white nannofossil chalk with light greenish gray millimeter-scale color banding and chert layers. The chert shows many different colors including black, dark greenish gray, very dark greenish gray, dark gray, olive-yellow, dark brown, and pink. The Unit II–III transition is identified by the uppermost common occurrence of chert. Below 289 m CSF, nannofossil chalk contains increasing amounts of micrite and the cherts vary in color. The lowermost cherts are olive-yellow, then pink, and, finally, dark brown at the base. The chalk changes color to white below 298.54 m CSF. $CaCO_3$ contents remain >88 wt% in the chalk layers. Igneous basement was not recovered at Site U1336.

All major microfossil groups were found in sediments from Site U1336, representing a complete biostratigraphic succession at the shipboard sample resolution level of middle Miocene to lower Oligocene sediments. They provide a coherent, high-resolution biochronology through a complete sequence (Fig. F3). Calcareous nannofossils are moderately to poorly preserved throughout the succession. There appears to be a complete sequence of nannofossil zones from Zone NN6 (middle Miocene) through NP22 (lower Oligocene), except for Zone NN3, which could not be resolved. Planktonic foraminifers are present throughout the succession ranging from

Zones N12 through O1. They are moderately well preserved in the Miocene and less well preserved in the Oligocene.

Benthic foraminifers are present throughout the section, although abundances are overall quite low. The preservation of tests is moderate in the upper part of Site U1336 (Samples 320-U1336A-1H-CC through 19H-CC, 8.22–170.63 m CSF, and 320-U1336B-1H-CC through 20H-CC, 1.68–174.01 m CSF) but deteriorates below this level. The Oligocene to middle Miocene benthic foraminifer assemblage is relatively diverse and indicates oligotrophic lower bathyal to abyssal paleodepths.

The Oligocene/Miocene boundary is placed between the first occurrence of *Paragloborotalia kugleri* (23.0 Ma) and the extinction of *Sphenolithus delphix* (23.1 Ma). The former occurs between Samples 320-U1336A-16H-CC and 17H-2, 38–40 cm (142.96 m CSF) and Samples 320-U1336B-16H-1, 52–54 cm, and 17H-3, 80–82 cm (137.72 m CSF). The top of *S. delphix* is recognized between Samples 320-U1336A-17X-2, 90 cm, and 17X-4, 90 cm (145.9 m CSF), and between Samples 320-U1336B-16H-CC and 17H-1, 150 cm (137.56 m CSF).

The radiolarian stratigraphy at Site U1336 spans the interval from just above the Zone RN6/RN5 boundary (middle Miocene) to the upper part of Zone RP22 (upper Oligocene) at ~170 m CSF. Below this level the sediments are barren of radiolarians. Above this level the assemblages tend to have good to moderate preservation with intermittent intervals of good preservation in Zones RN3 and RN4 (lower to middle Miocene). The downsection decrease in preservation and ultimate disappearance of the radiolarians below Core 320-U1336A-19H appears to be associated with dissolution and reprecipitation of the biogenic silica as intergranular cement and as chert.

Diatom stratigraphy in Hole U1336B spans the interval from just above the *Cestodiscus peplum* zone (middle Miocene) in Core 320-U1336B-1H to the lowermost part of the *Crucidenticula nicobarica* zone (upper lower Miocene) in Core 320-U1336B-7H. Below Sample 320-U1336B-7H-CC, the sediments are barren of diatoms. Above this level the valves tend to be mostly poorly preserved. Sample 320-U1336B-1H-CC contains the highest diversity with *Cestodiscus pulchellus* as dominant component, accompanied by *Cavitatus jouseana* and *Thalassiosira yabei*. Fragments of the large centric diatom *Ethmodiscus* are present in the upper part of Hole U1336B.

Paleomagnetic measurements were conducted on archive-half sections of 21 APC cores from Hole U1336A and 20 APC cores from Hole U1336B. Measurements of natural remanent magnetization (NRM) above ~80 m CSF in Holes U1336A and U1336B indicate moderate magnetization intensities (~1×10^{-3} A/m) with a patchy but generally weak viscous remanent magnetization (VRM) or isothermal remanent magnetization (IRM) drilling overprint. Polarity reversal sequences are clearly recognized (Fig. **F3**). Demagnetization data from discrete samples above ~ 80 m CSF indicate that the characteristic remanent magnetization of the sediments is identified at the 10–20 mT demagnetization steps. The reversals pattern can be correlated with the geomagnetic polarity timescale (GPTS) from the base of Chrons C5r to C6n (~12 to 19 Ma).

Below ~80 m CSF, a zone of diagenetic alteration involving dissolution of remanence carriers reduces remanence intensities after alternating-field (AF) demagnetization of 20 mT to values close to magnetometer noise level in the shipboard environment (~1×10^{-5} A/m). In this zone, sediment magnetizations have been partly or entirely overprinted during the coring process and remanence inclinations are sometimes steep after AF demagnetization at peak fields of 20 mT. At ~130–140 m CSF (Cores 320-U1336A-15H through 16H and 320-U1336B-15H) and below ~160 m CSF (Cores 320-U1336A-19H through 21H and 320-U1336B-18H through 20H), polarity reversals are apparently present but the inclinations are steep (as much as 80°), indicating that the drilling overprint has not been effectively removed during shipboard demagnetization.

A complete physical property program was conducted on whole cores, split cores, and discrete samples. Whole-Round Multisensor Logger (WRMSL) (gamma ray attenuation [GRA] bulk density, magnetic susceptibility, *P*-wave velocity, and electrical noncontact resistivity), thermal conductivity, and natural gamma radiation (NGR) measurements comprised the whole-core measurements. Compressional wave velocity measurements on split cores and moisture and density (MAD) analyses on discrete core samples were made at a frequency of 1 per undisturbed section in Cores 320-U1336A-1H through 35X. Compressional wave velocities were measured toward the bottom of sections. MAD analyses were located 10 cm downsection from carbonate analyses (see **"Geochemistry"**). Lastly, the Section Half Multisensor Logger (SHMSL) was used to measure spectral reflectance on archive-half sections. Physical properties measurements on whole-round sections and samples from split cores reflect the differences among lithologies drilled at Site U1336 (Fig. **F3**). Nannofossil ooze with varying amounts of clay, radiolarians, and diatoms makes up lithologic Unit I and is characterized by high-amplitude and high-frequency variations in bulk density, magnetic sus-

ceptibility, NGR, and color reflectance. Magnetic susceptibility is highest in Unit I, with values ranging from 5×10^{-5} to 30×10^{-5} SI. NGR is also high in this unit, with values to 56 cps near the seafloor. Wet bulk densities are lowest in Unit I, with values ranging from 1.4 to 1.7 g/cm^3. Porosity is highest in this interval, ranging from 65% to 80%. The grain density of most of the sediments of Unit I, as well as Units II and III, ranges from 2.6 to 2.9 g/cm^3, reflecting the dominance of carbonate constituents at Site U1336. The sediment velocity in Unit I is low, averaging 1500 m/s. The color reflectance of Unit I is marked by luminance (L*) values that are slightly lower and more variable than values determined for sediments in Units II and III.

Below Unit I, a more uniform increase in wet bulk density and decrease in porosity in Units II and III reflects the increasing compaction of the sediments. A slight step increase in wet bulk density marks the transition between Units II and III. In Unit III wet bulk density and porosity average 1.9 g/cm^3 and 51%, respectively. Magnetic susceptibility and NGR are low and nearly uniform in Units II and III. Magnetic susceptibility is typically below 5×10^{-5} SI, and NGR is ~2 cps. Lower clay abundance in Unit II is marked by an increase in L* at the boundary between Units I and II. At 92 m CSF, within Unit II, sharp decreases in the a* and b* reflectance parameters mark the change in sediment color from pale yellow to greenish gray. One of the most pronounced changes in physical properties at Site U1336 is the sharp increase in velocity that accompanies the change from nannofossil ooze to nannofossil chalk at the boundary between Units II and III. The velocity at the base of Unit II is ~1700 m/s. Below 190 m CSF, in Unit III, the rate at which velocity increases with depth increases, ultimately reaching ~2200 m/s at 290 m CSF, near the base of Hole U1336A.

Special Task Multisensor Logger (STMSL) data were collected at 5 cm intervals from Hole U1336B and compared to the WRMSL data obtained at 2.5 cm resolution from Hole U1336A during Expedition 320. Features in the magnetic susceptibility and gamma ray attenuation density are well aligned between Holes U1336A and U1336B to a depth of ~94 m core composite depth below seafloor (CCSF-A; see **"Core composite depth scale"** in the "Methods" chapter). Below 94 m CCSF-A, the magnetic susceptibility signal drops to very low values but the density data are good enough to sustain a correlation to interval 320-U1334B-14H-4, 122 cm. At this point (138.50 m CCSF-A) sediments recovered in both holes are disturbed.

Paleomagnetic reversals were used to calculate the average linear sedimentation rate (LSR) for the upper 74 m of the section at Site U1336 on the corrected core composite depth below seafloor (CCSF-B; see **"Corrected core composite depth scale"** in the "Methods" chapter) depth scale. Below 74 m CSF only biostratigraphic datums were used to calculate the average LSR. The LSR at Site U1336 decreases from 15 m/m.y. in the upper Oligocene to 12 m/m.y. in the lower Miocene and stays relatively constant at 9 m/m.y. in the remainder of the section.

Standard geochemical analyses of pore water and organic and inorganic sediment properties were undertaken on Site U1336 samples. Alkalinity is relatively constant at values >2.5 mM in the upper 110 m CSF, with a pronounced decline to 1 mM by 170 m CSF. Sulfate concentrations decrease with depth to values as low as 22 mM. Dissolved manganese has a broad peak in the depth range from ~25 to 120 m CSF, and dissolved iron appears then peaks below 100 m CSF. The increase of dissolved iron occurs where Mn decreases downhole. Concentrations of dissolved silicate increase with depth from <400 to 800 µM.

Highlights

Miocene sedimentary section and cyclic sedimentation

One of the highlights from Site U1336 is the recovery of a thick Miocene carbonate section from the central equatorial Pacific, one of the high-priority objectives of the PEAT program. We recovered the complete early Miocene sequence (7.1 m.y. duration) in a ~110 m thick section, with a sedimentation rate of 12 m/m.y. and the middle Miocene sequence (4.4 m.y. duration) in a ~45 m thick interval with a sedimentation rate of ~21 m/m.y. These high sedimentation rates will facilitate the study of paleoceanographic processes at unprecedented resolution for the equatorial Pacific.

The obvious variations of both color and biogenic composition within nannofossil oozes represent cyclic fluctuations of CCD and upwelling intensity during the middle Miocene through early Miocene. The variable lithology also results in the variations of many petrophysical signals of physical properties including L*, b*, magnetic susceptibility, NGR, and GRA bulk density.

Oligocene–Miocene transition and depth transects

Site U1336 was planned as part of a latitudinal transect for early Miocene age slices and the PEAT Oligocene–Miocene depth transect compound in conjunction with Sites U1335 and U1337. The Miocene sequence

at these sites includes the critical intervals of the Mi-1 glaciation and middle Miocene ice sheet expansion (Holbourn et al., 2005; Zachos et al., 2001b; Pälike et al., 2006b). The dominant lithologies of nannofossil ooze and chalk at Sites U1336 and U1335, with good preservation of calcareous microfossils, will allow us to achieve the prime objective for this site.

The Oligocene–Miocene transition in Hole U1336A occurs in homogeneous nannofossil ooze within the alternations of white and light greenish gray ooze. The same alternating sequence is observed above the Oligocene–Miocene transition at Site U1334. Biostratigraphy reveals that the Oligocene/Miocene boundary exists between 142.96 and 145.9 m CSF at Site U1336; this will allow the high-resolution study of this critical interval.

Geochemical front

Site U1336 recovered an interval of greenish gray carbonates that exhibit a distinct peak in dissolved Fe concentrations in pore water with similar characteristics as geochemical alteration fronts at Sites U1334 and U1335. At Site U1336, this zone is ~200 m thick. The remanent magnetization intensity is very weak in most parts of this section (80–180 m CSF). High dissolved Fe and Mn concentrations in pore water are caused by changes in the oxidation state of the sediments. The oxidation-reduction reactions are likely fueled by variable availability of organic carbon in the sediments. This site may provide the opportunity to study organic matter degradation.

Site U1336 migrated from south to north through the equatorial belt of high productivity. Based on paleolatitude reconstructions these geochemical alteration fronts can be mapped to similar equatorial positions between Sites U1334 and U1335, roughly between the Equator and ~4°N.

Chert formation in the early Oligocene

The sequence at Site U1336 includes barren intervals of radiolarian fossils and many thin intercalated chert layers and fragments. The radiolarians decrease in preservation downsection and disappear below Core 320-U1336A-19H. Instead, the sediments contain several chert fragments. Some inferred chert layers occur at ~120–140 m CSF and blocked APC penetration. Below ~190 m CSF, various colored chert layers and fragments occurred within the cores. The chert frequently contains foraminifer tests, reflecting diagenetic process of dissolution and reprecipitation of the biogenic silica.

The dissolution of biogenic silica is the source of porcellanite and chert and, on crust younger than 65 Ma, almost all cherts in the Pacific Ocean lie <150 m above basement. Although we did not recover basement rocks at this site, the sediments became hard, lithified limestones and the drilled section is probably close to basement. The dissolution of silica in the basal sedimentary section is likely associated with the circulation of warm hydrothermal waters in the upper oceanic crust that extend into the lower sediments where they are cut by fractures and faults (Moore, 2008a, 2008b). This site will provide information on chert formation in the equatorial Pacific regions.

Operations

Times for Site U1336 are given in local ship time, which was Universal Time Coordinated (UTC) – 9 h.

Transit to Site U1336

The 185 nmi transit from Site U1335 to Site U1336 took 17.8 h at an average speed of 10.4 kt.

Site U1336

Hole U1336A

The ship slowed as it approached Hole U1336A and was in dynamic positioning mode at 1545 h on 22 April 2009. Once the ship was stabilized over the new site, the drill string was deployed and the bit positioned 5 m shallower than the corrected precision depth recorder depth of 4300.4 m drilling depth below rig floor (DRF). Hole U1336A was spudded with the APC at 0135 h on 23 April. The seafloor depth estimated from recovery in the first core was 4296.9 m DRF (4285.3 mbsl) (Table T1).

APC Cores 320-U1336A-1H through 21H were taken from 0 to 184.8 m CSF and recovered 190.2 m (103%) (Table T1). Nonmagnetic core barrels were used to obtain Cores 320-U1336A-1H through 16H; steel barrels were used for all other cores. Three cores (320-U1336A-14H, 16H, and 21H) only partially stroked and were advanced by recovery. A hard layer at ~124 DSF prevented Core 320-U1336A-14H from achieving a full stroke; the layer was ~0.5 ft thick and was not recovered. Based on how it drilled, we inferred it may have been chert. The last piston core (320-U1336A-21H) required drilling over to free the barrel from the formation.

Cores 320-U1336A-22X through 35X were taken from 184.8 to 302.9 m CSF and recovered 69.0 m (58%). We stopped coring before reaching the basement objective because of decreasing rates of penetration (as low as ~3 m/h for Cores 320-U1336A-34X and 35X), relatively low recovery, and the possibility of obtaining a stratigraphically complete Miocene section by coring in a second hole. We pulled out of

the hole and the bit cleared the seafloor at 0400 h on 25 April. We offset the ship 25 m south of Hole U1336A.

Hole U1336B

After positioning the bit at 4284 m DRF (5 m shallower than in Hole U1336A), we started coring in Hole U1336B at 0540 h on 25 April. Based on recovery in the first core, the seafloor depth was 4298.1 m DRF (4286.5 mbsl). Cores 320-U1336B-1H through 20H were taken from 0 to 173.9 m CSF and recovered 179.6 m (103%). Nonmagnetic core barrels were used for Cores 320-U1336B-1H through 16H; steel barrels were used for the others. Core 320-U1336B-16H only achieved a partial stroke and was advanced by recovery. Once coring was completed, the drill string was pulled out of the hole with the bit clearing the seafloor at 0400 h on 26 April. Once all drilling equipment was secured, the vessel departed for Honolulu, Hawaii, at 1315 h on 26 April.

Transit to Honolulu, Hawaii

The 1954 nmi transit from Site U1336 to Honolulu, Hawaii took 7.8 days at an average speed of 10.4 kt. At 2400 on 27 April 2009, the shipboard clocks were set back one hour so that ship local time was UTC – 10 h (Hawaii Standard Time). Expedition 320 concluded with the first line ashore at 0736 h on 4 May.

Lithostratigraphy

Drilling at Site U1336 recovered a ~300 m thick section of pelagic sediments (Fig. F4). The sedimentary sequence at Site U1336 is divided into three lithologic units (Fig. F4; Table T2). Unit I (0–74 m CSF) is composed of nannofossil ooze of Miocene age that displays submeter-scale alternations of white (10YR 8/1) to brown (10YR 5/3) nannofossil oozes with varying amounts of radiolarians, foraminifers, diatoms, and clay as minor constituents. Two white (10YR 8/1) diatom nannofossil oozes (Samples 320-U1336A-5H, 22–36 cm, and 6H-2, 87–92 cm) are present within Unit I. These intervals were not observed in Hole U1336B. Unit II (74–189 m CSF) consists of ~115 m thick nannofossil ooze of early Miocene to late Oligocene age with very weak magnetic susceptibility and vivid color changes. Sediment color changes downhole from pale yellow (2.5Y 8/2) to light greenish gray (10Y 8/1) at 92 m CSF. Below this boundary, the coloration of the Unit II nannofossil oozes alternates between light greenish gray (10Y 8/1) and white (N 8/) to 184.80 m CSF. Unit III is composed of light greenish gray (10GY 7/1) nannofossil chalks with interbedded greenish gray (10GY 6/1) to black (10YR 2/1), olive-yellow (2.5Y 6/6), and pink (7.5YR 7/3) chert layers (189.50–299.6 m CSF) of Oligocene age. Units II and III have similar color alternations with occasional sharply defined packets of light greenish gray (5G 8/1) color bands below 120.86 m CSF.

Lithologic units and boundaries (Table T2) are defined by differences in lithology, physical property data, and calcium carbonate ($CaCO_3$) content as measured by coulometry (see "Geochemistry"). Lithologic differences, based on both visual core description and smear slide analysis, reflect varying distributions of biogenic components such as nannofossils, radiolarians, diatoms, and clay-sized lithogenic material (Fig. F4; see "Site U1336 smear slides" in "Core descriptions"). Lithologic descriptions are based on sediments recovered in Holes U1336A and U1336B. Sediments from Hole U1336A were described by the scientific party during Expedition 320, whereas those from Hole U1336B were examined and described by the Expedition 321 scientific party.

Unit I

Intervals: 320-U1336A-1H-1, 0 cm, through 8H-7, 5 cm; 320-U1336B-1H-1, 0 cm, through 9H-5, 84 cm
Depths: Hole U1336A = 0–73.05 m CSF; Hole U1336B = 0–75.14 m CSF
Age: middle to lower Miocene
Lithology: nannofossil ooze and diatom nannofossil ooze

Major lithologies in Unit I are white (10YR 8/1) to brown (10YR 5/3) nannofossil ooze. The unit is characterized by alternating submeter-scale light and dark bands of nannofossil ooze. Based on smear slides, the darker bands contain greater amounts of radiolarians and/or clay and some of the white bands are nannofossil ooze with foraminifers (Figs. F5, F6). The alternating white to brown sequence is punctuated by two white (10YR 8/1) layers of diatom nannofossil ooze (Samples 320-U1336A-5H-2, 22–36 cm, and 6H-2, 87–92 cm); however, these sediments were not recovered in Hole U1336B and were likely missed by coring gaps or sampled for whole-round studies before cores were described. Pumice fragments, sometimes as large as 2.0 cm in diameter, occur in Unit I. Most are well rounded and light gray to gray (N7/ to N6/) in color. Throughout Unit I, physical properties, including magnetic susceptibility, b* and L* reflectance, and GRA bulk density, all show higher amplitude variability than underlying units. $CaCO_3$ content is also more variable in Unit I relative to Unit II, ranging between 48 and 90 wt% (Fig. F4). The transition to Unit II is indicated by an overall decrease in the amplitude of variation in the physical properties, a downhole increase

in density and L*, a decrease in magnetic susceptibility, and a lesser abundance of the minor constituent radiolarians, clay, and foraminifers (Fig. F4).

Unit II

Intervals: 320-U1336A-8H-7, 5 cm, through 22X-4, 20 cm; 320-U1336B-9H-5, 84 cm, through 20H-7, 58 cm (end of Hole U1336B)
Depths: Hole U1336A = 73.05–189.50 m CSF; Hole U1336B = 75.14–173.98 m CSF (end of hole)
Age: early Miocene to late Oligocene
Lithology: nannofossil ooze

The dominant lithology in Unit II is nannofossil ooze with vivid coloring. The uppermost 9.6 m of Unit II is pale yellow (2.5Y 8/2 to 2.5Y 8/3) nannofossil ooze that sharply overlies a sequence of alternating white (2.5Y 8/1 and N 8/) and light greenish gray (10GY 8/1) nannofossil ooze at 92.14 m CSF in Hole U1336A (Figs. F7, F8). Below 120 m CSF, light greenish gray (5G 8/1) millimeter-scale color bands are observed in centimeter-scale packets in nearly every core. Chert was encountered in the lower portion of this unit hampering coring recovery, but no layers were recovered directly. Numerous small angular fragments of chert were found in Section 320-U1336B-16H-CC and soupy intervals near tops of Cores 320-U1336B-17H through 19H, representing fall-in sediment. A small fragment of in situ chert was recovered in interval 320-U1336B-18H-4, 106 cm. Bioturbation is generally minor or nonvisible throughout the unit. $CaCO_3$ content in Unit II is relatively constant, typically >85 wt% (Fig. F4; see "Geochemistry"). Color reflectance parameter b* decreases abruptly at 92.14 m CSF in Hole U1336A and 91.85 m CSF in Hole U1336B and remains low throughout the unit. L* increases across the Unit I/II boundary, reaching a maximum near the top of Unit II (~90) and gradually decreases with depth to ~65–70 at ~180–190 m CSF (Fig. F7). Working downhole through Unit II, GRA bulk density increases from ~1.6 to 1.9 g/cm^3. Magnetic susceptibility is very low (typically $<5 \times 10^{-5}$ SI), sometimes below zero, throughout the unit (Fig. F4; see "Physical properties").

Unit III

Intervals: 320-U1336A-22X-4, 20 cm, through 35X-CC, 38 cm
Depths: Hole U1336A = 189.5–299.6 m CSF
Age: Oligocene
Lithology: nannofossil chalk, and chert

The Unit II–III transition is identified by the transition to chalk. Dominant lithologies of Unit III are light greenish gray (10GY 8/1 and 10GY 7/1) and white (7.5YR 8/1 and N 8/) nannofossil chalk with light greenish gray (5G 8/1) millimeter-scale color banding and chert layers. In the upper 100 m of Unit III cherts are black (10YR 2/1) to dark greenish gray (10GY 4/1). Below 289 m CSF nannofossil chalk contains increasing amounts of micrite and cherts occur in different colors: olive yellow (2.5Y 6/6), dark brown (7.5Y 3/2), and pink (7.5YR 7/3) (see "Site U1336 thin sections" in "Core descriptions"). Thin section analyses show increasing abundance with depth of foraminifers in the cherts (see "Site U1336 thin sections" in "Core descriptions"). Foraminifer tests in the cherts have been filled with microcrystalline quartz or occasionally filled or replaced by opaques, likely pyrite (Fig. F9). GRA density continues to increase with depth, from ~1.9 g/cm^3 at the top of the unit and reaching a maximum of ~2.0–2.1 g/cm^3 from 282 m CSF and below (Fig. F4; see "Physical properties"). Magnetic susceptibility in Unit III is generally low ($<5 \times 10^{-5}$ SI) with thin instances of much higher values that correspond to the chert layers. L* is overall more variable and generally lower in Unit III, whereas b* shows more variability than overlying units. $CaCO_3$ contents remain >88 wt% in the chalk layers. Igneous rocks were not recovered at Site U1336.

Discussion

Unit I light–dark color cycles

Pronounced submeter-scale color variations are common within the nannofossil oozes of Miocene age found in Unit I. These light–dark cycles are associated with variations in the relative amounts of accessory lithologic components within the nannofossil oozes, including clay, radiolarians, and diatoms (Fig. F5). These lithologic cycles are also apparent in a higher amplitude of variation in physical properties, including L*, b*, magnetic susceptibility, and GRA bulk density (Fig. F4; see "Physical properties"). Nannofossils dominate these sediments, making up between 50% and 95% of smear slide samples. The remainder is made up of clay, radiolarians, or diatoms (Fig. F5; see "Site U1336 smear slides" in "Core descriptions"). Two white (10YR 8/1) diatom nannofossil ooze layers (Samples 320-U1336A-5H-2, 22–36 cm, and 6H-2, 87–92 cm) occur at 38.34 and 48.40 m CSF. These layers stand out because they are visually brighter than the surrounding sediments (nearest L* measurements are 88 and 83.5 for the upper and lower layers, respectively) and also have a unique spongy texture that causes pilling during surface scraping in preparation for line scan imaging. Smear slide analysis indicates that the diatom assemblage is composed primarily of pennate taxa, with abundant needlelike *Thalassiothrix* spp. (Fig. F6). The low abundance of diatoms (<5%) in most dark layers,

where abundance of radiolarians increases relative to nannofossils, suggests that the observed lithologic variations within the nannofossil oozes could be the product of dissolution cycles; however, more detailed mass accumulation rate data are needed to test this.

Redox-related color changes

Site U1336 sediments are marked by vivid color changes that are made obvious against the backdrop of otherwise relatively white nannofossil oozes and chalks. Sediment color shows a downhole shift from white (10YR 8/1) to very pale brown (10YR 7/3) through pale yellow (2.5Y 8/2) to light greenish gray (10GY 8/1) over a 30 m thick interval (65–95 m CSF). This greenish gray color starts abruptly (Fig. **F8**) at 92.14 m CSF in Hole U1336A and at 91.8 m CSF in Hole U1336B and spans a ~198 m thick interval before shifting to white and pink below 290.41 m CSF in Hole U1336A (not recovered in Hole U1336B). Reflectance parameters a* and b*, which measure green–red and blue–yellow portions of the spectrum, respectively, shift in a steplike manner to lower values with these observed color changes (Fig. **F7**). Magnetic susceptibility drops to near zero in the transition from very pale brown to pale yellow and remains very weak throughout the light greenish gray interval, the same pattern observed at Sites U1334 and U1335. With elevated Fe and Mn pore water concentrations, discrete millimeter- to centimeter-scale color bands occur within the interval of light greenish gray to white nannofossil ooze where Fe reduction has occurred in Units II and III. Although there is no obvious lithologic specificity, the banded sediments are sometimes more consolidated than the immediately overlying and underlying sediments.

The pattern of changing sediment color, physical and magnetic properties, and pore water chemistry seen at Site U1336 suggests loss of Fe-bearing minerals during diagenesis by microbial Fe reduction. A diagenetic origin for the color bands is suggested by their occurrence in the interval of the sequence that has undergone Fe reduction, their lack of lithologic specificity, and induration sometimes associated with discrete beds with particularly prominent banding. Similar "light gray-green banded chalk" is reported from DSDP Site 79 (2°33.02′N, 121°34.00′W) with high Fe (105 µM/kg) and Mn (1000 µM/kg) interstitial water concentrations (Presley and Kaplan, 1972).

Summary

At Site U1336 ~300 m of pelagic sediments are divided into three major lithologic units. Sediments are composed mainly of nannofossil oozes, nannofossil chalks, and chert. The early to middle Miocene sedimentary sequence of Unit I contains more radiolarians, clay, foraminifers, and diatoms relative to the early Miocene to early Oligocene sediments below ~75 m CSF. Subtle changes in the relative proportions of these minor components produce meter-scale dark–light color cycles and two diatom-rich layers. Numerous rounded fragments of pumice occur throughout this unit. The oxidation-reduction reactions responsible for the observed vivid colors and pore water chemistry changes are likely fueled by enhanced availability of organic carbon relative to overlying and underlying sediments. Thin chert layers were encountered near 124 m CSF in Unit II, but mainly broken fragments were recovered, except for a small in situ chert fragment at 159.6 m CSF in interval 320-U1336B-18H-4, 106 cm. More abundant chert layers are common in Unit III.

Biostratigraphy

At Site U1336 we recovered a 300 m thick sequence of middle Miocene to lower Oligocene nannofossil ooze and chalk with thin chert layers toward the base. Calcareous nannofossils are present throughout the succession, and there appears to be a complete sequence of nannofossil zones from Zone NN6 (middle Miocene) through Zone NP22 (lower Oligocene), except for Zone NN3, which could not be resolved. Radiolarians are present in the upper half of the section only, and Zones RN6–RP22 are present. Similarly, diatoms are only found in the upper cores and are poorly preserved. Planktonic foraminifers are present throughout the succession, and Zones N12 (Subzone M9b)–O1 are recognized. Planktonic foraminifers are abundant and moderately well preserved in the Miocene but less well preserved in the Oligocene. No preservational changes were associated with the sediment color shift from brown and very pale brown to light greenish gray. Ostracodes were occasionally observed in samples. The nannofossil, foraminifer, radiolarian, and diatom datums and zonal determinations agree well, and an integrated calcareous and siliceous microfossil biozonation is shown in Figure **F10.** An age-depth plot including biostratigraphic and paleomagnetic datums is shown in Figure **F11.** Benthic foraminifers are present throughout the section and indicate lower bathyal to abyssal paleodepths.

Calcareous nannofossils

Calcareous nannofossil biostratigraphy is based on analysis of core catcher and core section samples from both holes. Depth positions (CSF) and age estimates of biostratigraphic marker events are presented in Table **T3.** Nannofossils are abundant and

moderately well preserved in the Miocene with intervals of poor preservation. Preservation is poor to moderate through most of the Oligocene.

The uppermost sample investigated (Sample 320-U1336A-1H-1, 110 cm) contains *Coronocyclus nitescens* and *Calcidiscus premacintyrei* without *Sphenolithus heteromorphus*, indicating a Zone NN6 age. Sample 320-U1336B-1H-CC lacks *C. nitescens* and *C. premacintyrei*. The top common occurrence of *Cyclicargolithus floridanus* (lowermost Zone NN6) is recognized in Sample 320-U1336A-2H-6, 80 cm, just above the top *S. hetermorphus* (base of Zone NN6) in Sample 320-U1336A-3H-2, 90 cm. In Hole U1336B, both events occur within Core 320-U1336B-3H. Nannofossil Zones NN4 and NN5 cannot be differentiated in this succession because of the absence of the zonal marker *Helicosphaera ampliaperta*; however, the presence of *Discoaster petaliformis* between Samples 320-U1336A-3H-4, 90 cm, and 5H-4, 64 cm, indicates a position in upper Zones NN4 to NN5 (Young, 1999; Raffi et al., 2006). The base of *D. petaliformis* has been calibrated at 15.70 Ma at ODP Sites 925 and 926 (as *Discoaster signus* in Raffi et al., 2006). This event was observed in Sample 320-U1336A-5H-4, 64 cm. The intra–Zone NN4 datum top common *Discoaster deflandrei* occurs in Sample 320-U1336A-4H-4, 90 cm, at a level that appears to be too high in comparison with surrounding biostratigraphic datums. This may be due to difficulties in distinguishing *D. deflandrei* from *Discoaster exilis* in material where discoaster identification is impaired by relatively poor preservation. In Hole U1336B, the top common datum of *D. deflandrei* is quite distinct because of the lower sample resolution used; it occurs within Core 320-U1336B-5H.

The base of *S. heteromorphus* occurs in Sample 320-U1336A-7H-2, 50 cm, together with frequent *Sphenolithus belemnos* in Hole U1336A, and in Core 320-U1336B-7H. Zone NN3 is defined by the extinctions of *S. belemnos* (top) and *Triquetrorhabdulus carinatus* (bottom). As these events are only 1.5 m apart (i.e., in adjacent samples), this suggests that Zone NN3 is missing or confined to a condensed interval between Samples 320-U1336A-7H-2, 50 cm, and 7H-3, 53 cm. Alternatively, the ranges of one or both of these taxa may be modified in the equatorial Pacific Ocean.

The intra–Zone NN2 datums, base of *S. belemnos* and top acme of *T. carinatus* (Raffi et al., 2006) are recognized in Samples 320-U1336A-8H-CC and 13H-CC, respectively. The lowermost occurrence of *Discoaster druggii* was observed in Samples 320-U1336A-14H-CC and 320-U1336B-14H-CC. Its rare and discontinuous distribution makes it difficult to exactly place the Zone NN1/NN2 boundary. The base of *Sphenolithus disbelemnos* occurs in Sample 320-U1336A-15H-CC and Sample 320-U1336B-15H-1, 10 cm. The top and base of *S. delphix* occurs in Samples 320-U1336A-17H-4, 90 cm, and 17H-6, 90 cm, respectively, although the species is rare and difficult to distinguish in these relatively poorly preserved assemblages. In Hole U1336B, *S. delphix* occurs from Sample 320-U1336B 17H-1, 150 cm, to 17H-3, 149 cm. The extinction of this species occurs just prior to (<100 k.y.) the Oligocene/Miocene boundary.

The Oligocene succession is predominantly nannofossil chalk with abundant nannofossils but poor to moderate preservation. The top of Zone NP25 is recognized by the top of *Sphenolithus ciperoensis* in Sample 320-U1336A-20H-CC. The intra–Zone NP24 abundance crossover from *Triquetrorhabdulus longus* to *T. carinatus* is difficult to place because of the poor preservation of these nannolith taxa—especially calcitic overgrowth of the slender rodlike taxa *T. longus,* which makes it indistinct from the thicker *T. carinatus*—but our initial analysis places it between Samples 320-U1336A-20H-CC and 20H-5, 100 cm, close to the top of *S. ciperoensis* datum. As at Sites U1332–U1335, the top of *Cyclicargolithus abisectus* was picked at this site in Sample 320-U1336A-19H-6, 70 cm, at a level consistent with the calibration for the top acme of *C. abisectus* (also Sites U1332–U1335). In Hole U1336B, this species was only observed in the lowermost core catcher sample (320-U1336B-20H-CC). The top of this species thus appears to have biostratigraphic potential in the paleoequatorial Pacific Ocean. The base of Zone NP25 is placed at the top of *Sphenolithus distentus* in Sample 320-U1336A-24X-3, 73 cm, and the base of Zone NP24 at the base of *S. ciperoensis* in Sample 320-U1336A-24X-5, 53 cm. The first appearance of *S. distentus* occurs within Zone NP23, in Sample 320-U1336A-29X-3, 40 cm. The top of *Reticulofenestra umbilicus* occurs in Sample 320-U1336A-35X-1, 34 cm, at the base of the sedimentary succession marking the base of Zone NP23.

Radiolarians

Radiolarian stratigraphy at Site U1336 (Table **T4**) spans the interval from just above the Zone RN6/RN5 boundary (middle Miocene) to the upper part of Zone RP22 (upper Oligocene). Below this level the sediments are barren of radiolarians. Above this level assemblages tend to have good to moderate preservation, with intermittent intervals of good preservation in Zones RN3 and RN4 (lower to middle Miocene). Species abundance and preservation are shown in Tables **T5** and **T6.** One of the unusual aspects of this site was the recovery of well-preserved upper middle Miocene sediments practically at the seafloor. There is no sign of younger sedimentary material and only

minor reworking of older microfossils into the sediments of Cores 320-U1336A-1H and 2H. Most of the other sites drilled in the region a few degrees north of the Pacific Equator encounter a layer of barren clay or radiolarian clay of variable thickness at the sediment surface. This clay usually contains radiolarian microfossils of widely ranging ages. The sediment surface at Site U1336 appears swept clean.

The downsection decrease in preservation and ultimate disappearance of the radiolarians below Core 320-U1336A-19H appears to be associated with dissolution and reprecipitation of the biogenic silica as intergranular cement and chert. It has been proposed that the dissolution of biogenic silica is the source of silica forming porcellinite and chert, and on crust <65 Ma in age, almost all cherts in the Pacific lie <150 m above basement (Moore, 2008b). Chert encountered at this site (see **"Lithostratigraphy"**) fits within these criteria. What is unusual about silica dissolution at this site is that it extends so far up into the section. Normally the silica-free zone (the zone of the sediments at the base of a sedimentary section that is devoid of siliceous microfossils) extends only ≤40 m above the basement in Pacific sediments (Moore, 2008a). Here the silica-free zone extends >120 m above basement, something that is usually seen only in sites on the older crust of the western Pacific. Moore (2008a, 2008b) proposes that the dissolution of the silica in basal sedimentary sections is associated with the circulation of warm hydrothermal waters in the upper oceanic crust that extends into the lower sediments when they are cut by permeable fractures and faults. Such small-offset faults appear to be present in the section near this site (Fig. **F2**). These faults, combined with possible higher heat flow so close to a major fracture zone (located 10 km south of the site), may have aided in a much more pervasive dissolution of the biogenic silica in the basal sediments at Site U1336.

The topmost part of the section corresponds to the lowest part of Zone RN6 (uppermost middle Miocene) that is based on the presence of *Diarutus pettersoni* and *Dorcadospyris alata* (Samples 320-U1366A-1H-4, 104–106 cm, and 320-U1336B-1H-CC). Only core catcher samples were investigated in Hole U1336B. Zone RN5 is well distinguished by four datum events (Table **T4**). The Zone RN5/RN4 boundary occurs between Samples 320-U1336A-4H-2, 105–107 cm, and 4H-4, 105–107 cm, and in Core 320-U1336B-5H. This boundary is defined by the evolutionary transition from *Dorcadospyris dentata* to *D. alata*.

In Hole U1336A, the Zone RN4/ RN3 boundary was recognized by the base of *Calocycletta (Calocyclissima) costata* between Samples 320-U1336A-6H-4, 105–107 cm, and 6H-CC. The base of Zone RN3 is distinguished by the evolutionary appearance of *Stychocorys wolffii* between Samples 320-U1336A-8H-2, 105–107 cm, and 8H-4, 105–107 cm. The top of Zone RN1, defined by the top of *Theocyrtis anossa*, occurs between Samples 320-U1336A-12H-2, 105–107 cm, and 12H-4, 105–107 cm, and in Core 320-U1336B-14H. The base of Zone RN1 is determined by the base of *Cyrtocapsella tetrapera* between Sample 320-U1336A-15H-4, 105–107 cm, and Sample 320-U1336A-15H-CC and in Core 320-U1336B-15H. The lower sections contain *Lychnocanomma elongata*, indicating Zone RP22. Eight radiolarian events are observed within Zone RP22 in Hole U1336A.

The Oligocene/Miocene boundary occurs between Sample 320-U1336A-16H-CC and Sample 320-U1336A-17H-4, 105–107 cm, as suggested by the presence of *Dorcadospyris cyclacantha,* which has a short stratigraphic range across the Oligocene/Miocene boundary. It appears at 23.29 Ma and disappears just after the Oligocene/Miocene boundary at 22.98 Ma. In Hole U1336B, *D. cyclacantha* was observed only in Sample U1336B-17H-CC.

Diatoms

The diatom stratigraphy in Hole U1336B (Table **T7**) spans the interval from just above the *C. peplum* zone (middle Miocene) in Core 320-U1336B-1H to the lowermost part of *C. nicobarica* zone (upper lower Miocene) in Sample 320-U1336B-7H-CC. Below Sample 320-U1336B-7H-CC, the sediments are barren of diatoms. Above this level the valves tend to be mostly poorly preserved. Sample 320-U1336B-1H-CC contains the highest diversity with *C. pulchellus* as dominant component, accompanied by *C. jouseana,* and *T. yabei*. Fragments of the large centric diatoms *Ethmodiscus* are present in the upper part of Hole U1336B.

Planktonic foraminifers

A high-resolution planktonic foraminifer biostratigraphy was generated at Site U1336 using core catchers and supplementary additional samples, usually two per core. The sedimentary succession at this site ranges from Subzone M9b (Zone N12) (middle Miocene) to Zones O1–O2 (lower Oligocene) (Fig. **F10;** Table **T8**), which agrees well with calcareous nannofossil and radiolarian biostratigraphy (Fig. **F11**). Species abundance and preservation are shown in Tables **T9** and **T10.** The preservation and abundance of planktonic foraminifers is moderate in the upper part of the succession and deteriorates to poor downcore with extensive infilling and encrustation. Preservation of planktonic foraminifer tests is inferior to nearby equatorial Pacific Ocean sites drilled during DSDP Leg 9 (Jenkins and Orr, 1972). Planktonic

foraminifer tests can account for >70% of the total residue in each sample, but some intervals are characterized by lower abundance and assemblages are dominated by dissolution-resistant forms (i.e., Samples 320-U1336A-6H-4, 38–40 cm, and 320-U1336B-17H-3, 80–82 cm); in such cases identification of datum events is difficult. As a result of the extensive infilling we applied a very broad definition to *Globoquadrina venezuelana*, which is dominant to abundant in most samples. Preservation is poor in the lowest part of the sedimentary succession consisting of nannofossil chalk. Planktonic foraminifers are encrusted with calcite in this section and it is difficult to identify and/or estimate the percentage of planktonic foraminifers in each sample because the washing process failed to successfully extract all the foraminifers from the chalk.

A continuous record of the middle to lower Miocene is observed from Subzone M9b (Zone N12) to Subzone M1a. Subzone M9a through Zone M8 (Zone N12) are distinguished on the basis of several datum events within the *Globorotalia (Fohsella) fohsi* group (Table **T8**). The base of *Globorotalia (Fohsella) fohsi robusta* occurred in Samples 320-U1336A-1H-3, 38–40 cm, and 320-U1336B-1H-CC. The Zone M7/M8 (N11/N12) boundary is defined by the base of *G. (Fohsella) fohsi* sensu lato in Samples 320-U1336A-2H-CC and 320-U1336B-2H-CC. The base of Zone N11 is indicated by the base of *Globorotalia (Fohsella) "praefohsi"* in Samples 320-U1336A-3H-5, 38–40 cm, and 320-U1336B-3H-CC.

It was not possible to fully constrain the boundary between Zones M6–M7 (N9–N10) because the base of *Globorotalia (Fohsella) peripheroacuta* (14.24 Ma) on which it is defined appears to occur deeper than the base of *Orbulina* spp. (14.74 Ma), which separates Zones M6 and M5. Higher resolution samples in Cores 320-U1336A-3H and 4H may be needed in order to fully resolve these zonal boundaries. However, Zone M5 is identified between the base of *Orbulina* spp. in Samples 320-U1336A-3H-CC and 320-U1336B-3H-CC and the base of *Praeorbulina sicana* in Samples 320-U1336A-6H-2, 38–40 cm, and 320-U1336B-6H-CC. The rarity of *Catapsydrax dissimilis* in Hole U1336A made it difficult to distinguish the Zone M3/M4 boundary; however, in Hole U1336B the top of *C. dissimilis* was constrained to the interval between Samples 320-U1336B-7H-CC and 8H-CC. It was not possible to identify the boundary between Zones M3 and M2 because of the absence of *Globigerinatella insueta*. The top of *P. kugleri* defines the top of Subzone M1b and was found between Samples 320-U1336A-10H-CC and 11H-2, 30–32 cm. The base of Subzone M1b was between Samples 320-U1336A-15H-2, 38–40 cm, and 15H-4, 38–40 cm, using the base of *Globoquadrina dehiscens*. The co-occurrence of *P. kugleri, Paragloborotalia pseudokugleri,* and *G. dehiscens* in Sample 320-U1336A-11H-2, 38–40 cm, and Samples 320-U1336B-12-CC, 13-CC, and 14-CC indicate Subzone M1b.

The base of Zone M1 is marked by the base of *P. kugleri* and is employed to approximate the Oligocene/Miocene boundary (Steininger et al., 1997). It occurs between Samples 320-U1336A-16H-CC and 17H-2, 38–40 cm, and between Samples 320-U1336B-16H-1, 52–54 cm, and 17H-3, 80–82 cm. Only specimens with a subacute periphery and more than six chambers in the final whorl were considered to be *P. kugleri* (see Pearson and Wade, 2009, for discussion). Sample 320-U1336B-16H-CC contained many reworked specimens of early and middle Oligocene age and could not be used to provide further constraint on the base of Zone M1.

In the upper part of Zone O6, robust dentoglobigerinids and paragloborotaliids are more abundant. The upper part of Zone O6 is indicated by the presence of *P. pseudokugleri*. The 150–250 µm size fraction contains assemblages abundant and diverse in paragloborotaliids, but they are rare in the >250 µm size fraction. This is consistent with the size change in paragloborotaliids documented at Site 1218 (Wade et al., 2007). Frequent specimens of *Dentoglobigerina galavisi, Dentoglobigerina tripartita, G. venezuelana,* and *Paragloborotalia nana* are found in lowermost part of Zone O6. The top of *Paragloborotalia opima* marks the top of Zone O5, and whereas at previous sites it was not observed, the lower boundary of this zone is fully identified in Hole U1336A by the top of the common occurrence of *Chiloguembelina cubensis* (28.0 Ma) that occurs between Samples 320-U1336A-25X-2, 45–47 cm, and 25X-CC. The base of *Globigerina angulisuturalis* defines the base of Zone O4 and occurs between Samples 320-U1336A-27X-CC and 28X-2, 20–22 cm. Zone O3 is partially distinguished by the co-occurrence of *Subbotina angiporoides, Turborotalia ampliapertura,* and *P. opima* (i.e., Sample 320-U1336A-29X-CC). Zones O1 and O2 at the base of the succession are not fully constrained, although the lack of *P. opima* and the presence of *P. nana, C. dissimilis, Dentoglobigerina* spp., and *Turborotalia ampliapertura* indicate that the lower Oligocene is preserved. Further age control is difficult because of the poor preservation of the planktonic foraminifers in the deeper part of the section.

Benthic foraminifers

Benthic foraminifers were examined in core catcher samples from Holes U1336A and U1336B. The occurrence of benthic foraminifers at this site is shown in Tables **T11** and **T12.** The sample intervals

from Samples 320-U1336A-1H-CC through 35X-CC (8.22–299.61 m CSF) and 320-U1336B-1H-CC through 20H-CC (1.68–174.01 m CSF) contain benthic foraminifers continuously, although abundances are low overall. Samples 320-U1336A-34X-CC (294.10 m CSF), within a chert interval, and 6H-CC (49.87 m CSF), within a radiolarian ooze, contain rare benthic foraminifers. Benthic to planktonic foraminifer ratios are ~1%–2% in Samples 320-U1336B-1H-CC through 16H-CC (8.22–136.86 m CSF), except in Sample 320-U1336B-6H-CC (49.87 m CSF), where the benthic to planktonic foraminifer ratio rises to 25%. In Samples 320-U1336B-16H-CC through 20H-CC (136.81–174.01 m CSF), benthic to planktonic foraminifer ratios increase to 5%–10%. Fish teeth and ostracodes are present in most of the core catcher samples examined. Benthic foraminifer tests are moderately well preserved in the upper part of Site U1336 (Samples 320-U1336A-1H-CC through 19H-CC, 8.22–170.63 m CSF; and 320-U1336B-1H-CC through 20H-CC, 1.68–174.01 m CSF), but preservation deteriorates and tests are frequently abraded and infilled below this level.

The Oligocene to middle Miocene benthic foraminifer assemblage at Site U1336 is relatively diverse and indicates oligotrophic, lower bathyal to abyssal paleodepths. Characteristic taxa are *Cibicidoides mundulus, Globocassidulina subglobosa*, *Gyroidinoides* spp., *Laticarinina pauperata, Nuttallides umbonifer*, *Oridorsalis umbonatus*, *Pullenia bulloides*, and *Siphonodosaria* spp. *Brizalina pusilla* is abundant (39%) in Sample 320-U1336A-30X-CC (264.48 m CSF). The benthic foraminifer assemblage at Site U1336 closely resembles Oligocene and early Miocene assemblages previously described from the eastern equatorial Pacific Ocean (ODP Site 573, Thomas, 1985; ODP Sites 1218 and 1219, Takata and Nomura, 2005). The assemblage from Site U1336 also shows close affinity to Oligocene and middle Miocene assemblages from Sites U1332–U1334, although *N. umbonifer* occurs less frequently at Site U1336 than at these other sites.

Paleomagnetism

We conducted a paleomagnetic study of archive-half sections of 21 APC cores from Hole U1336A and 20 APC cores from Hole U1336B with the primary objective of determining the magnetostratigraphy of the site and providing chronostratigraphic constraints. To accomplish this, we measured the NRM of each section at either 5 or 2.5 cm intervals (depending on time availability) before and after demagnetization at a peak AF of 20 mT. AF demagnetization at a peak field of 10 mT was also carried out for most Hole U1336B core sections. We processed the paleomagnetic data by removing measurements made within 5 cm (or 7.5 cm when measured at 2.5 cm intervals) of section ends and data from disturbed intervals (Table **T13**).

The FlexIt core orientation tool was not deployed at the site because the conclusion, derived from Sites U1331 and U1332, that the output of the tool was erratic and inconsistent with expected remanence directions for sediments of this age from this location (we expected Neogene declinations to lie close to north for the normal polarity and close to south for the reversed polarity). The remanence inclination is close to zero, as expected for a site located close to the paleoequator, making inclination not diagnostic of polarity. The lack of core orientation gave us an unwelcome degree of freedom in the assignment of polarity, as each core can be rotated in azimuth through 180° to change the sign of any polarity zone. Azimuthal core orientation had to be determined solely by correlating distinct reversals patterns as recorded by the paleomagnetic declination with the GPTS (see **"Paleomagnetism"** in the "Methods" chapter and **"Paleomagnetism"** in the "Site U1331" chapter). Although this process is aided by biostratigraphic age constraints, which limit the range of possible correlations with the GPTS (see **"Biostratigraphy"**), it is the polarity zone pattern and its fit to the GPTS that provided the basis for the match. Once we had identified a possible reversal pattern, data were oriented so that normal and reversed polarity zones had declinations of ~0° and ~180°, respectively.

We measured magnetic susceptibilities and masses of 138 discrete samples. Volumes of samples were recalculated using sediment MAD data (see **"Physical properties"**) and the magnetic susceptibilities were subsequently normalized using recalculated volumes and masses. Of these samples, 20 were stepwise AF demagnetized and measured at 5 mT steps to a peak field of 40 mT and 10 mT steps to 60 mT.

Results

Downhole paleomagnetic data for Holes U1336A and U1336B are presented in Figures **F12, F13, F14, F15,** and **F16.** Measurements of NRM above ~80 m CSF in Holes U1336A and U1336B indicate moderate magnetization intensities (~1 × 10^{-3} A/m) with a patchy but generally weak VRM or isothermal remanent magnetization IRM drilling overprint (see **"Paleomagnetism"** in the "Site U1331" chapter). Polarity reversal sequences are clearly recognized in general. Demagnetization data from discrete samples above ~80 m CSF (Fig. **F17;** Table **T14**) indicate that the characteristic remanent magnetization (ChRM) of the sediments is identified at the 10–20 mT de-

magnetization steps. Principal component analysis directions of the ChRM components above ~80 m CSF agree with measurements of coeval intervals from the archive halves (Fig. F12), indicating that the magnetic directions after 20 mT demagnetization provide a reliable indicator of the ChRM of the sediments.

Below ~80 m CSF, a zone of diagenetic alteration involving dissolution of remanence carriers (see "Paleomagnetism" in the "Site U1334" chapter) reduces remanent intensities after 20 mT AF demagnetization to values close to magnetometer noise level in the shipboard environment (~2 × 10^{-5} A/m). In this zone, sediment magnetizations have been partly or entirely overprinted during the coring process and remanent inclinations are sometimes steeply negative after AF demagnetization at a peak field of 20 mT. At ~130–140 m CSF (Cores 320-U1336A-15H through 16H and 320-U1336B-15H) and below ~160 m CSF (Cores 320-U1336A-19H through 21H and 320-U1336B-18H through 20H), polarity reversals are apparently present but the inclinations are steep (as much as 80°), indicating that the drilling overprint has not been effectively removed during shipboard demagnetization.

Magnetostratigraphy

In the upper ~80 m CSF, correlation of polarity zones with the GPTS is guided by the biostratigraphic framework of key nannofossil and foraminifer datums from core catcher and additional samples (see "Biostratigraphy") but is based largely on the polarity zone pattern fit to the GPTS. Reversal depths are provided in Table T15 and polarity interpretation is shown in Figure F16. At the top of Holes U1336A and U1336B, polarity assignments are constrained by the tops of nannofossils *C. nitescens* and *C. premacintyrei,* which have ages of 12.12 Ma and 12.45 Ma, respectively. We correlate the uppermost reversed polarity zone to the base of Chron C5r of the GPTS (Fig. F16). Cores 320-U1336A-3H and 320-U1336B-4H contain a ~10 m thick normal polarity zone, which we tentatively correlate to normal polarity Chrons C5ACn and C5ADn; Chron C5ACr was not identified. The base of Core 320-U1336A-4H has an age of 15.7 Ma (see "Biostratigraphy"); therefore, we correlate the reversal sequence within Cores 320-U1336A-4H, 320-U1336B-4H, and 5H with Chrons C5ADr and C5Bn (Fig. F16). The top of the polarity zone corresponding to Chron C5Br occurs at the base of Core 320-U1336-4H and top of Core 320-U1336B-5H, with the base of the polarity zone at the base of Core 320-U1336A-5H and at the top of Core 320-U1336B-6H. Below the polarity zone corresponding to Chron C5Br, our correlation with the GPTS is relatively unambiguous through Core 320-U1336A-9H, which contains the upper portions of Chron C6n. Below ~90 m CCSF-A the magnetization intensity of the sediments decreases below analytical noise level; however, below ~160 m CSF a reversal pattern is discernible (Figs. F13, F15) but difficult to correlate with GPTS in the absence of core orientation data.

Geochemistry

Sediment gases sampling and analysis

Headspace gas samples were taken at a frequency of one sample per core in Hole U1336A as part of the routine environmental protection and safety monitoring program. All headspace sample analyses resulted in nondetectable levels of methane (C_1; <2 ppmv), with no higher hydrocarbons.

Interstitial water sampling and chemistry

Twenty-two interstitial water samples were collected from Hole U1336B (Table T16) in the APC-cored interval using the whole-round squeezing method. Chemical constituents were determined according to the procedures outlined in "Geochemistry" in the "Methods" chapter. Chlorinity varies from ~555 mM in the shallowest sample to ~565–570 mM in deeper samples (Fig. F18). Chlorinity values have a distinct increase from ~555 to ~570 mM in the uppermost 40 m CSF, potentially reflecting the change from the more saline ocean at the Last Glacial Maximum to the present (Adkins and Schrag, 2003). Alkalinity is relatively constant at >2.5 mM in the upper 110 m CSF, with a pronounced decline to 1 mM by 170 m CSF. Sulfate concentrations decrease with depth to values of 22 mM. Dissolved phosphate concentrations are ~5 µM at ~9 m CSF, decreasing to ~1 µM by ~15 m CSF. Dissolved manganese has a broad peak to >5 µM from ~25 to 120 m CSF and then returns to ~1.8 µM in the deepest four samples. Below 100 m CSF, dissolved iron increases coincident with manganese decline, with concentrations reaching >10 µM below 130 m CSF.

Because of the relatively high sulfate concentrations, dissolved Ba concentrations are below detection (0.5 µM). Concentrations of dissolved silicate increase with depth from <400 to 800 µM.

Calcium and magnesium concentrations increase and decrease with depth, respectively, with calcium values from 10 to 29 mM and magnesium values from 50 to 28 mM (Fig. F18). This is indicative of diffusional control of Mg and Ca profiles between seawater at the top and the reaction zone of fluid and basalt in the underlying basement (e.g., Gieskes, 1981).

Lithium concentrations decrease from ~26 µM at the surface to <10 µM below 130 m CSF, and potassium concentrations decrease with depth to values as low as 8 mM. Strontium concentrations increase from near-seawater values in the shallowest sample to >400 µM in the deepest samples, the highest values seen during this expedition. Boron concentrations range between 440 and 490 µM, showing a slight decrease downcore.

Bulk sediment geochemistry

Calcium carbonate ($CaCO_3$) and inorganic carbon concentrations were determined on sediment samples from Hole U1336A (Table **T17;** Fig. **F19**), and calcium carbonate, inorganic carbon, and total organic carbon (TOC) concentrations were determined on 39 sediment samples from Hole U1336B. TOC was not run on samples from Hole U1336A because samples from Hole U1336A were accidently sent to the Gulf Coast Repository during the Expedition 320/321 port call (Table **T17;** Fig. **F19**). Calcium carbonate concentrations ranged between 48 and 96 wt%. In the uppermost ~90 m CSF, $CaCO_3$ concentrations vary between 48 and 95 wt%, with a distinct low at 48 m CSF. Below 90 m CSF, $CaCO_3$ concentrations are consistently high (77 to 96 wt%). Variations in $CaCO_3$ concentrations correspond to lithostratigraphic observations (see **"Lithostratigraphy"**). TOC content is generally low throughout the sediment column, ranging between 0.05 and 0.08 wt%; however, relatively high TOC concentrations (0.10 to 0.30 wt%) are observed at 0.71 and 51.52 m CSF and in the interval between 108.51 and 135.22 m CSF.

In Hole U1336B, bulk sediment samples were analyzed at a frequency of one per core for silicon, aluminum, iron, manganese, magnesium, calcium, sodium, potassium, titanium, phosphorus, barium, copper, chromium, scandium, strontium, vanadium, yttrium, and zirconium (Table **T18**). Concentrations of noncarbonate components like SiO_2, Al_2O_3, and Fe_2O_3 display similar patterns, with the highest values occurring in the uppermost sediments and decreasing to a minimum between 100 and 140 m CSF before a small peak at the base of the section. Ca (carbonate) content displays the opposite pattern, indicating the important role of carbonate dilution in determining the bulk sediment composition at this site.

Physical properties

Physical properties at Site U1336 were measured on whole cores, split cores, and discrete samples. WRMSL measurements (GRA bulk density, magnetic susceptibility, and *P*-wave velocity), thermal conductivity, and NGR measurements comprised the whole-core measurements. For Hole U1336A, compressional wave velocity measurements on split cores and MAD analyses on discrete core samples were made at a frequency of one per undisturbed section in Cores 320-U1336A-1H through 35X. The SHMSL, configured with the Ocean Optics sensor, was used to measure spectral reflectance on archive-half sections. Resolution was reduced from 2.5 to 5 cm for Hole U1336A cores as a result of time constraints.

Hole U1336B cores were analyzed by the WRMSL and NGR detector during Expedition 320 and placed directly into cold storage unsplit. During Expedition 321, thermal conductivity measurements were made on whole-round sections. After the cores were split, MAD and velocity measurements were made on samples from every other section. Sediment reflectance was measured on all archive-half cores with the SHMSL at a resolution of 2.5 cm.

Density and porosity

Two methods were used to determine bulk sediment properties at Site U1336, GRA for the bulk density of whole-round sections (Fig. **F20**), and MAD analyses for wet bulk density, dry bulk density, grain density, water content, and porosity of discrete samples (Fig. **F21;** Table **T19**). MAD and GRA bulk density measurements display the same trends and are similar in absolute values through the entire section (Fig. **F21B**). Cross-plots of wet bulk density and dry bulk density versus interpolated GRA bulk density (Fig. **F22**) show excellent correlation between MAD and GRA density data.

Generally, wet bulk density corresponds with changes in lithology (Fig. **F21B**). Wet bulk density is lowest in lithologic Unit I (1.4–1.7 g/cm^3) and reflects variations in the amount of minor lithologic components (clay, radiolarians, and diatoms) within the major lithology of nannofossil ooze. In Unit II, bulk density increases slightly and becomes more uniform (~1.7 g/cm^3). In Unit III, which also corresponds to the XCB-cored interval, bulk density becomes highly irregular, ranging from lower density at the top of cores to higher density at the base of cores. This pattern reflects drilling disturbance at the top of XCB cores. The average wet bulk density for the XCB portion can be determined from the discrete MAD analyses that were cut directly from undisturbed intervals. Wet bulk density values in Unit III average 1.9 g/cm^3, reflecting increased compaction of the sediments at depths >180 m CSF.

Variations in grain density (ρ_S) in Hole U1336A generally match changes in lithology (Fig. **F21C**). At the top of Hole U1336A grain density is 3.0 g/cm^3 and decreases rapidly, reflecting clay-rich sediments that grade rapidly into nannofossil ooze. Grain density

averages 2.7 g/cm³ for most of the section, varying from 2.6 to 2.9 g/cm³. This average and range reflect the dominance of carbonate material (calcite; ρ_S = 2.70 g/cm³) at Site U1336. Grain densities determined for Hole U1336B average ~0.1 g/cm³ less than grain densities determined for the same interval in Hole U1336A. The lower density of Hole U1336B material most likely reflects a larger sample volume and reduction of measurement error and error associated with mass and volume values derived from the assumed salt content of the pore fluid.

Porosity and water content vary inversely with wet bulk density (Fig. **F21A**). The highest porosities occur in lithologic Unit I, varying from 65% to 80%. At the boundary between Units I and II porosity begins to decrease gradually toward the base of Unit II, where values average from 55% to 60% at ~184 m CSF. A shift to lower porosity accompanies the shift to higher density in Unit III. Porosity in this interval ranges from 45% to 60%.

Magnetic susceptibility

Whole-round magnetic susceptibility measurements correlate well with the major differences in lithology at Site U1336 (Fig. **F20**). Magnetic susceptibility values are highest in lithologic Unit I and show high amplitude and high frequency variations from 5×10^{-5} to 30×10^{-5} SI. Across the boundary between Units I and II, susceptibility decreases from ~10×10^{-5} to near 0 SI and remains low to the bottom of Hole U1336A. There is a slight increase in the amplitude and frequency of the variation of magnetic susceptibility in Unit III.

Compressional wave velocity

Shipboard results

Velocity measurements made with the *P*-wave logger (PWL) on whole-round sections and discrete measurements from split cores follow similar trends of increasing velocity with increasing depth as a result of increased compaction (Fig. **F23**). Discrete velocity measurements along the *x*-axis (contact probe) follow the trend of the PWL results in Hole U1336A (Fig. **F23;** Table **T20**) but exceed the PWL velocities on average by 20 m/s. An offset of 40 m/s is present in the first 25 m of the section in Hole U1336A. The cores in this interval appeared dry and fractured, which may account for the disparity. The *x*-axis velocities determined in Hole U1336B average 50 m/s higher than those over the comparable interval in Hole U1336A. Differences in the pressure applied in making contact between the sediment and transducers may account for this difference. Velocity measurements in the *y*- and *z*-axis directions (insertion probe) generally exceed the PWL velocity by 10 m/s. Differences between the whole-core and split-core measurements possibly reflect the presence of water in the space between the core liner and sediment in the whole cores, sediment fracturing as the *y*- and *z*-axis transducers penetrate the split core, and slight compaction of the sediment in the contact probe technique. No *y*- or *z*-axis velocity measurements were made below ~150 m CSF, as the XCB-cored sediment was hard and fractured easily with insertion of the transducers.

Velocities are between 1480 and 1500 m/s in lithologic Unit I and between 1480 and 1530 m/s in Unit II. At ~176 m CSF, velocities begin to increase rapidly into Unit III, from 1530 to ~1960 m/s at 208 m CSF. The remainder of Unit III shows high frequency and high amplitude variation, averaging 1910 m/s in this lithified and highly biscuited interval.

Postcruise correction

The *x*-direction velocities for Hole U1336A were determined using a liner thickness of 3.2 mm, the correction that was initially applied at Site U1334 (see **"Physical properties"** in the "Site U1334" chapter). This correction was not applied to velocities determined for Hole U1336B. These velocities were determined using a core liner thickness of 2.7 mm for the liner correction. During the analysis of Hole U1337A cores, it was determined that high *x*-direction velocities do not result from thicker than expected core liner but instead are the result of using an incorrect value for the system delay associated with the contact probe (see **"Physical properties"** in the "Site U1337" chapter). Critical parameters used in this correction are system delay = 19.811 µs, liner thickness = 2.7 mm, and liner delay = 1.26 µs. During the analysis of Hole U1337A cores, it also was determined that consistently low PWL velocities required the addition of a constant value that would produce a reasonable velocity of water (~1495 m/s) for the quality assurance/quality control liner (see **"Physical properties"** in the "Site U1337" chapter). These corrections have not been applied to the velocity data presented in this chapter.

Natural gamma radiation

NGR was measured in both holes at Site U1336 (Fig. **F20**). The highest counts per second are present at the seafloor (~56 cps). The NGR signal rapidly decreases with depth in lithologic Unit I, with small variations centered at 5 cps. At the boundary between Units I and II, NGR values decrease to ~2 cps. NGR is uniform at ~2 cps through Units II and III.

Thermal conductivity

Thermal conductivity was measured on the third section of each core from Hole U1336A and the fourth section of each core from Hole U1336B (Table T21). Thermal conductivity increases slightly with depth at the site (Fig. F24) and is inversely related to porosity (Fig. F25). Lower conductivity occurs with higher porosity as increased interstitial spacing attenuates the applied current from the probe. Overall, thermal conductivity decreases from 1.2 to 1 W/(m·K) through lithologic Unit I, with a minimum conductivity of 0.91 W/(m·K) at 31 m CSF. Through Units II and III, thermal conductivity increases from 1 to 1.4 W/(m·K), whereas porosity decreases over a similarly gradual trend of 75% to 50% (Fig. F21A). Below 183 m CSF, thermal conductivity decreases in XCB-cored sediment, possibly as a result of increased fractures and occurrence of sediment biscuits. Thermal conductivity values were not recorded deeper than 189 m CSF because the sediment was too hard to insert the probe.

Reflectance spectroscopy

Spectral reflectance was measured on the archive-half sections from Holes U1336A and U1336B using the SHMSL (Fig. F26). Variations in luminance (L*) correspond to pronounced lithologic changes. In lithologic Unit I, L* values are lowest (50–80) and display high-amplitude variations, reflecting changes in minor lithologic components. Values in Unit II are higher and more uniform, reflecting the relatively pure nannofossil ooze of this unit. Luminance values are slightly lower and more variable in Unit III. Variations in a* (blue–yellow) and b* (green–red) also reflect changes in lithology, with higher and more variable values in Unit I compared to Unit II. Both a* and b* exhibit a steplike decrease at 92 m CSF that is associated with a sharp change in the color of the nannofossil ooze from pale yellow to greenish gray.

Stratigraphic correlation and composite section

STMSL data were collected at 5 cm intervals from Hole U1336B and compared to WRMSL data obtained at 2.5 cm resolution from Hole U1336A during Expedition 320. In this way, drilling was monitored in Hole U1336B in real time to maximize the opportunity for the recovery and construction of a stratigraphically complete composite section. Cores from Hole U1336B were also measured on the WRMSL during Expedition 320 and left onboard as whole-round sections to be split and described during Expedition 321. After the cores were split and described a composite section was constructed.

Magnetic susceptibility and GRA density proved most useful for correlating between holes at Site U1336 (Figs. F27, F28). Features in the magnetic susceptibility and GRA density are well aligned between Holes U1336A and U1336B to ~94 m CCSF-A. The correlation between the two holes is presented in Figures F27 and F28. Offsets and composite depths are listed in Table T22. Below ~94 m CCSF-A, the magnetic susceptibility signal drops to very low values but density data are good enough to sustain a correlation to interval 320-U1334B-14H-4, 122 cm. At this point (138.50 m CCSF-A) sediments recovered in both holes are disturbed. Core 320-U1336B-15H was appended to the bottom of the splice (Table T23). Near the bottom of Core 320-U1336B-18H the splice shifts to Core 320-U1336A-18H and continues to the base of the hole by appending Hole U1336A cores (Table T23). A preferred splice would have been to append Core 321-U1336A-15H just above the disturbed section at the base of Core 321-U1336B-14H. However, this was not allowed by Correlator software. The critical interval from Cores 320-U1336B-14H through 320-U1336A-18H is illustrated in Figure F29.

A growth factor of 1.13 is calculated by linear regression for the top ~94 m CCSF-A of Site U1336, indicating a 13% increase in CCSF-A relative to CSF depth (Fig. F30). We used this value to calculate CCSF-B depth presented in Table T22 to aid in the calculation of sedimentation and mass accumulation rates.

Sedimentation rates

All principal biostratigraphic datums and a set of 33 tentatively interpreted paleomagnetic reversals (restricted to the APC-cored sections) (Table T24; see also "Biostratigraphy" and "Paleomagnetism") were used in establishing age control (Fig. F11). Paleomagnetic reversals were used to calculate the average LSRs for the upper 74 m CCSF-B of the section at Site U1336, as depicted in Figure F11. Below 74 m CCSF-B, only biostratigraphic datums were used to calculate the average LSRs.

The LSR at Site U1336 decreases from 15 m/m.y. in the upper Oligocene to 12 m/m.y. in the lower Miocene and stays relatively constant at 9 m/m.y. in the remainder of the section (Fig. F11).

References

Adkins, J.F., and Schrag, D.P., 2003. Reconstructing Last Glacial Maximum bottom water salinities from deep-sea sediment pore fluid profiles. *Earth Planet Sci. Lett.,* 216:109–123. **doi:10.1016/S0012-821X(03)00502-8**

Amante, C., and Eakins, B.W., 2008. *ETOPO1 1 Arc-Minute Global Relief Model: Procedures, Data Sources and Analysis:* Washington, DC (DOC/NOAA/NESDIS/NGDC).

Billups, K., Pälike, H., Channell, J.E.T., Zachos, J.C., and Shackleton, N.J., 2004. Astronomic calibration of the late Oligocene through early Miocene geomagnetic polarity time scale. *Earth Planet. Sci. Lett.,* 224(1–2):33–44. **doi:10.1016/j.epsl.2004.05.004**

Cande, S.C., LaBrecque, J.L., Larson, R.L., Pitmann, W.C., III, Golovchenko, X., and Haxby, W.F., 1989. *Magnetic Lineations of the World's Ocean Basins.* AAPG Map Ser., 13.

Engebretson, D.C., Cox, A., and Gordon, R.G., 1985. *Relative Motions between Oceanic and Continental Plates in the Pacific Basin.* Spec. Pap.—Geol. Soc. Am., 206.

Gieskes, J.M., 1981. Deep-sea drilling interstitial water studies: implications for chemical alteration of the oceanic crust, Layers I and II. *In* Warme, J.E., Douglas, R.G., and Winterer, E.L. (Eds.), *The Deep Sea Drilling Project: A Decade of Progress*. Spec. Publ.—Soc. Econ. Paleontol. Mineral., 32:149–167.

Hays, J.D., et al., 1972. *Init. Repts. DSDP,* 9: Washington, DC (U.S. Govt. Printing Office). **doi:10.2973/dsdp.proc.9.1972**

Holbourn, A., Kuhnt, W., Schulz, M., and Erlenkeuser, H., 2005. Impacts of orbital forcing and atmospheric CO_2 on Miocene ice-sheet expansion. *Nature (London, U.K.),* 438(7067):483–487. **doi:10.1038/nature04123**

Jenkins, D.G., and Orr, W.N., 1972. Planktonic foraminiferal biostratigraphy of the eastern equatorial Pacific—DSDP Leg 9. *In* Hays, J.D., et al., *Init. Repts. DSDP,* 9: Washington, DC (U.S. Govt. Printing Office), 1059–1193. **doi:10.2973/dsdp.proc.9.125.1972**

Knappenberger, M., 2000. Sedimentation rates and Pacific plate motion calculated using seismic cross sections of the Neogene equatorial sediment bulge [M.Sc. thesis]. Boise State Univ., Idaho.

Koppers, A.A.P., Phipps Morgan, J., Morgan, J.W., and Staudigel, H., 2001. Testing the fixed hotspot hypothesis using $^{40}Ar/^{39}Ar$ age progressions along seamount trails. *Earth Planet. Sci. Lett.,* 185(3–4):237–252. **doi:10.1016/S0012-821X(00)00387-3**

Lyle, M., 2003. Neogene carbonate burial in the Pacific Ocean. *Paleoceanography,* 18(3):1059. **doi:10.1029/2002PA000777**

Lyle, M., Liberty, L., Moore, T.C., Jr., and Rea, D.K., 2002. Development of a seismic stratigraphy for the Paleogene sedimentary section, central tropical Pacific Ocean. *In* Lyle, M., Wilson, P.A., Janecek, T.R., et al., *Proc. ODP, Init. Repts.,* 199: College Station, TX (Ocean Drilling Program), 1–21. **doi:10.2973/odp.proc.ir.199.104.2002**

Lyle, M., Wilson, P.A., Janecek, T.R., et al., 2002. *Proc. ODP, Init. Repts.,* 199: College Station, TX (Ocean Drilling Program). **doi:10.2973/odp.proc.ir.199.2002**

Lyle, M.W., Pälike, H., Moore, T.C., Mitchell, N., and Backman, J., 2006. *Summary Report of R/V Roger Revelle Site Survey AMAT03 to the IODP Environmental Protection and Safety Panel (EPSP) in Support for Proposal IODP626:* Southampton, U.K. (Univ. Southampton). **http://eprints.soton.ac.uk/45921/**

Mayer, L.A., Shipley, T.H., Theyer, F., Wilkens, R.H., and Winterer, E.L., 1985. Seismic modeling and paleoceanography at Deep Sea Drilling Project Site 574. *In* Mayer, L., Theyer, F., Thomas, E., et al., *Init. Repts. DSDP,* 85: Washington, DC (U.S. Govt. Printing Office), 947–970. **doi:10.2973/dsdp.proc.85.132.1985**

Miller, K.G., Wright, J.D., and Fairbanks, R.G., 1991. Unlocking the ice house: Oligocene–Miocene oxygen isotopes, eustasy, and margin erosion. *J. Geophys. Res., [Solid Earth],* 96(B4):6829–6848. **doi:10.1029/90JB02015**

Moore, T.C., Jr., 2008a. Biogenic silica and chert in the Pacific Ocean. *Geology,* 36(12):975–978. **doi:10.1130/G25057A.1**

Moore, T.C., Jr., 2008b. Chert in the Pacific: biogenic silica and hydrothermal circulation. *Palaeogeogr., Palaeoclimatol., Palaeoecol.,* 261(1–2):87–99. **doi:10.1016/j.palaeo.2008.01.009**

Müller, R.D., Roest, W.R., Royer, J.-Y., Gahagan, L.M., and Sclater, J.G., 1997. Digital isochrons of the world's ocean floor. *J. Geophys. Res., [Solid Earth],* 102(B2):3211–3214. **doi:10.1029/96JB01781**

Pälike, H., Frazier, J., and Zachos, J.C., 2006b. Extended orbitally forced palaeoclimatic records from the equatorial Atlantic Ceara Rise. *Quat. Sci. Rev.,* 25(23–24):3138–3149. **doi:10.1016/j.quascirev.2006.02.011**

Pälike, H., Lyle, M.W., Ahagon, N., Raffi, I., Gamage, K., and Zarikian, C.A., 2008. Pacific equatorial age transect. *IODP Sci. Prosp.,* 320/321. **doi:10.2204/iodp.sp.320321.2008**

Pälike, H., Norris, R.D., Herrle, J.O., Wilson, P.A., Coxall, H.K., Lear, C.H., Shackleton, N.J., Tripati, A.K., and Wade, B.S., 2006a. The heartbeat of the Oligocene climate system. *Science,* 314(5807):1894–1898. **doi:10.1126/science.1133822**

Paul, H.A., Zachos, J.C., Flower, B.P., and Tripati, A., 2000. Orbitally induced climate and geochemical variability across the Oligocene/Miocene boundary. *Paleoceanography,* 15(5):471–485. **doi:10.1029/1999PA000443**

Pearson, P.N., and Wade, B.S., 2009. Taxonomy and stable isotope paleoecology of well-preserved planktonic foraminifera from the uppermost Oligocene of Trinidad. *J. Foraminifer. Res.,* 39(3):191–217. **doi:10.2113/gsjfr.39.3.191**

Petronotis, K.E., 1991. Paleomagnetic studies of the skewness of Pacific plate marine magnetic anomalies 25–32R: implications for anomalous skewness and the motion of the Pacific plate and hotspots [Ph.D. thesis]. Northwestern Univ., Evanston, IL.

Petronotis, K.E., Gordon, R.G., and Acton, G.D., 1994. A 57 Ma Pacific plate paleomagnetic pole determined

from a skewness analysis of crossings of marine magnetic anomaly 25r. *Geophys. J. Int.,* 118(3):529–554. **doi:10.1111/j.1365-246X.1994.tb03983.x**

Presley, B.J., and Kaplan, I.R., 1972. Interstitial water chemistry: Deep Sea Drilling Project, Leg 9. *In* Hayes, J.D., et al., *Init. Repts. DSDP,* 9: Washington, D.C. (U.S. Govt. Printing Office), 841–844. **doi:10.2973/dsdp.proc.9.116.1972**

Raffi, I., Backman, J., Fornaciari, E., Pälike, H., Rio, D., Lourens, L., and Hilgen, F., 2006. A review of calcareous nannofossil astrobiochronology encompassing the past 25 million years. *Quat. Sci. Rev.,* 25(23–24):3113–3137. **doi:10.1016/j.quascirev.2006.07.007**

Sager, W.W., and Pringle, M.S., 1988. Mid-Cretaceous to early Tertiary apparent polar wander path of the Pacific plate. *J. Geophys. Res., [Solid Earth],* 93(B10):11753–11771. **doi:10.1029/JB093iB10p11753**

Shackleton, N.J., Hall, M.A., Raffi, I., Tauxe, L., and Zachos, J., 2000. Astronomical calibration age for the Oligocene–Miocene boundary. *Geology,* 28(5):447–450. **doi:10.1130/0091-7613(2000)28<447:ACAFTO>2.0.CO;2**

Steininger, F.F., Aubry, M.P., Berggren, W.A., Biolzi, M., Borsetti, A.M., Brzobohaty, R., Cartlidge, J.E., Cati, F., Corfield, R., Gelati, R., Iacarrino, S., Mödden, C., Napoleone, D., Nolf, F., Ottner, B., Reichenbacher, B., Rögl, F., Roetzel, R., Spezzaferri, S., Tateo, F., Villa, G., Wielandt, U., Zevenboom, D., and Zorn, I., 1997. The global stratotype sample and point the GSSP for the base of the Neogene (the Paleogene/Neogene boundary). *Episodes,* 20:23–28.

Takata, H., and Nomura, R., 2005. Data report: Oligocene benthic foraminifers from the eastern equatorial Pacific, Sites 1218 and 1219, ODP Leg 199. *In* Wilson, P.A., Lyle, M., and Firth, J.V. (Eds.), *Proc. ODP, Sci. Results,*199: College Station, TX (Ocean Drilling Program), 1–26. **doi:10.2973/odp.proc.sr.199.224.2005**

Thomas, E., 1985. Late Eocene to Recent deep-sea benthic foraminifers from the central equatorial Pacific Ocean. *In* Mayer, L., Theyer, F., Thomas, E., et al., *Init. Repts. DSDP,* 85: Washington, DC (U.S. Govt. Printing Office), 655–694. **doi:10.2973/dsdp.proc.85.117.1985**

van Andel, T.H., 1975. Mesozoic/Cenozoic calcite compensation depth and the global distribution of calcareous sediments. *Earth Planet. Sci. Lett.,* 26(2):187–194. **doi:10.1016/0012-821X(75)90086-2**

Wade, B.S., Berggren, W.A., and Olsson, R.K., 2007. The biostratigraphy and paleobiology of Oligocene planktonic foraminifera from the equatorial Pacific Ocean (ODP Site 1218). *Mar. Micropaleontol.,* 62(3):167–179. **doi:10.1016/j.marmicro.2006.08.005**

Young, J.R., 1999. Neogene. *In* Bown, P.R. (Ed.), *Calcareous Nannofossil Biostratigraphy:* Dordrecht, The Netherlands (Kluwer Academic Publ.), 225–265.

Zachos, J., Pagani, M., Sloan, L., Thomas, E., and Billups, K., 2001a. Trends, rhythms, and aberrations in global climate 65 Ma to present. *Science,* 292(5517):686–693. **doi:10.1126/science.1059412**

Zachos, J.C., Flower, B.P., and Paul, H., 1997. Orbitally paced climate oscillations across the Oligocene/Miocene boundary. *Nature (London, U. K.),* 388(6642):567–570. **doi:10.1038/41528**

Zachos, J.C., Shackleton, N.J., Revenaugh, J.S., Pälike, H., and Flower, B.P., 2001. Climate response to orbital forcing across the Oligocene–Miocene boundary. *Science,* 292(5515):274–278. **doi:10.1126/science.1058288**

Publication: 30 October 2010
MS 320321-108

Figure F1. A. ETOPO1 (Amante and Eakins, 2008) bathymetric overview map of Site U1336 and PEAT drilling locations with previous ODP and DSDP sites. F.Z. = fracture zone. **B.** Swath bathymetry from AMAT-03 site survey, Site U1336 region. White line = survey Line 6.

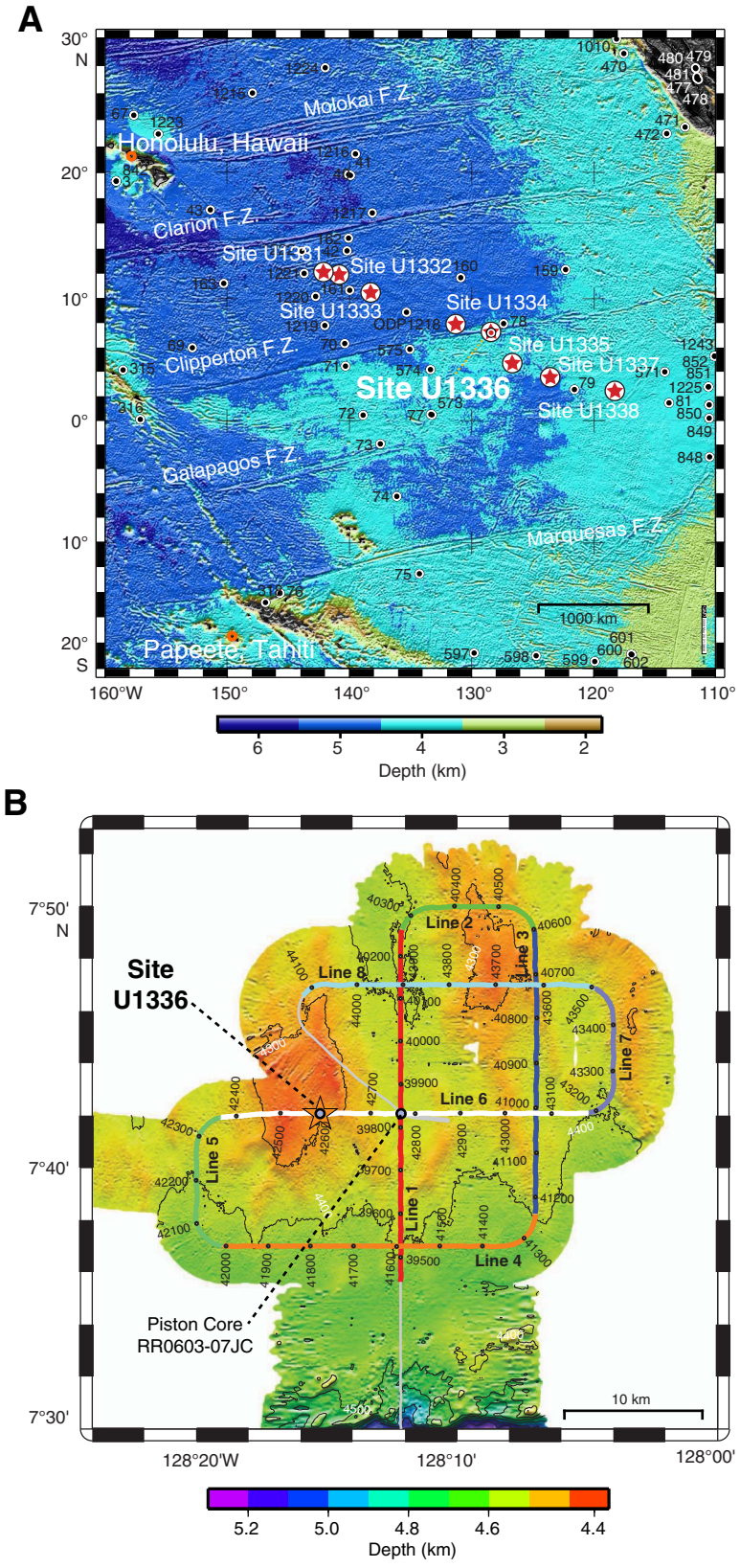

Figure F2. Seismic reflection profile Line 6 from 48-channel seismic reflection survey (Lyle et al., 2006). Data are filtered, stacked, and migrated. SP = shotpoint.

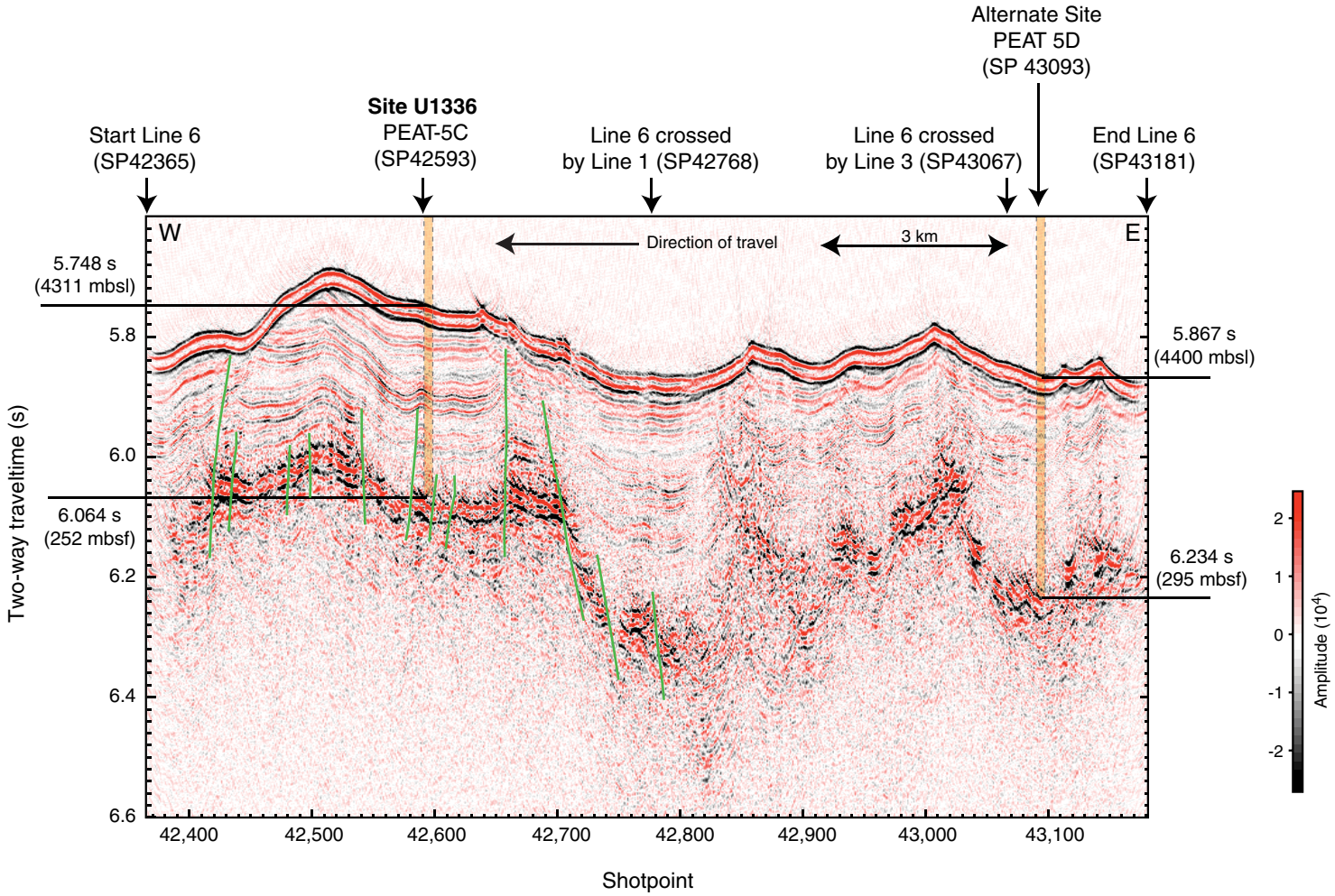

Figure F3. Site U1336 summary.

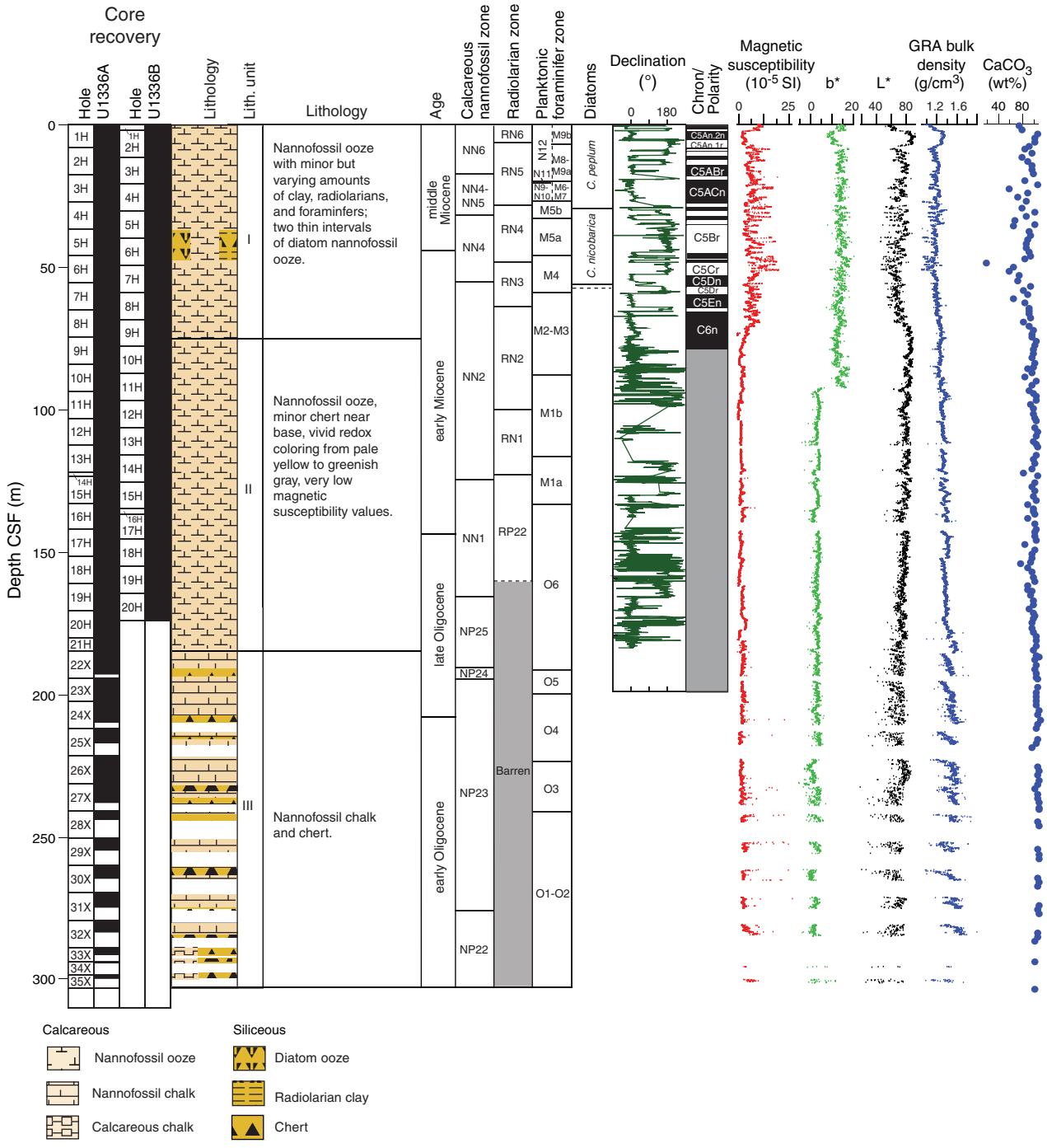

Figure F4. Lithostratigraphy summary, Site U1336. L*, b* = lightness reflectance value of sediment as defined in the LAB color model, GRA = gamma ray attenuation.

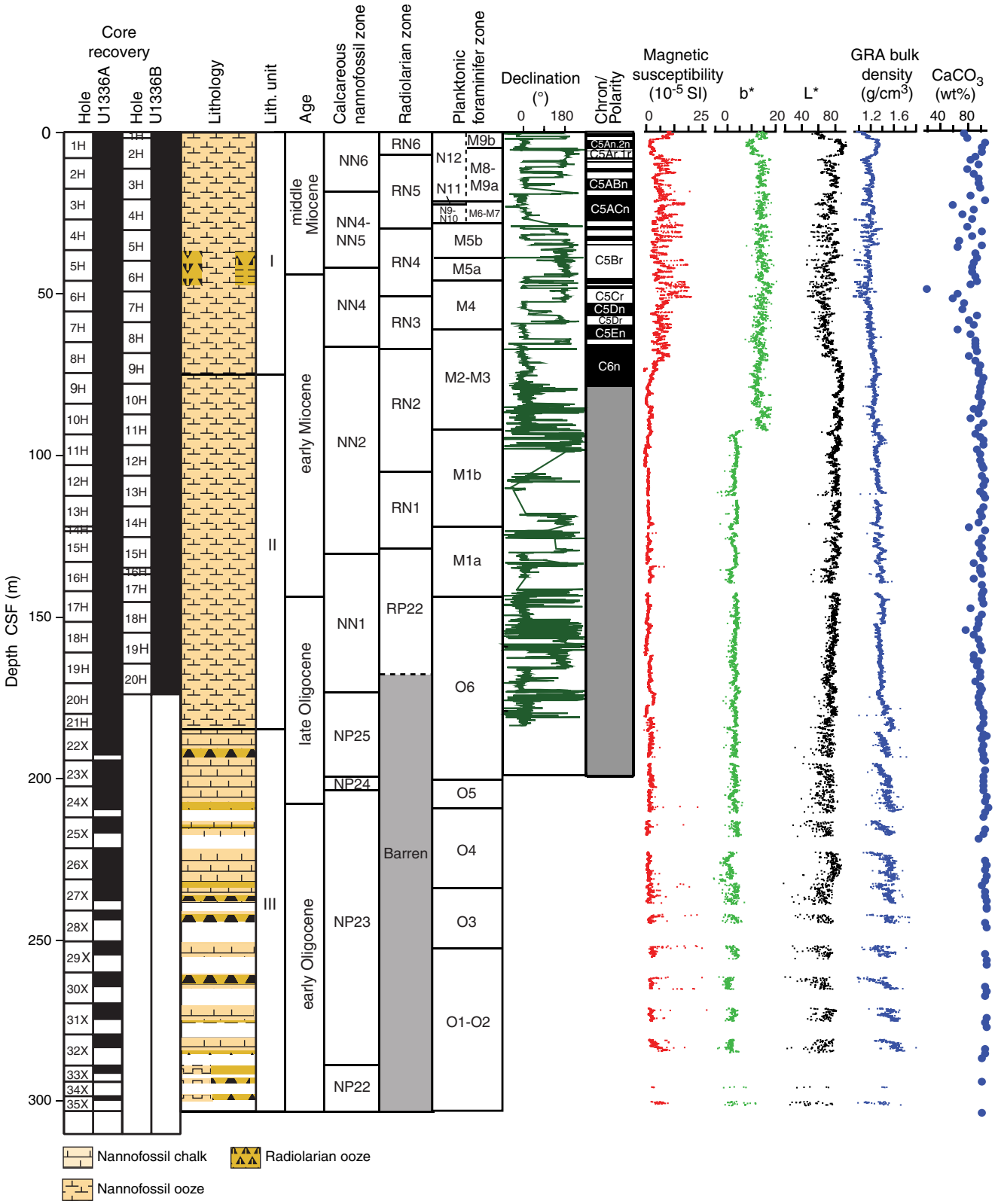

Figure F5. Light–dark sediment alternations of Miocene age including the two diatom-rich intervals. Pie charts show lithologic variability observed in smear slides.

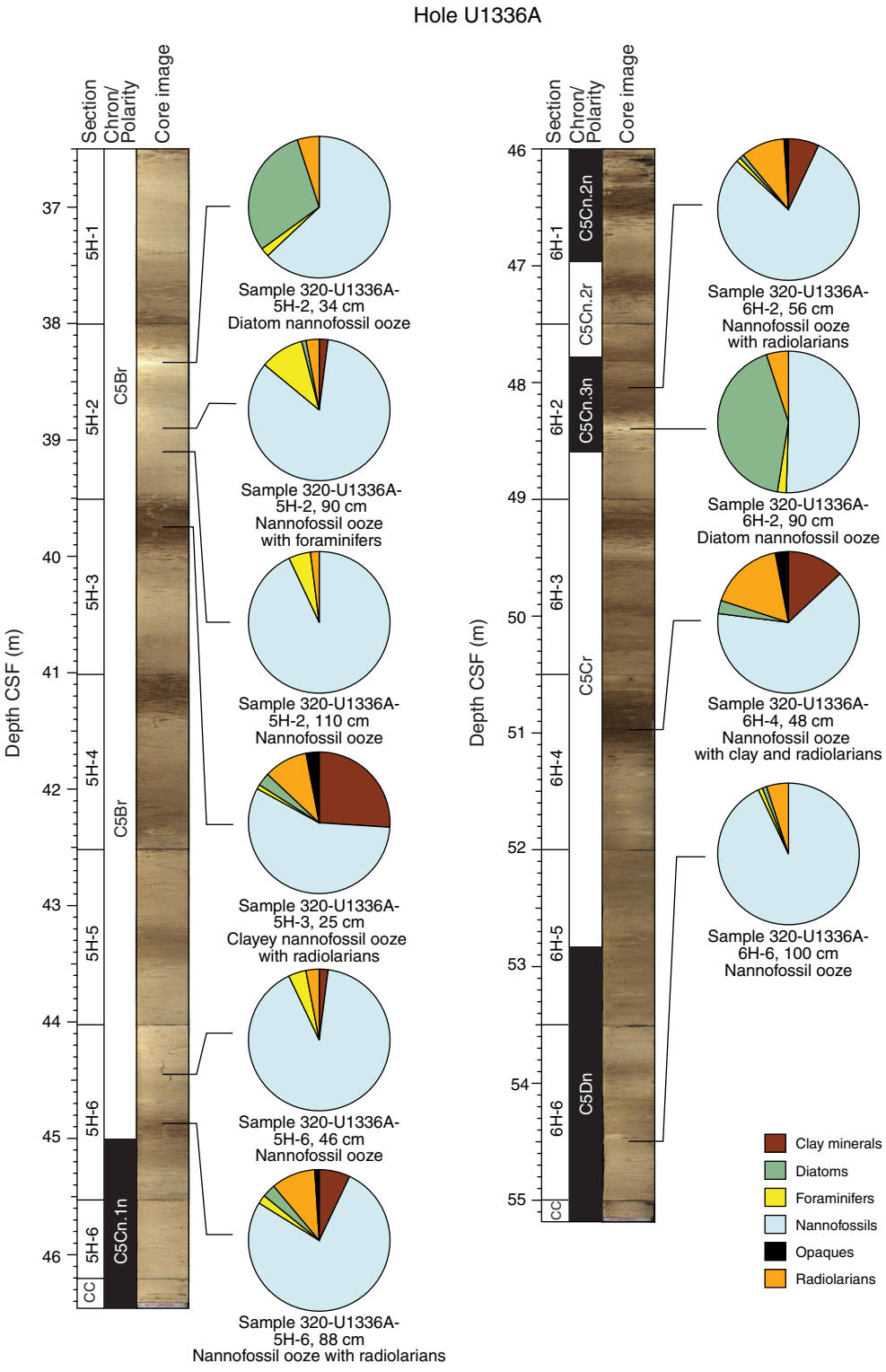

Figure F6. Smear slide photomicrographs of diatom-rich layers and adjacent lithologies. Left image = plane-polarized light, right image = cross-polarized light. **A.** Diatom nannofossil ooze (Sample 320-U1336A-5H-2, 34 cm). **B.** Nannofossil ooze with foraminifers (Sample 320-U1336A-5H-2, 90 cm). **C.** Nannofossil ooze with radiolarians (Sample 320-U1336A-6H-2, 56 cm). **D.** Diatom nannofossil ooze (Sample 320-U1336A-6H-2, 90 cm).

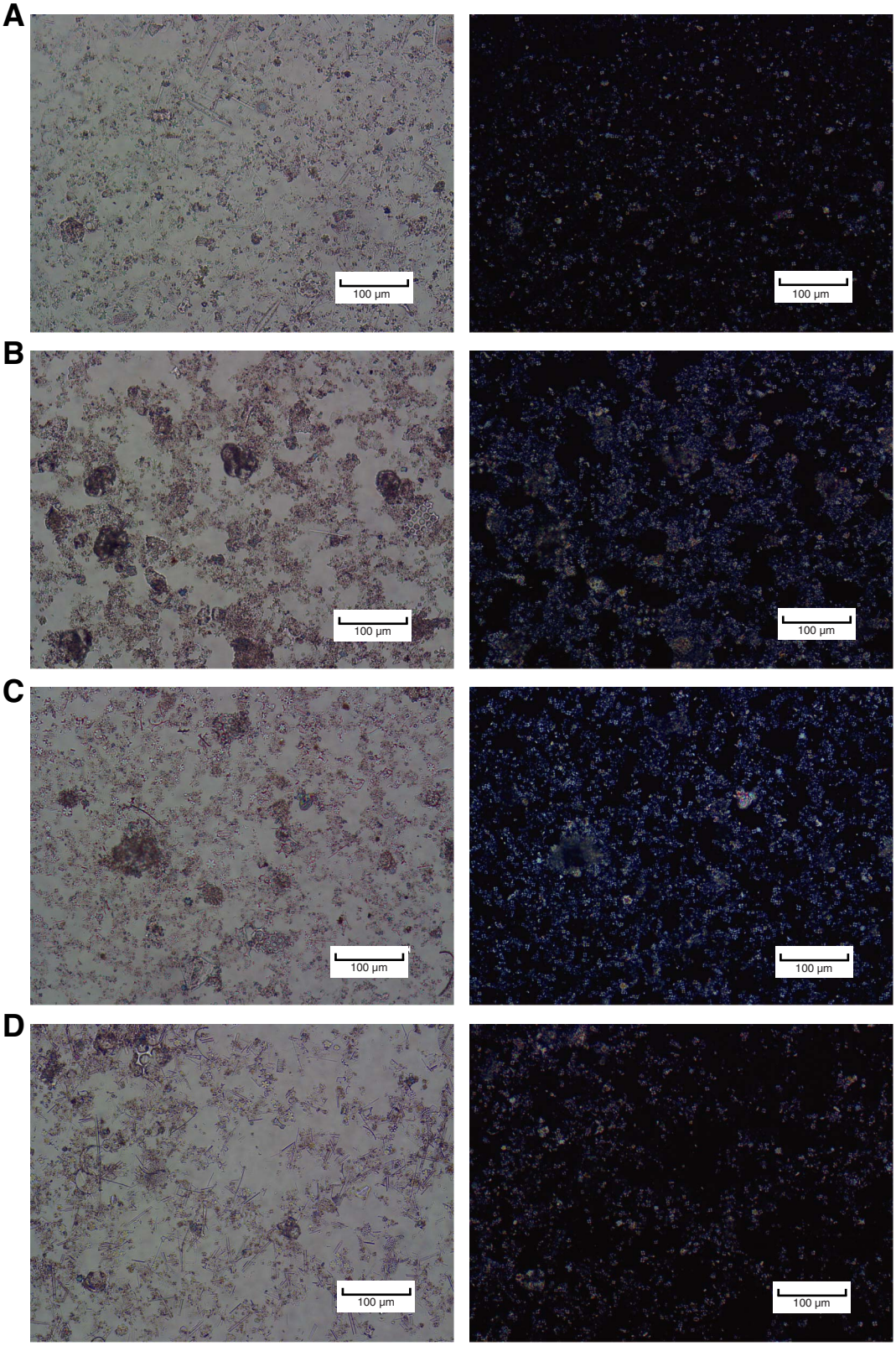

Figure F7. Color reflectance and magnetic susceptibility, Hole U1336A. Line scan images from Cores 320-U1336A-8H through 11H highlight observed color changes. L*, a*, b* = lightness reflectance value of sediment as defined in the LAB color model.

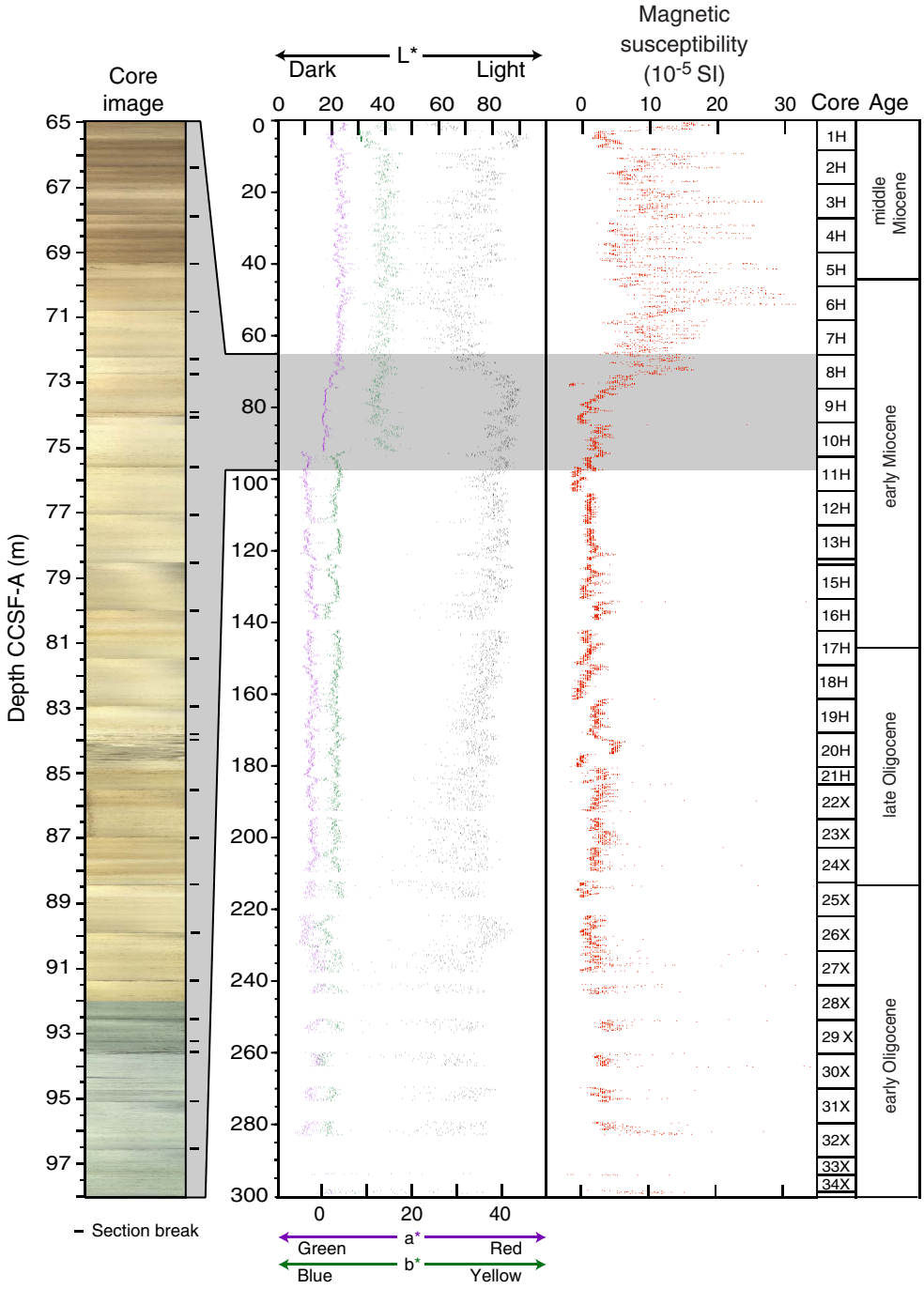

Figure F8. Line scan image of interval 320-U1336A-10H-6, 55–75 cm, showing sharp redox-related color change.

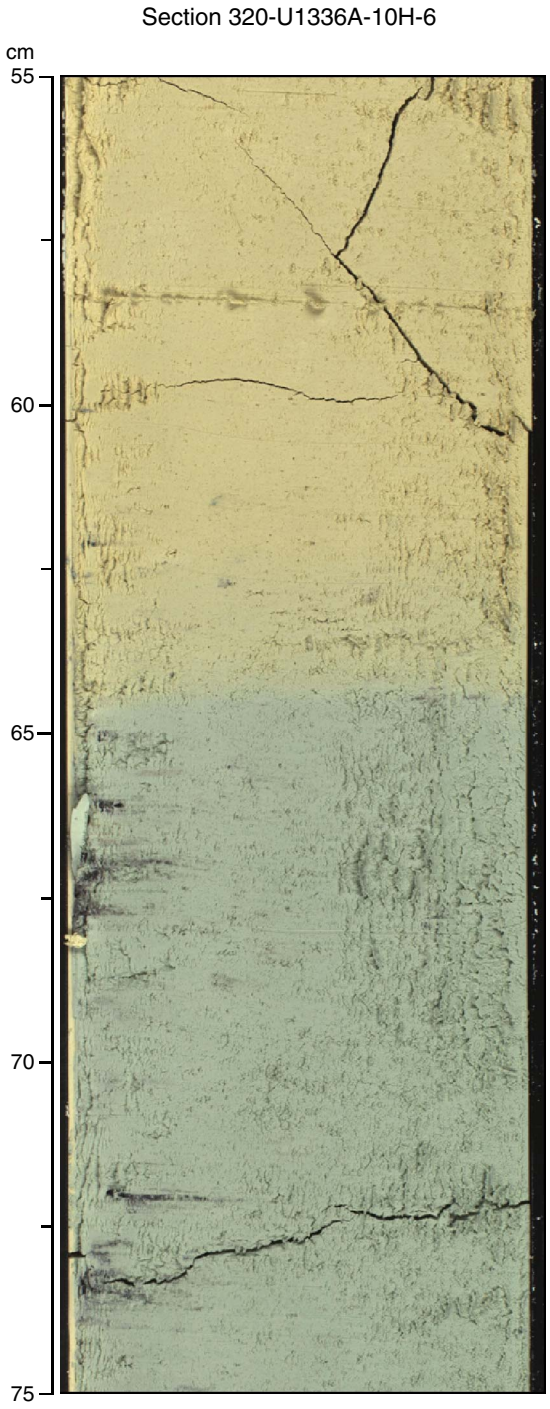

Figure F9. Thin section photomicrographs of foraminifer-bearing cherts, Site U1336. Left image = plane-polarized light, right image = cross-polarized light. **A.** Sample 320-U1336A-33X-1, 2–3 cm. **B.** Sample 320-U1336A-35X-1, 78–80 cm. **C, D.** Sample 320-U1336A-27X-1, 0–2 cm.

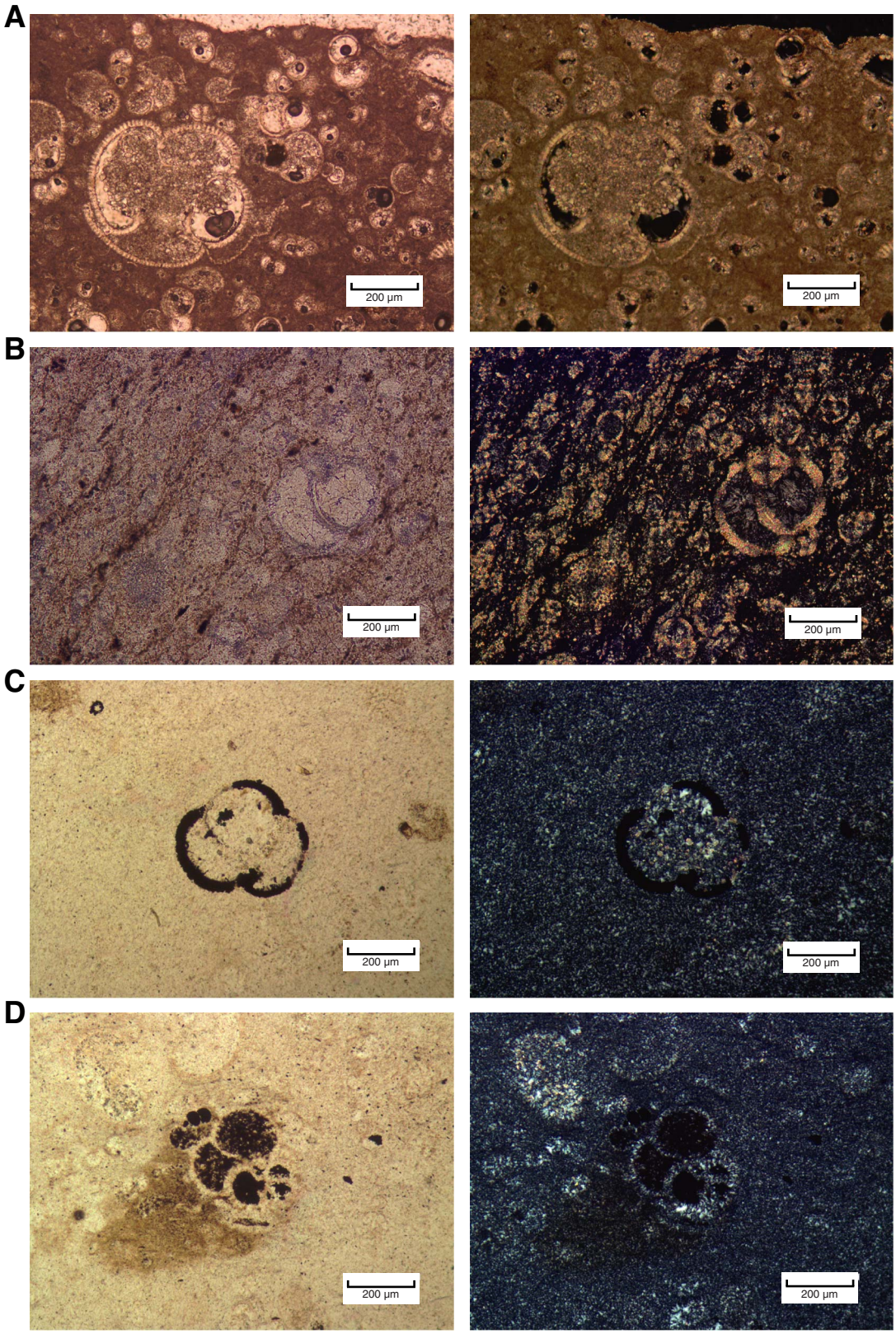

Figure F10. Integrated calcareous and siliceous microfossil biozonation, Site U1336.

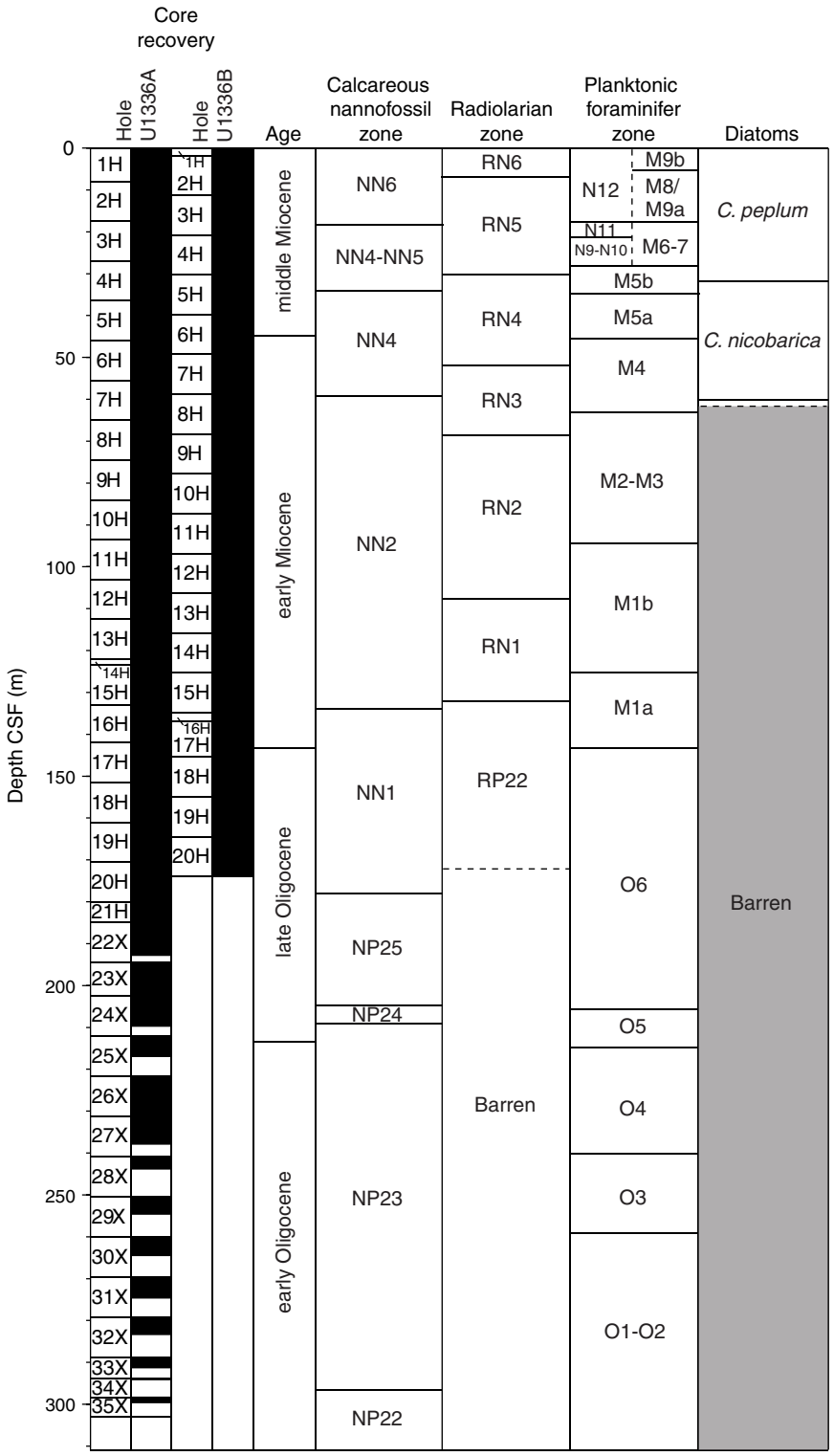

Figure F11. Linear sedimentation rates and chronostratigraphic markers, Site U1336.

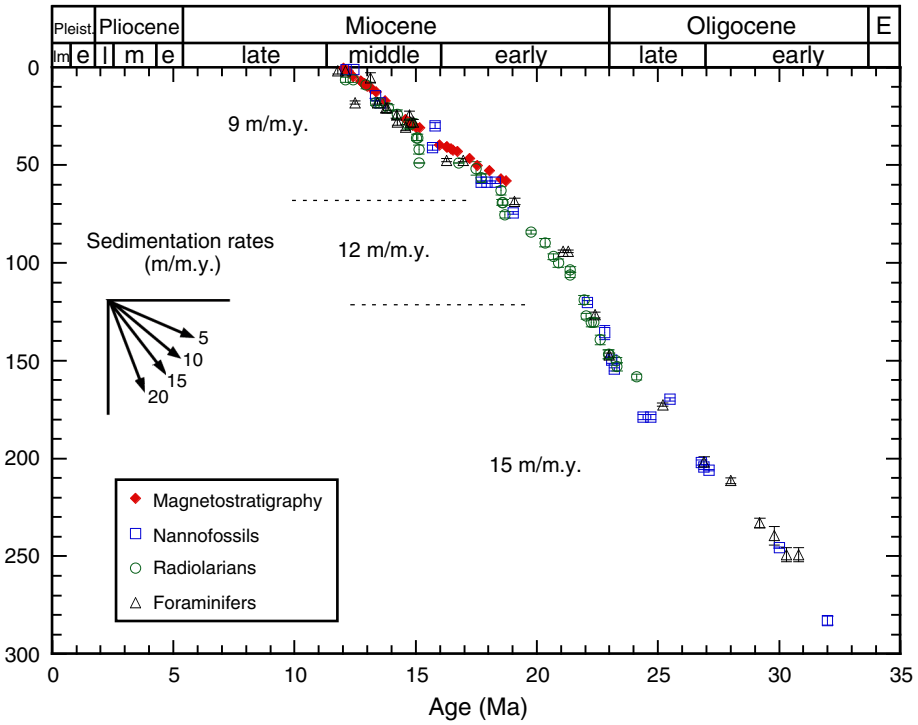

Figure F12. Magnetic susceptibility and paleomagnetic summary, Hole U1336A, 0–100 m CSF. Gray lines = measurements before demagnetization, red lines = measurements after 20 mT alternating-field demagnetization, blue squares = discrete sample data.

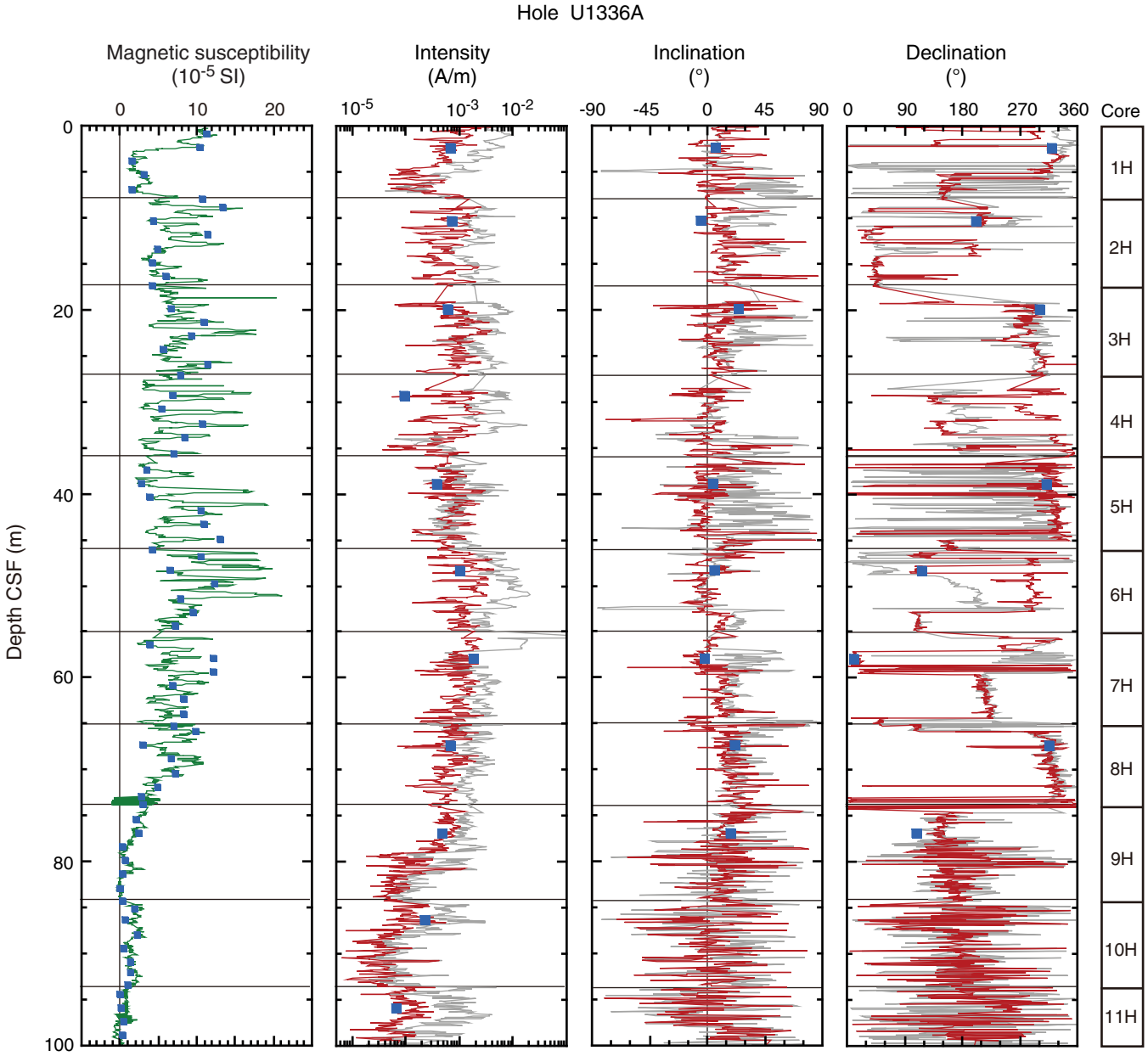

Figure F13. Magnetic susceptibility and paleomagnetic summary, Hole U1336A, 100–200 m CSF. Gray lines = measurements before demagnetization, red lines = measurements after 20 mT alternating-field demagnetization, blue squares = discrete sample data.

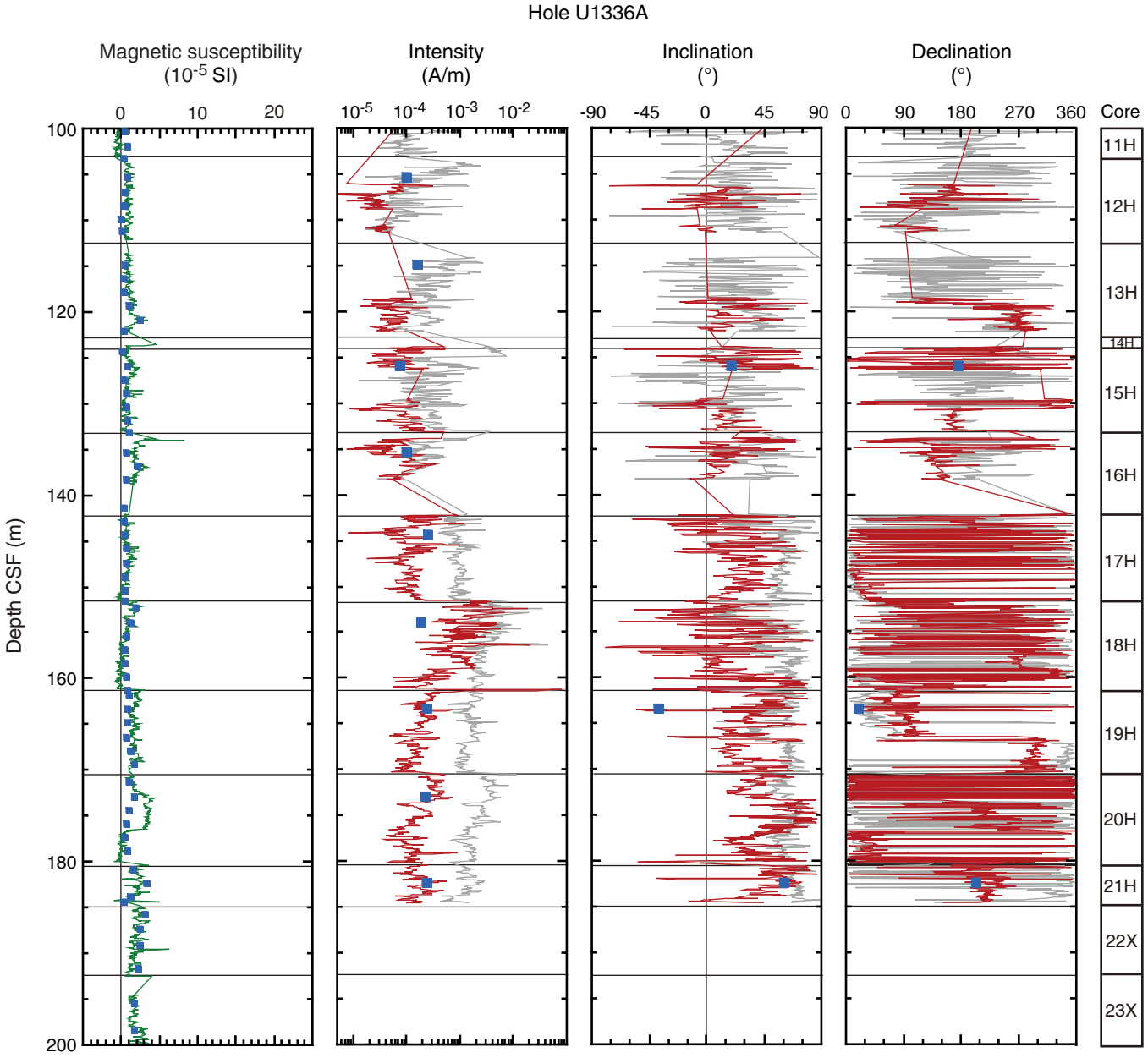

Figure F14. Magnetic susceptibility and paleomagnetic summary, Hole U1336B, 0–100 m CSF. Gray lines = measurements before demagnetization, red lines = measurements after 20 mT alternating-field demagnetization.

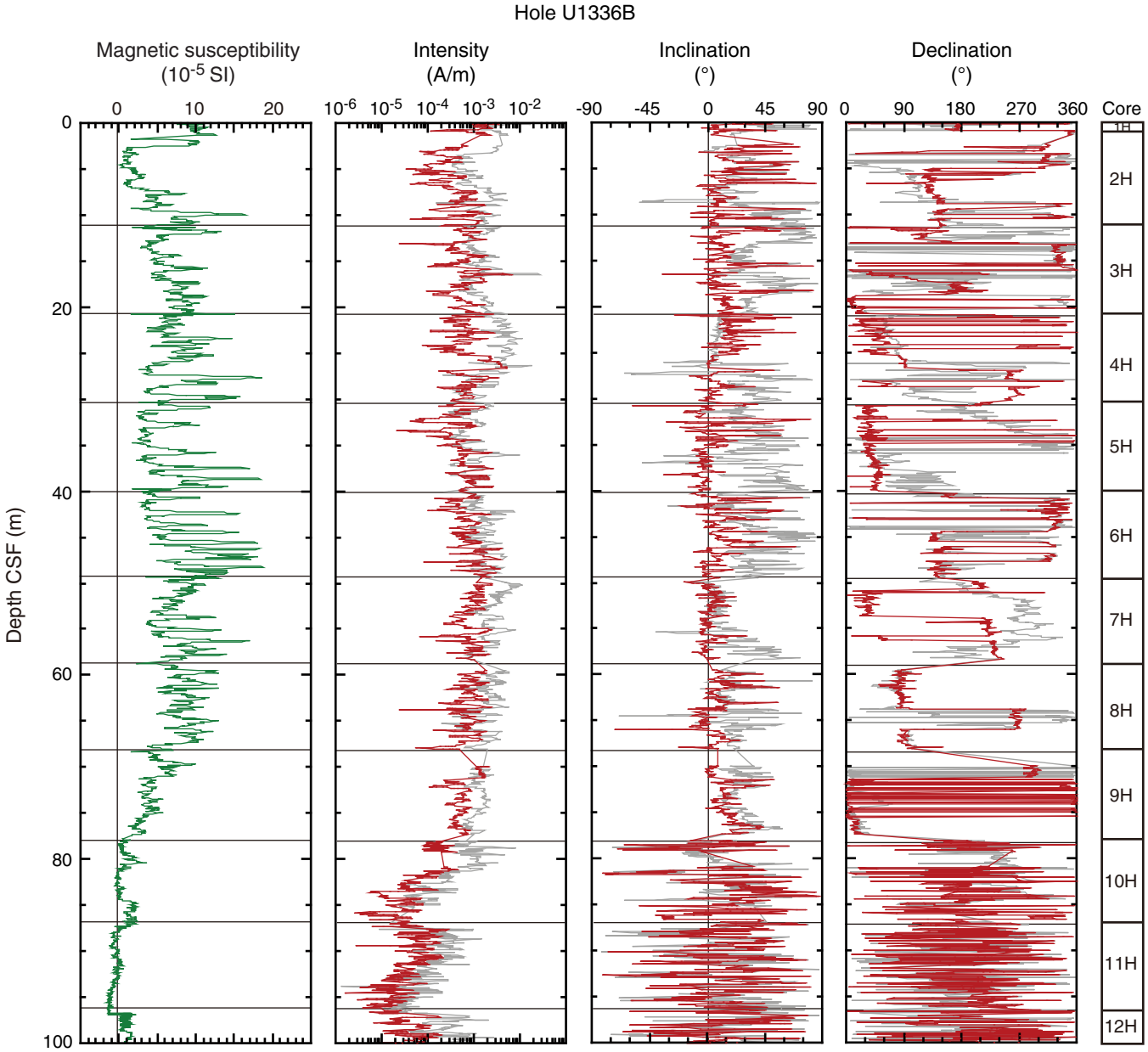

Figure F15. Magnetic susceptibility and paleomagnetic summary, Hole U1336B, 100–180 m CSF. Gray lines = measurements before demagnetization, red lines = measurements after 20 mT alternating-field demagnetization.

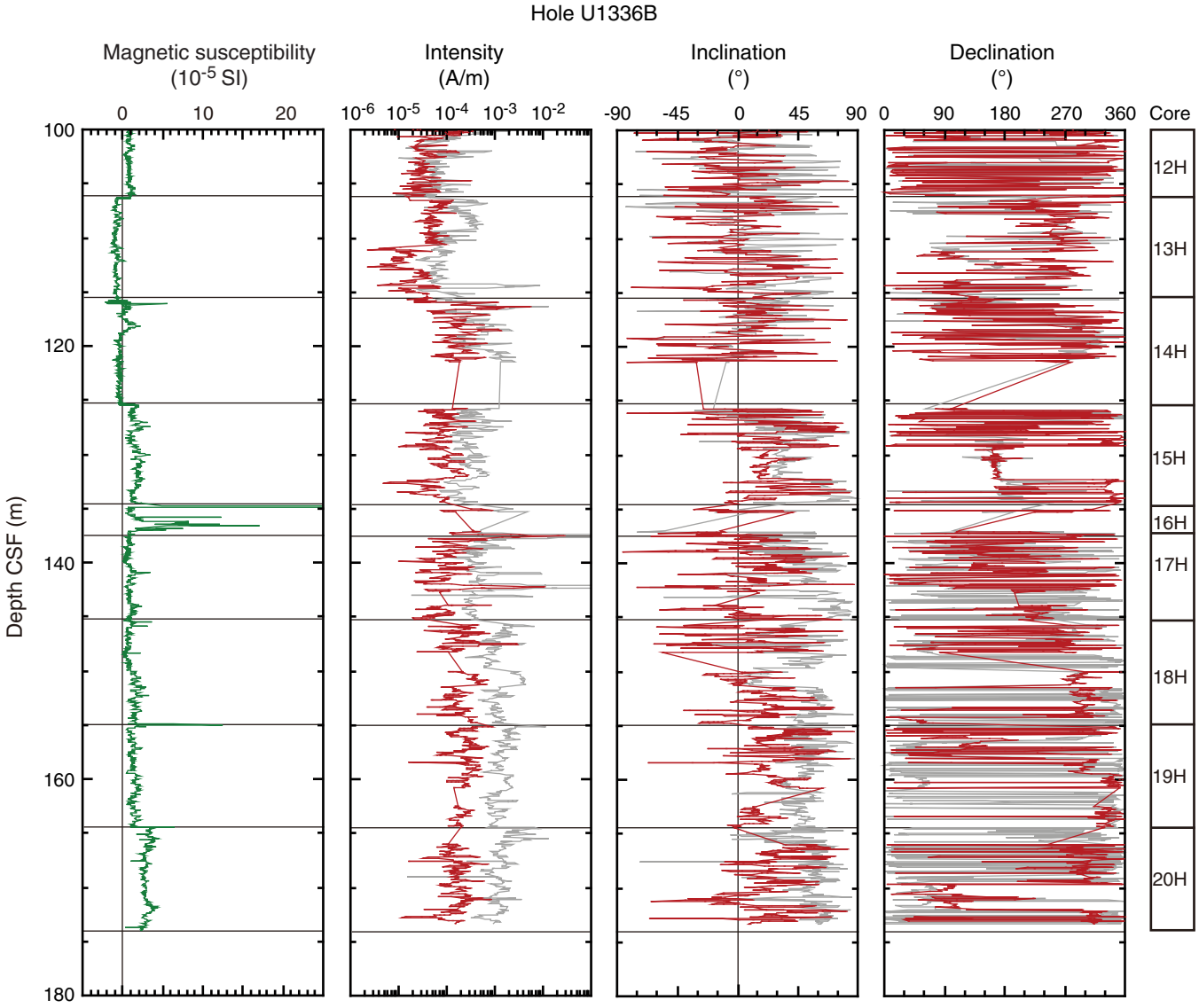

Figure F16. Declination of natural remanent magnetization after 20 mT alternating-field demagnetization. Red = cores. Note that in this interpretation polarity zones corresponding to Chrons C5ADn and C5ACn are concatenated into a single polarity zone, with Chron C5ACr not recorded. CCSF-A depths for holes were determined independent of the polarity record. See Table **T15.**

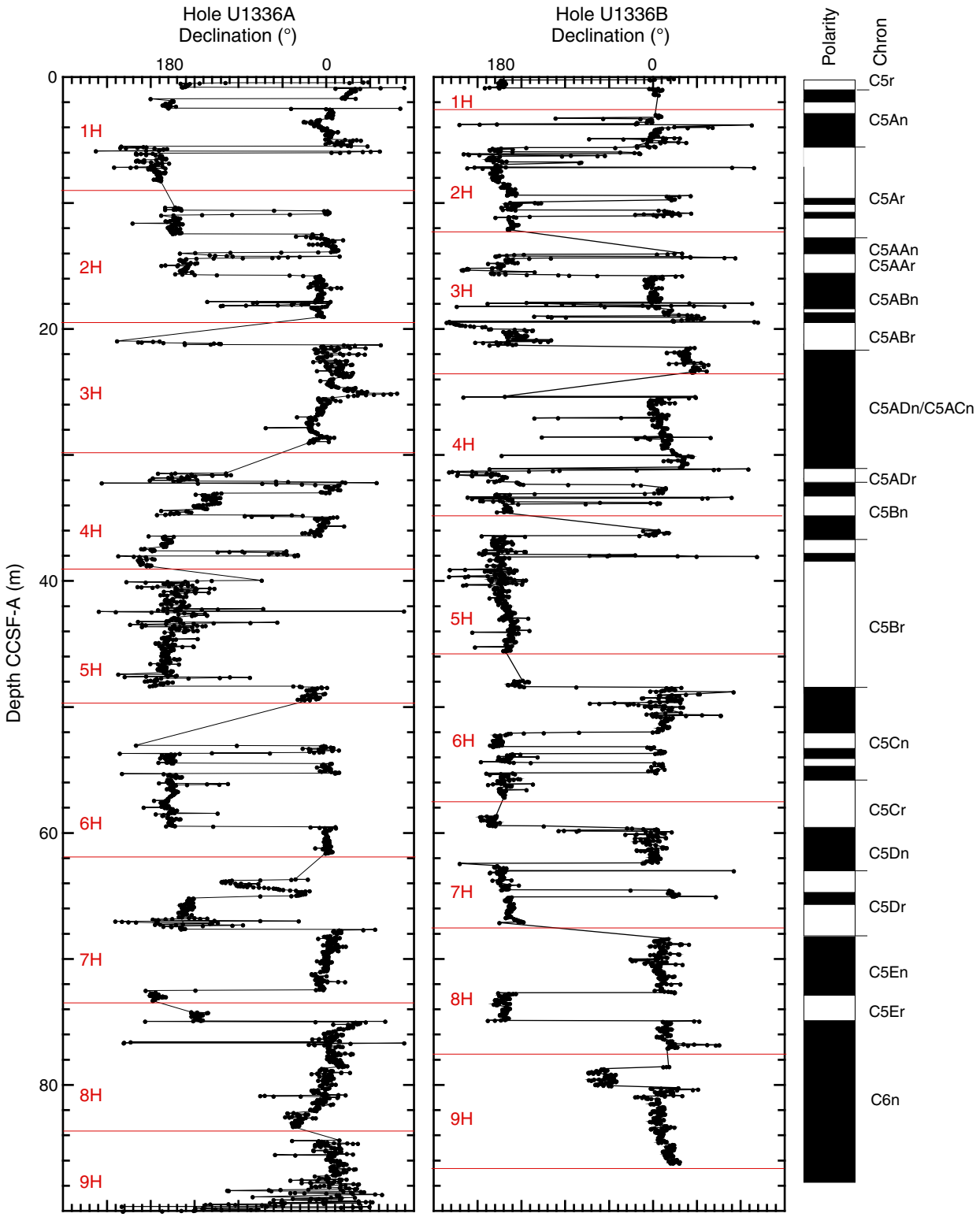

Figure F17. Alternating-field (AF) demagnetization results representative of Site U1336 discrete samples. Left plot = vector endpoints of paleomagnetic directions on vector demagnetization diagrams or modified Zijderveld plots (open squares = inclinations [Inc], solid squares = declinations [Dec]), top right plot = intensity variation with progressive demagnetization, bottom right plot = directions plotted on an equal-area stereonet. Data in A and B illustrate removal of a drilling overprint by ~10 mT, with remaining magnetization providing a relatively well-resolved characteristic remanent magnetization. C shows a sample from base of the hole, illustrating that a steep drilling overprint is dominant and a stable ChRM is not isolated during AF demagnetization. Maximum angular deviation (MAD) values provide an estimate quality of principal component analysis (PCA), where values <10 indicate good agreement between PCA vector and paleomagnetic data. See Table **T14.** **A.** Hole U1336A (2.35 m CSF). **B.** Hole U1336A (10.35 m CSF). **C.** Hole U1336A (172.85 m CSF).

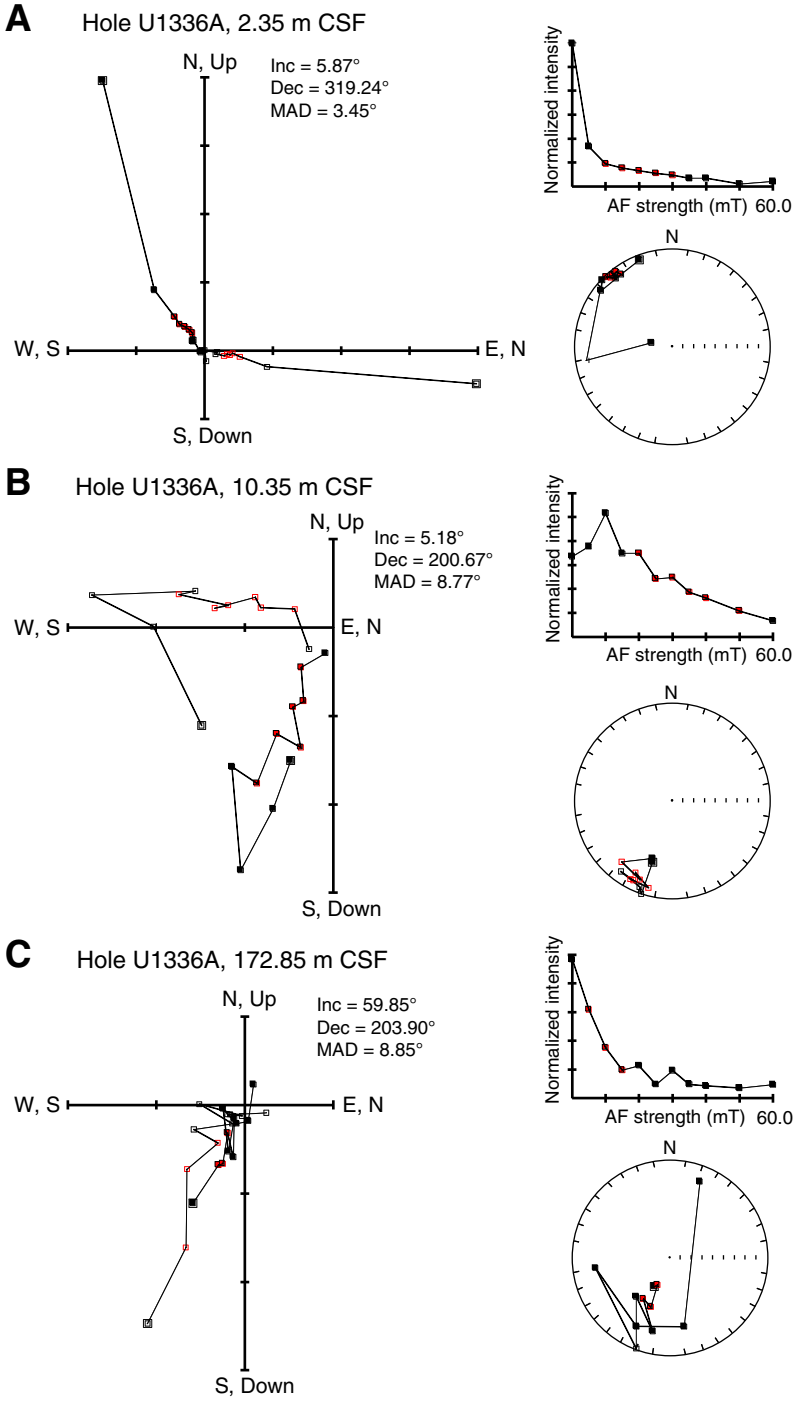

Figure F18. Interstitial water chemistry, Hole U1336B. Values below detection limit (see Table T16) plotted as zero.

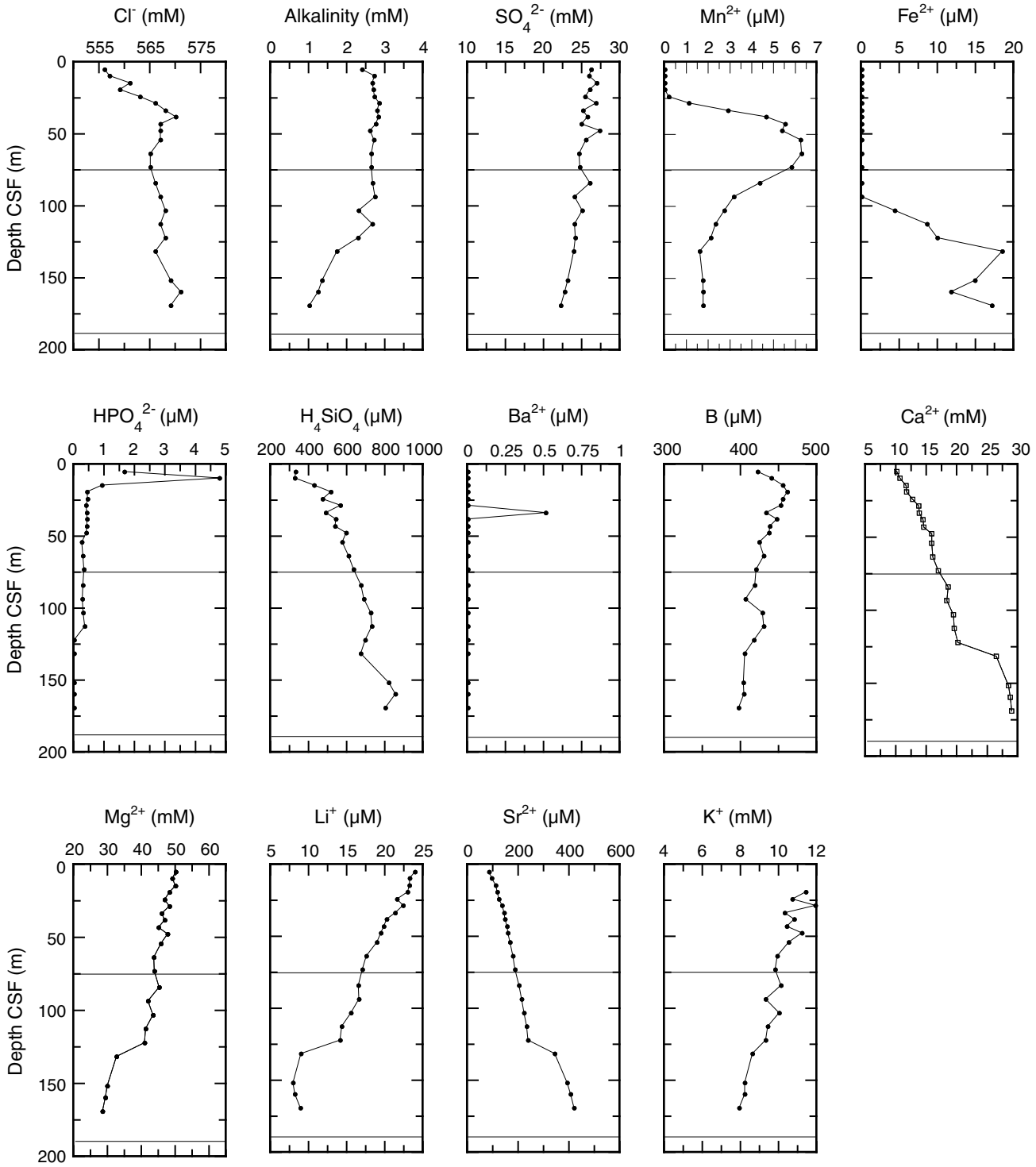

Figure F19. Calcium carbonate in sediments, Holes U1336A and U1336B. Total organic carbon (TOC) content from Hole U1336B.

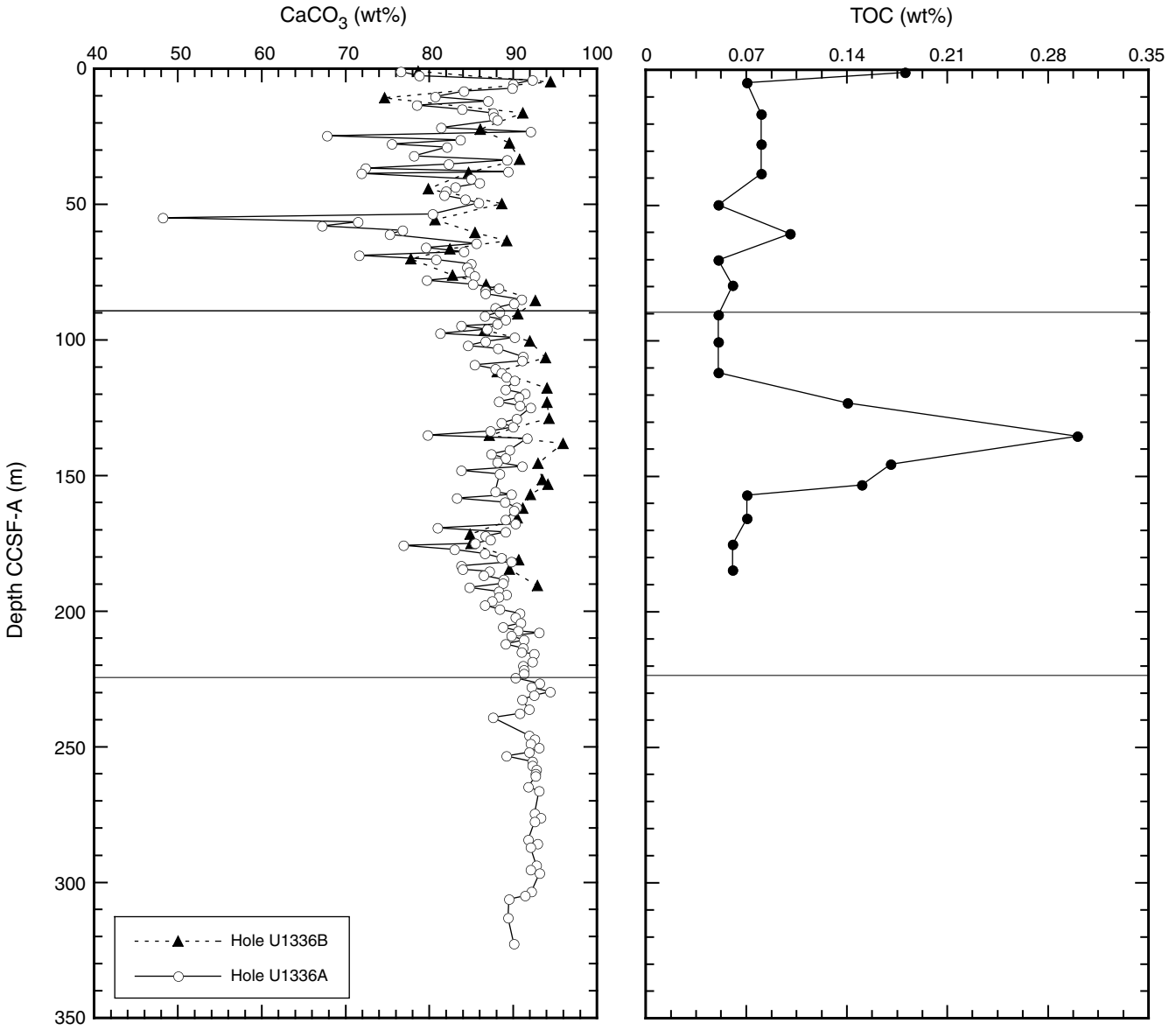

Figure F20. Whole-round measurements, Holes U1336A (black) and U1336B (red). Data for Hole U1336B are plotted using offsets of 0.5 g/cm^3 for bulk density, 30 × 10^{-5} SI for magnetic susceptibility, 100 m/s for *P*-wave velocity, and 10 cps for natural gamma radiation.

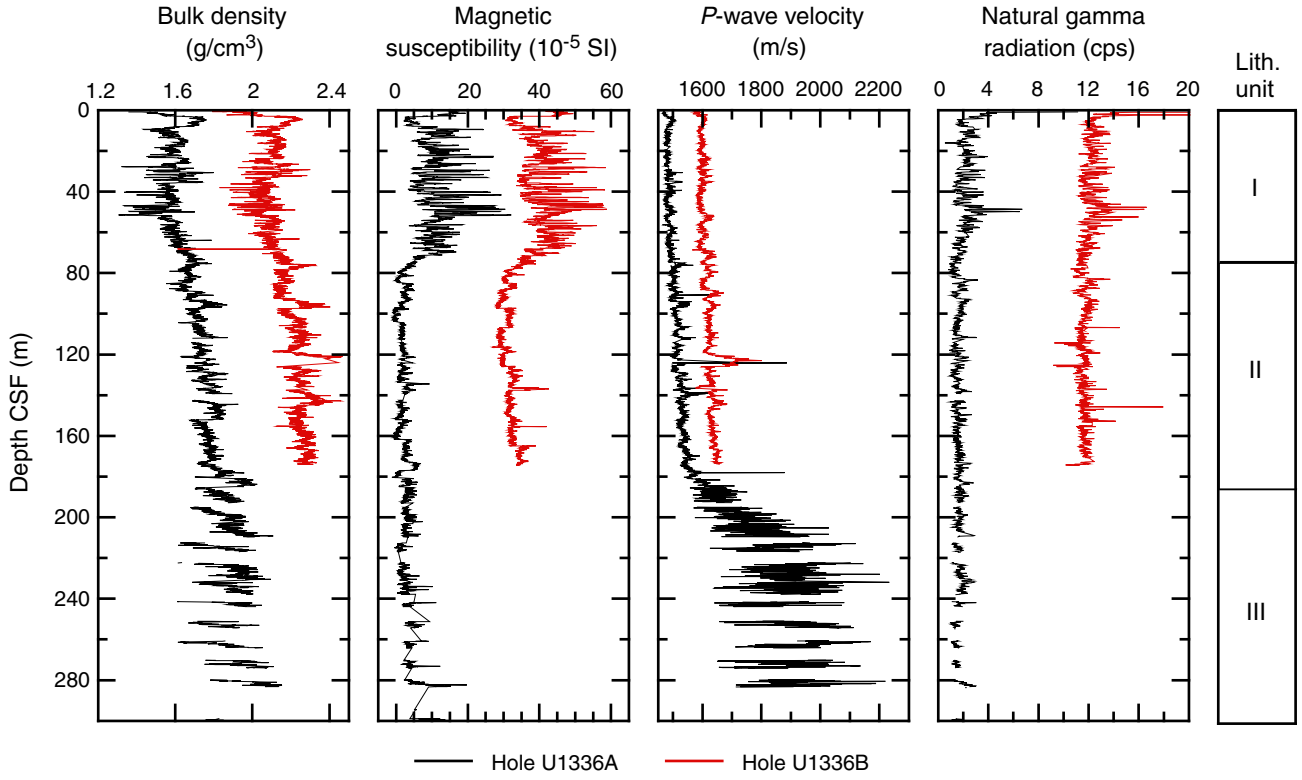

Figure F21. MAD measurements, Holes U1336A (black) and U1336B (red). **A.** Porosity (solid circles) and water content (open circles). **B.** Discrete-sample wet bulk density (solid circles) and gamma ray attenuation (GRA) bulk density (gray line). **C.** Grain density.

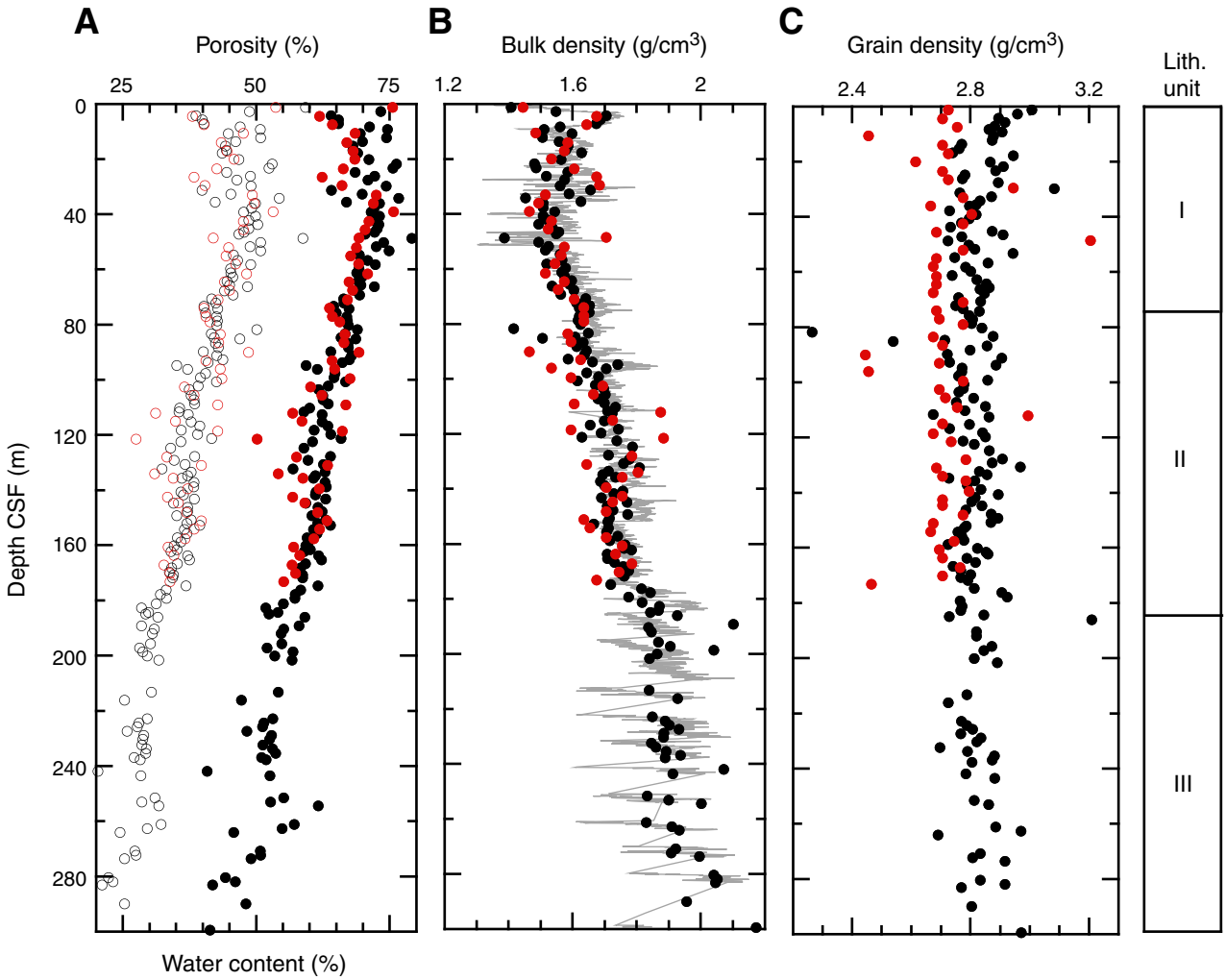

Figure F22. (**A**) Wet and (**B**) dry bulk density from MAD analysis of discrete samples from Holes U1336A (black) and U1336B (red) plotted with gamma ray attenuation (GRA) bulk density interpolated with a 20 cm wide Gaussian window.

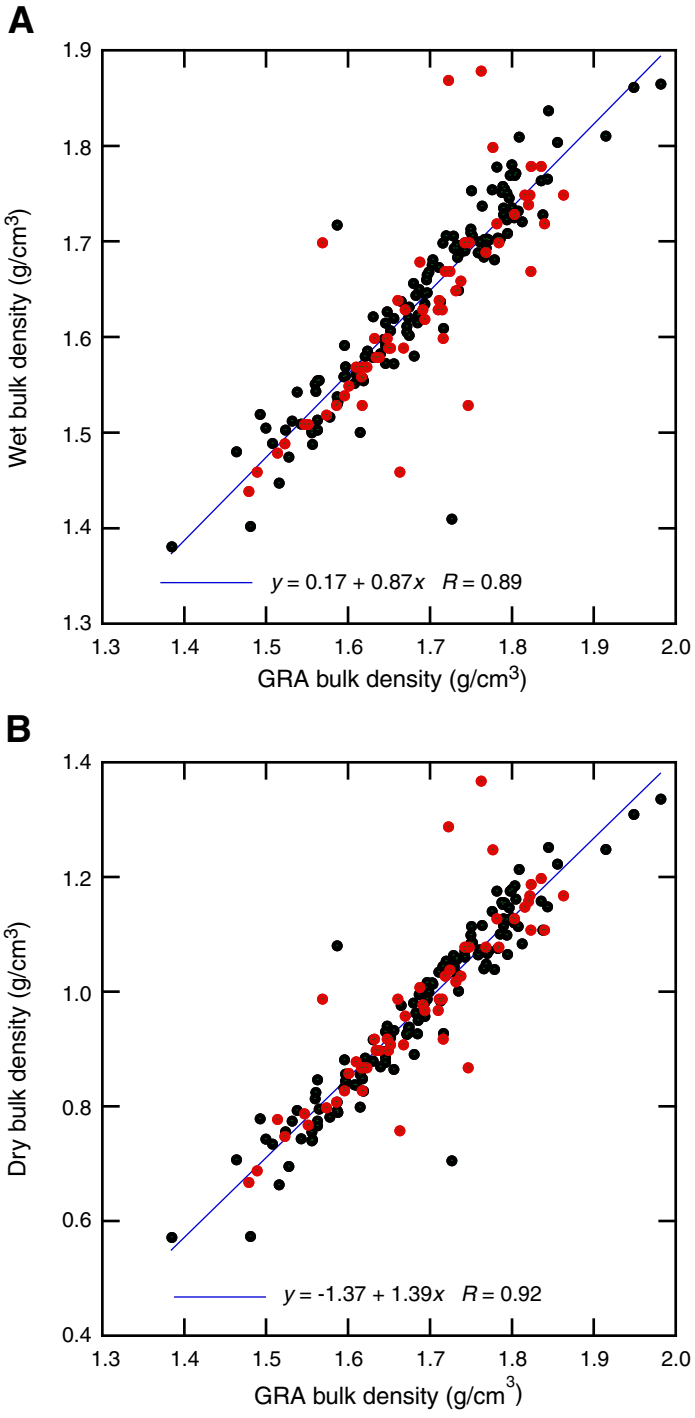

Figure F23. Compressional wave velocity from the PWL (gray lines) and discrete velocity measurements on split core using the contact probe for *x*-axis measurements and insertion probes for *y*- and *z*-axis measurements. Black circles = Hole U1336A, red circles = Hole U1336B. (See **"Compressional wave velocity"** for a note on postcruise velocity correction.)

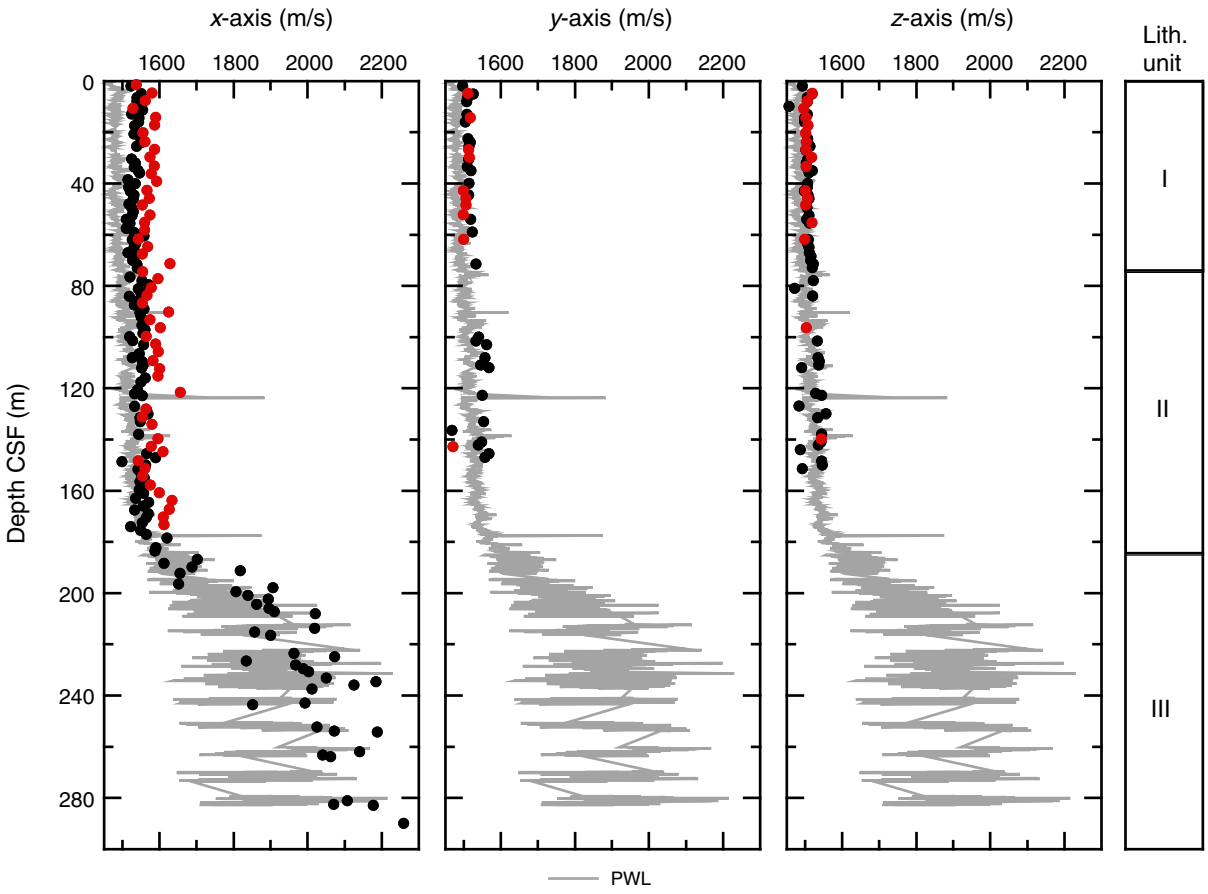

Figure F24. Thermal conductivity vs. depth, Holes U1336A (black) and U1336B (red).

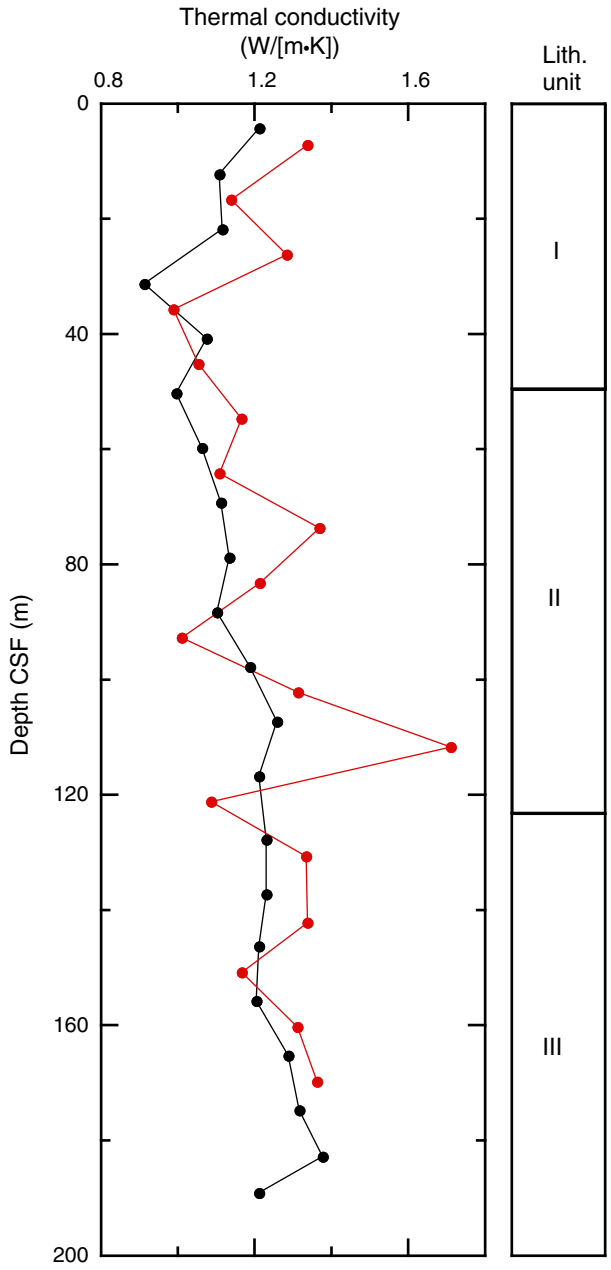

Figure F25. Thermal conductivity vs. porosity from MAD analysis of discrete samples, Holes U1336A (black) and U1336B (red).

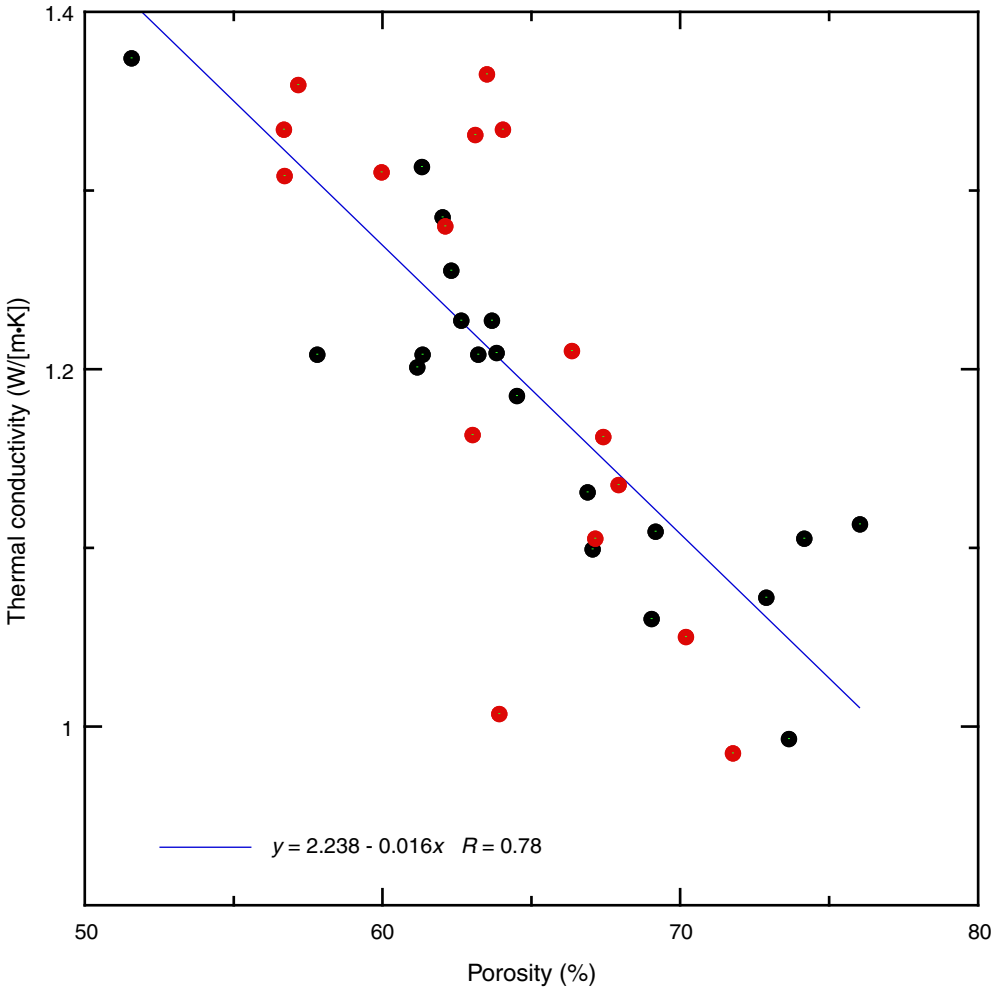

Figure F26. Reflectance spectrophotometry, Holes U1336A (black) and U1336B (red). Data for Hole U1336B are plotted using offsets of 20 for L* (luminance), 5 for a* (blue–yellow), and 5 for b* (green–red).

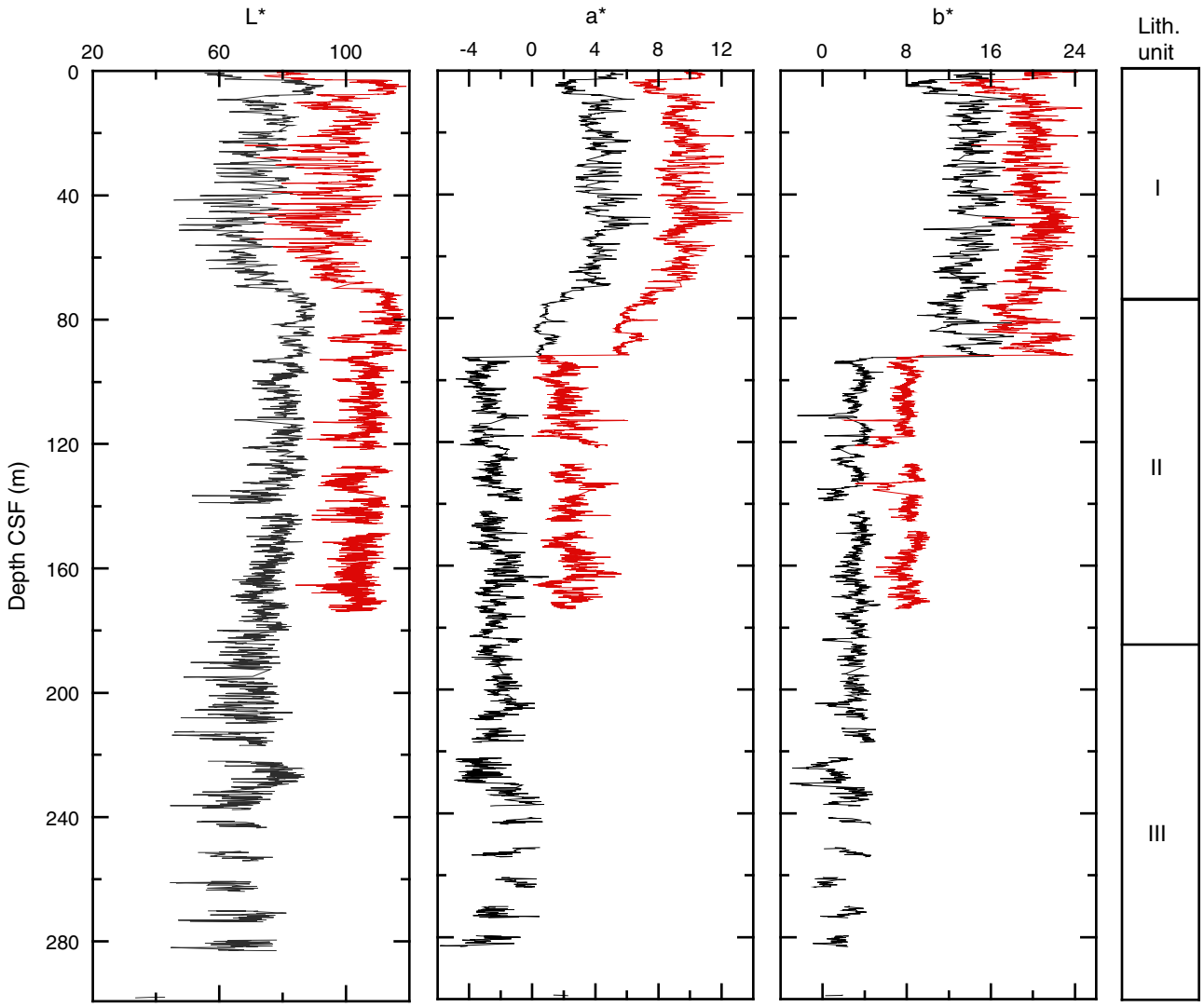

Figure F27. Magnetic susceptibility data, Holes U1336A (red) and U1336B (blue). Data are offset by a constant 10 SI units. Upper panels are the Site U1338 splices for the intervals. **A.** 0–50 m CCSF-A. (**Continued on next three pages.**)

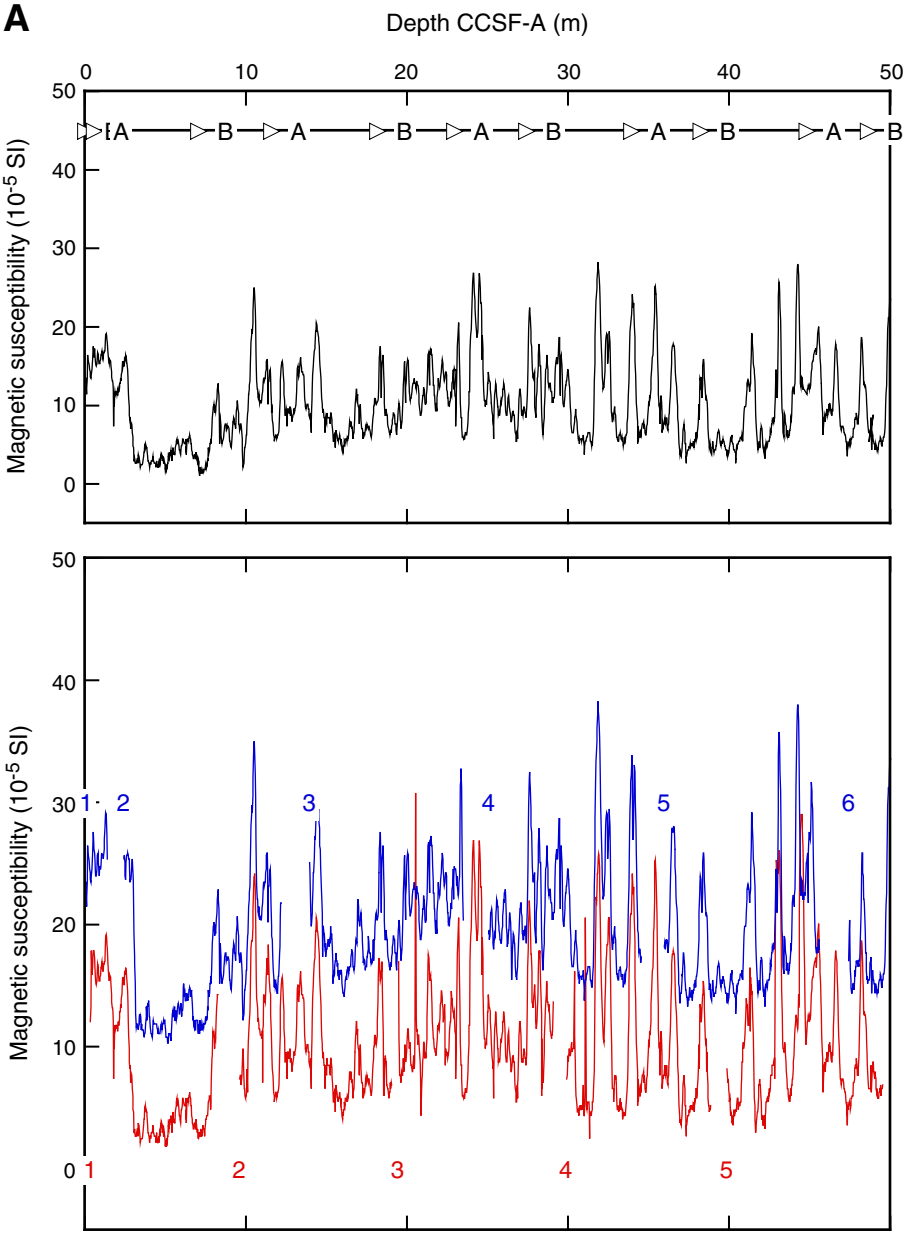

Figure F27 (continued). B. 50–100 m CCSF-A. (**Continued on next page.**)

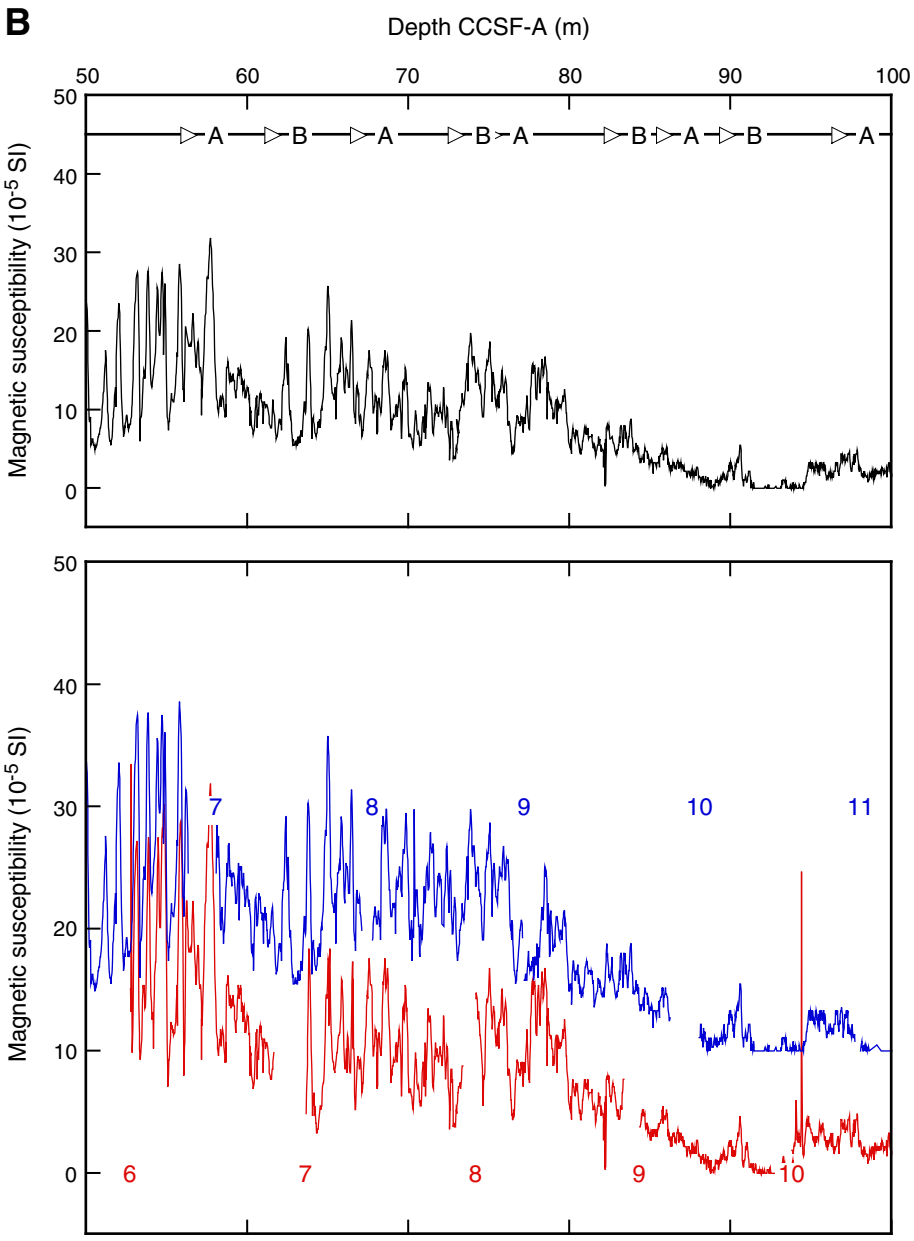

Figure F27 (continued). C. 100–150 m CCSF-A. (Continued on next page.)

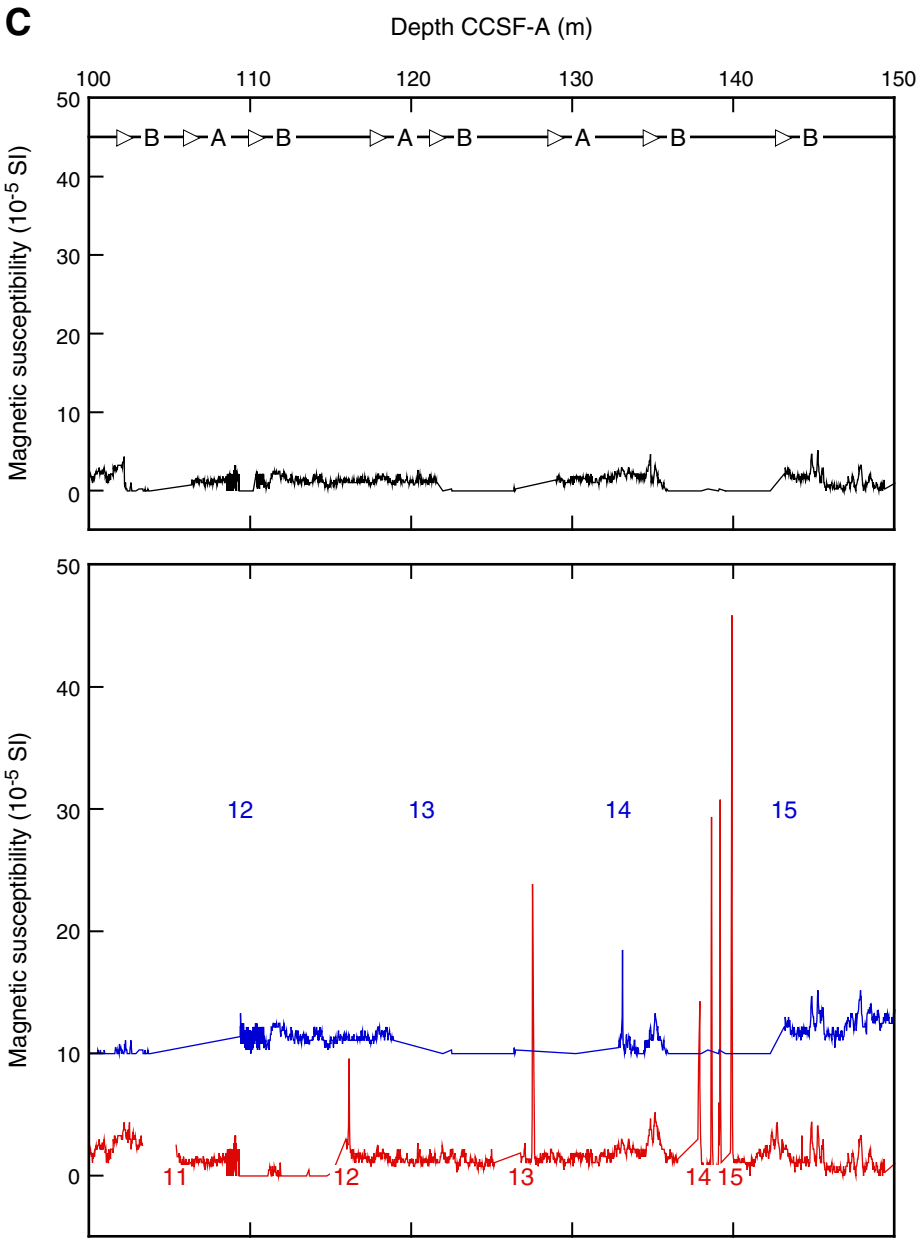

Figure F27 (continued). D. 150–200 m CCSF-A.

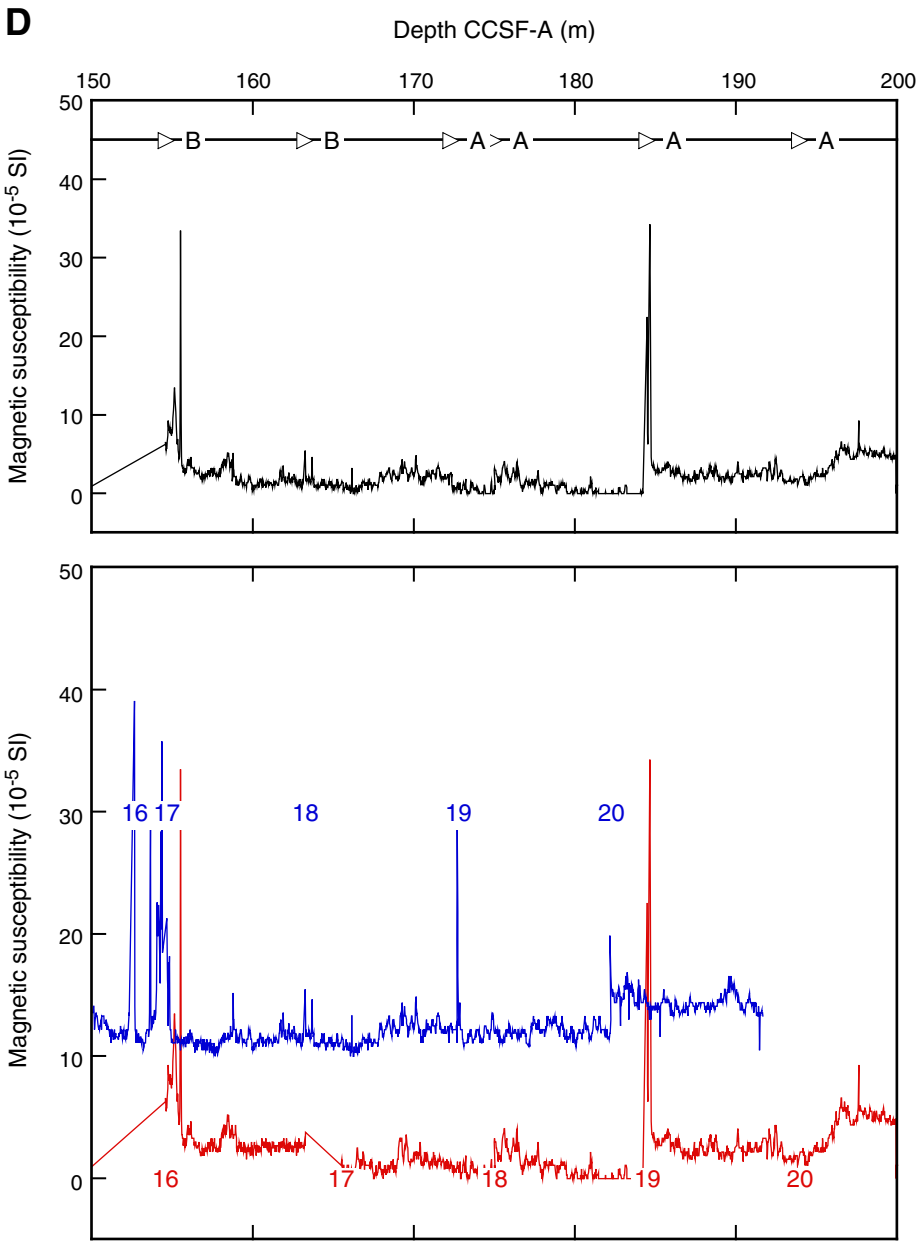

Figure F28. Gamma ray attenuation density data, Holes U1336A (red) and U1336B (blue). Data are offset by a constant 0.5 g/cm³. Upper panels are the Site U1338 splices for the intervals. **A.** 0–50 m CCSF-A. (**Continued on next three pages.**)

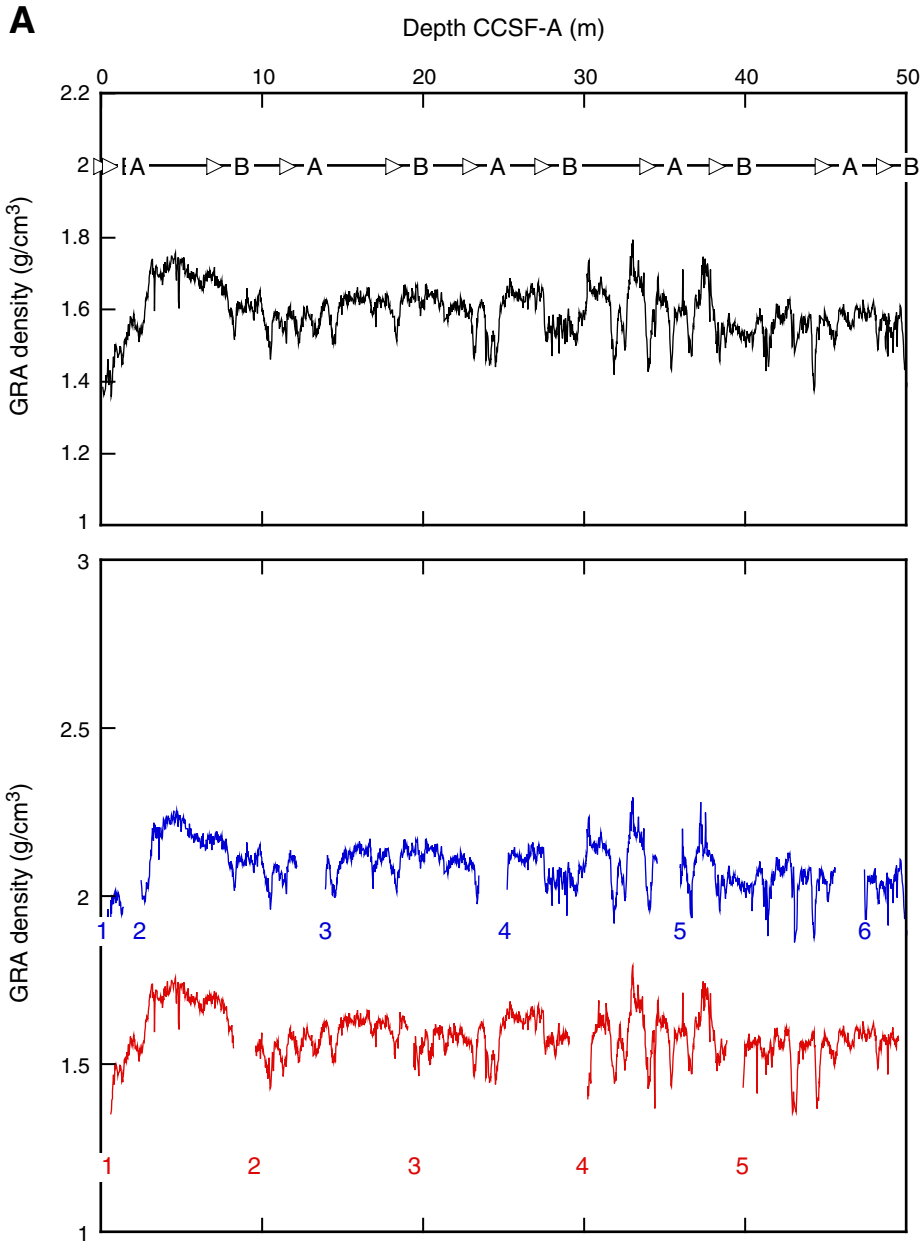

Figure F28 (continued). B. 50–100 m CCSF-A. (Continued on next page.)

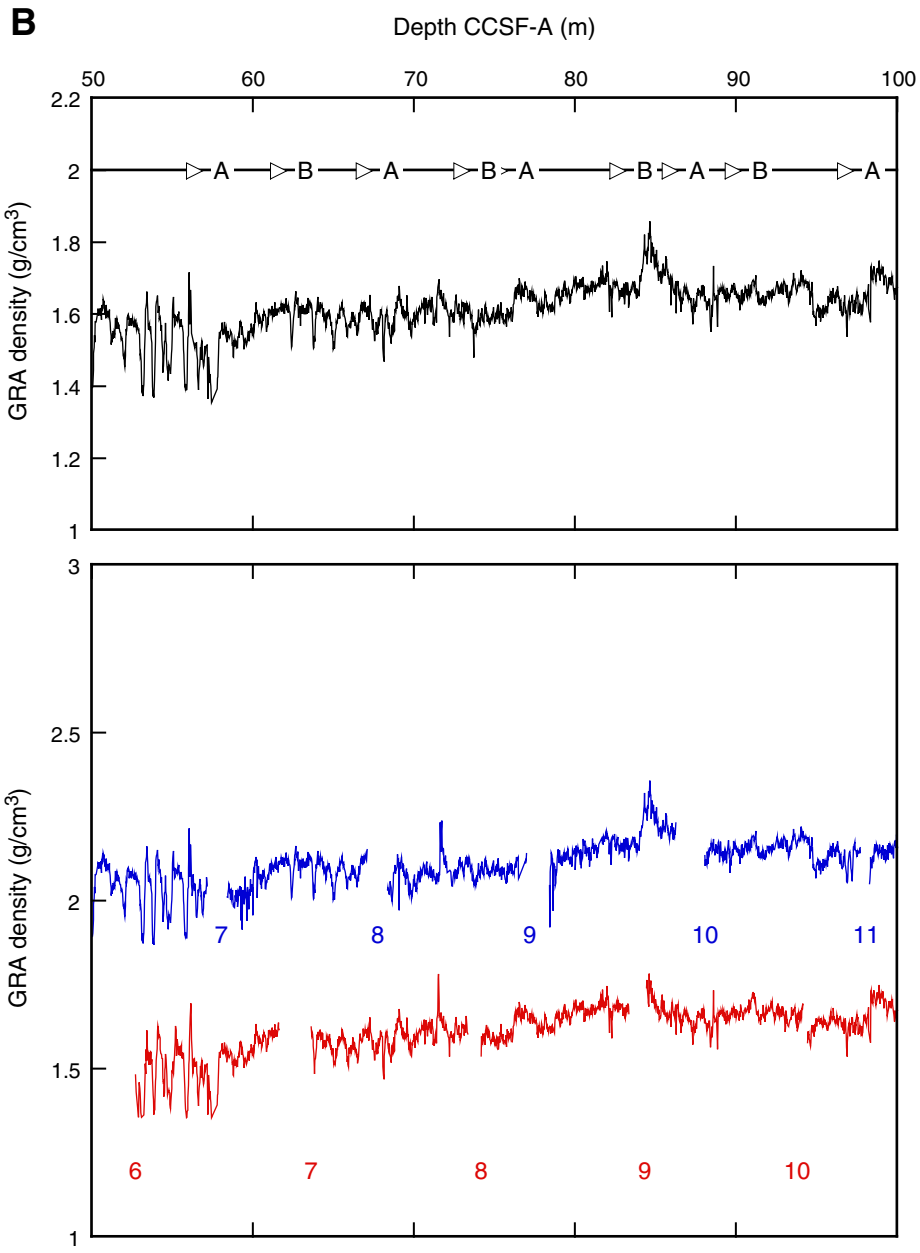

Figure F28 (continued). C. 100–150 m CCSF-A. (Continued on next page.)

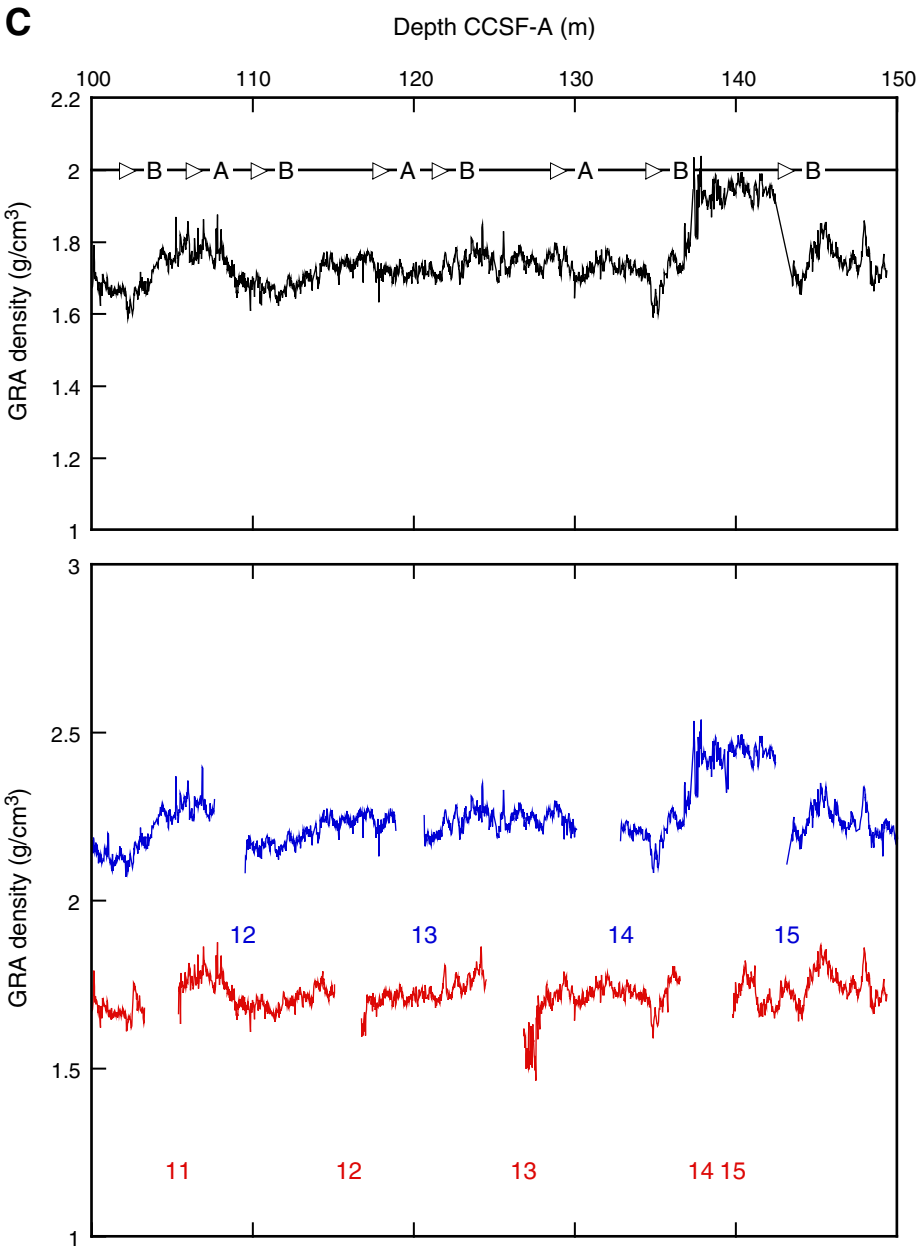

Figure F28 (continued). D. 150–200 m CCSF-A.

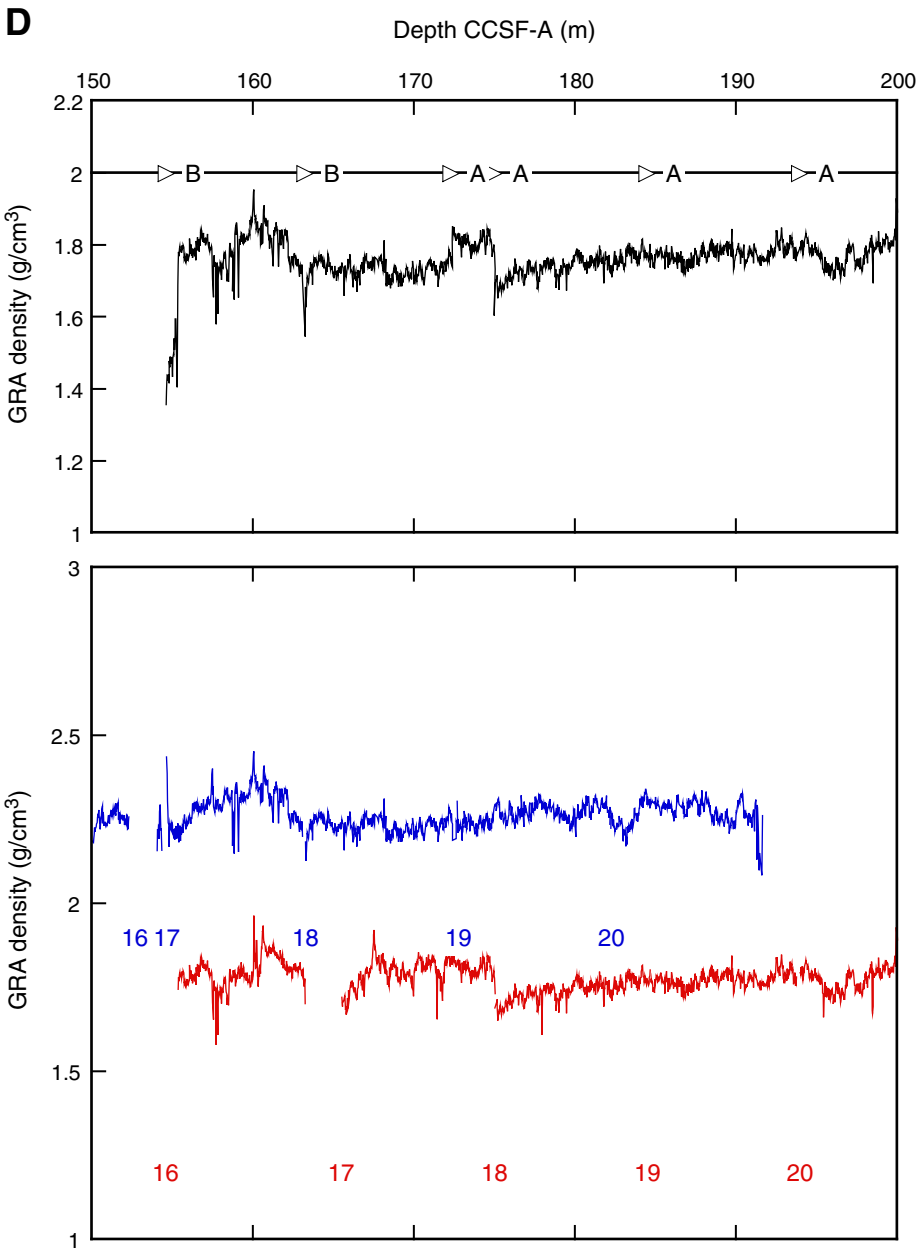

Figure F29. Core images, Holes U1336A and U1336B. Yellow line = top of deepest splice, black bars = disturbed intervals, green lines = floating ties or correlations (see text). Uninterrupted composite section ends at the top of disturbed section in Core 321-U1336B-14H. The most continuous splice appends Core 321-U1336A-15H at this point. Splice continues by appending Cores 320-U1336B-15H through 18H (blue arrow). Splice moves to Core 320-U1336A-18H and stays within Hole U1336A to total depth. Cores 320-U1336A-15H and 320-U1336B-15H can be correlated to one another, but neither can be tied to the rest of the section either above or below.

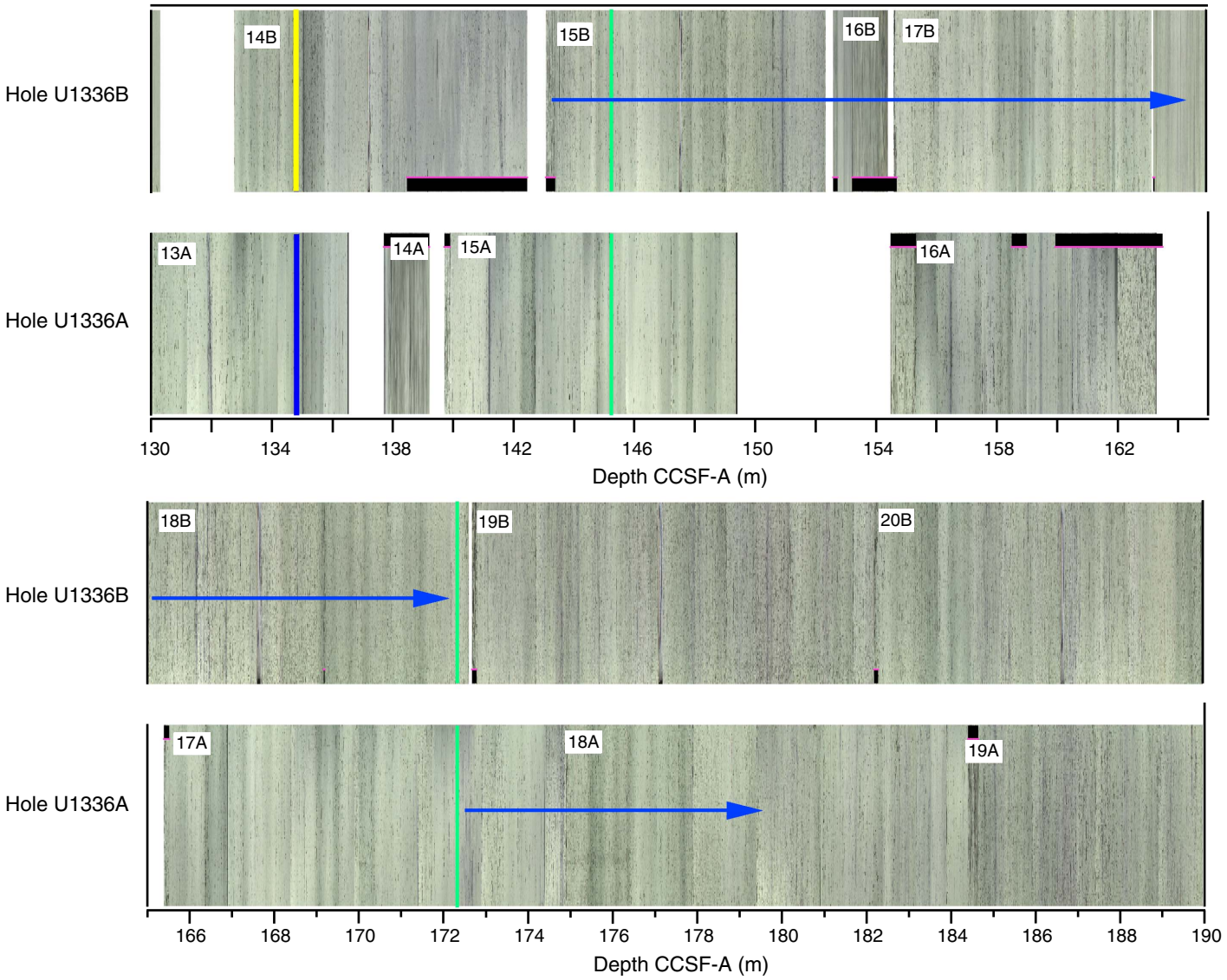

Figure F30. Core depth below seafloor vs. core composite depth below seafloor for tops of cores, Site U1336. Growth factor is slope of the regression line. On average, the core composite depth below seafloor of the spliced section is 13% greater than the core depth below seafloor.

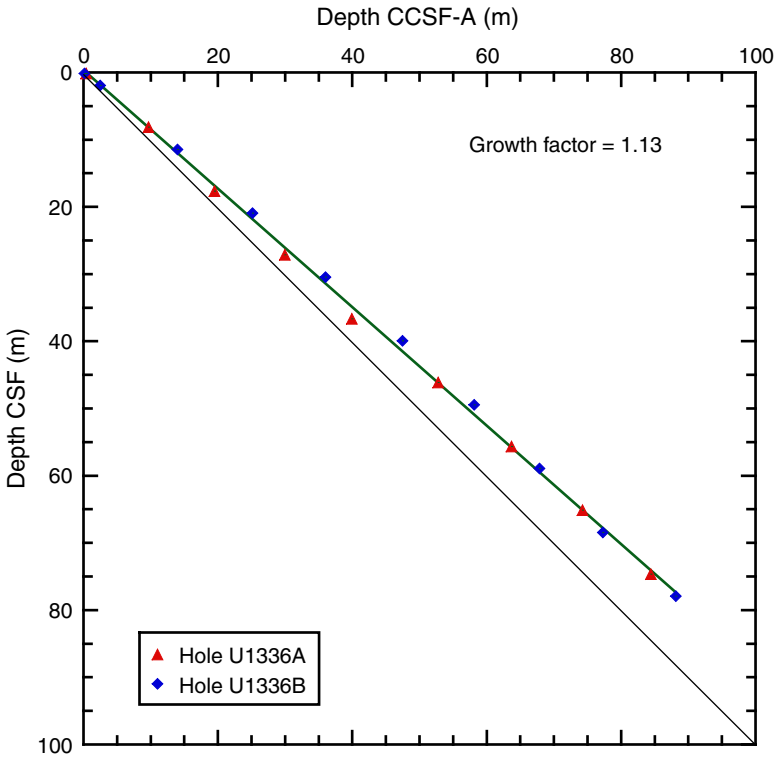

Table T1. Coring summary, Site U1336. (See table notes.) (Continued on next page.)

Site U1336
Time on site (h): 93.5 (1545 h, 22 April–1315 h, 26 April 2009)

Hole U1336A
Latitude: 7°42.074′N
Longitude: 128°15.253′W
Time on hole (h): 60.3 (1545 h, 22 April–0400 h, 25 April 2009)
Seafloor (drill pipe measurement below rig floor, m DRF): 4296.9
Distance between rig floor and sea level: 11.6 m
Water depth (drill pipe measurement from sea level, mbsl): 4285.3
Total depth (drill pipe measurement from rig floor, m DRF): 4599.8
Total penetration (drilling depth below seafloor, m DSF): 302.9
Total length of cored section (m): 302.9
Total core recovered (m): 259.1
Core recovery (%): 86
Total number of cores: 35

Hole U1336B
Latitude: 7°42.060′N
Longitude: 128°15.253′W
Time on hole (h): 33.3 (0400 h, 25 April–1315 h, 26 April 2009)
Seafloor (drill pipe measurement below rig floor, m DRF): 4298.1
Distance between rig floor and sea level: 11.6 m
Water depth (drill pipe measurement from sea level, mbsl): 4286.5
Total depth (drill pipe measurement from rig floor, m DRF): 4472.0
Total penetration (drilling depth below seafloor, m DSF): 173.9
Total length of cored section (m): 173.9
Total core recovered (m): 179.59
Core recovery (%): 103
Total number of cores: 20

Core	Date (2009)	Local time (h)	Depth DSF (m) Top of cored interval	Depth DSF (m) Bottom of cored interval	Interval advanced (m)	Depth CSF (m) Top of cored interval	Depth CSF (m) Bottom of cored interval	Length of core recovered (m)	Recovery (%)
320-U1336A-									
1H	23 Apr	0200	0.0	8.0	8.0	0.00	8.24	8.24	103
2H	23 Apr	0255	8.0	17.5	9.5	8.00	17.73	9.73	102
3H	23 Apr	0355	17.5	27.0	9.5	17.50	27.52	10.02	105
4H	23 Apr	0455	27.0	36.5	9.5	27.00	36.25	9.25	97
5H	23 Apr	0550	36.5	46.0	9.5	36.50	46.46	9.96	105
6H	23 Apr	0645	46.0	55.5	9.5	46.00	55.19	9.19	97
7H	23 Apr	0750	55.5	65.0	9.5	55.50	65.61	10.11	106
8H	23 Apr	0850	65.0	74.5	9.5	65.00	74.43	9.43	99
9H	23 Apr	0940	74.5	84.0	9.5	74.50	84.63	10.13	107
10H	23 Apr	1040	84.0	93.5	9.5	84.00	93.83	9.83	103
11H	23 Apr	1135	93.5	103.0	9.5	93.50	103.53	10.03	106
12H	23 Apr	1235	103.0	112.5	9.5	103.00	112.48	9.48	100
13H	23 Apr	1330	112.5	122.0	9.5	112.50	122.63	10.13	107
14H	23 Apr	1440	122.0	123.5	1.5	122.00	123.55	1.55	103
15H	23 Apr	1605	123.5	133.0	9.5	123.50	133.43	9.93	105
16H	23 Apr	1705	133.0	142.0	9.0	133.00	142.04	9.04	100
17H	23 Apr	1910	142.0	151.5	9.5	142.00	151.89	9.89	104
18H	23 Apr	2005	151.5	161.0	9.5	151.50	161.58	10.08	106
19H	23 Apr	2125	161.0	170.5	9.5	161.00	170.65	9.65	102
20H	23 Apr	2225	170.5	180.0	9.5	170.50	180.18	9.68	102
21H	23 Apr	2325	180.0	184.8	4.8	180.00	184.83	4.83	101
22X	24 Apr	0340	184.8	194.4	9.6	184.80	192.77	7.97	83
23X	24 Apr	0535	194.4	202.4	8.0	194.40	202.20	7.80	98
24X	24 Apr	0725	202.4	212.0	9.6	202.40	209.67	7.27	76
25X	24 Apr	0835	212.0	221.6	9.6	212.00	216.96	4.96	52
26X	24 Apr	0955	221.6	231.2	9.6	221.60	231.00	9.40	98
27X	24 Apr	1100	231.2	240.8	9.6	231.20	237.83	6.63	69
28X	24 Apr	1235	240.8	250.4	9.6	240.80	243.83	3.03	32
29X	24 Apr	1355	250.4	260.0	9.6	250.40	254.57	4.17	43
30X	24 Apr	1505	260.0	269.6	9.6	260.00	264.50	4.43	47
31X	24 Apr	1630	269.6	279.2	9.6	269.60	274.61	5.01	52
32X	24 Apr	1800	279.2	288.8	9.6	279.20	283.34	4.14	43
33X	24 Apr	1950	288.8	293.8	5.0	288.80	291.29	2.49	50

Table T1 (continued).

Core	Date (2009)	Local time (h)	Depth DSF (m) Top of cored interval	Depth DSF (m) Bottom of cored interval	Interval advanced (m)	Depth CSF (m) Top of cored interval	Depth CSF (m) Bottom of cored interval	Length of core recovered (m)	Recovery (%)
34X	24 Apr	2255	293.8	298.3	4.5	293.80	294.12	0.32	7
35X	25 Apr	0200	298.3	302.9	4.6	298.30	299.62	1.32	29
				Cored totals:	302.9			259.12	86
				Total interval cored:	302.9				
320-U1336B-									
1H	25 Apr	0610	0.0	1.8	1.8	0.00	1.73	1.73	96
2H	25 Apr	0710	1.8	11.3	9.5	1.80	11.88	10.08	106
3H	25 Apr	0815	11.3	20.8	9.5	11.30	21.16	9.86	104
4H	25 Apr	0910	20.8	30.3	9.5	20.80	30.57	9.77	103
5H	25 Apr	1010	30.3	39.8	9.5	30.30	40.30	10.00	105
6H	25 Apr	1110	39.8	49.3	9.5	39.80	49.90	10.10	106
7H	25 Apr	1205	49.3	58.8	9.5	49.30	58.68	9.38	99
8H	25 Apr	1300	58.8	68.3	9.5	58.80	68.50	9.70	102
9H	25 Apr	1355	68.3	77.8	9.5	68.30	77.77	9.47	100
10H	25 Apr	1450	77.8	87.3	9.5	77.80	87.80	10.00	105
11H	25 Apr	1550	87.3	96.8	9.5	87.30	97.25	9.95	105
12H	25 Apr	1645	96.8	106.3	9.5	96.80	106.60	9.80	103
13H	25 Apr	1740	106.3	115.8	9.5	106.30	116.41	10.11	106
14H	25 Apr	1845	115.8	125.3	9.5	115.80	125.89	10.09	106
15H	25 Apr	1940	125.3	134.8	9.5	125.30	134.83	9.53	100
16H	25 Apr	2045	134.8	136.8	2.0	134.80	136.86	2.06	103
17H	25 Apr	2150	136.8	145.4	8.6	136.80	145.66	8.86	103
18H	25 Apr	2315	145.4	154.9	9.5	145.40	155.05	9.65	102
19H	26 Apr	0020	154.9	164.4	9.5	154.90	164.74	9.84	104
20H	26 Apr	0150	164.4	173.9	9.5	164.40	174.01	9.61	101
				Cored totals:	173.9			179.59	103
				Total interval cored:	173.9				

Notes: DRF = drilling depth below rig floor, DSF = drilling depth below seafloor, CSF = core depth below seafloor. H = APC core, X = XCB core. Local time = UTC – 10 h.

Table T2. Lithologic unit boundaries, Site U1336. (See table notes.)

Unit	Lithologic summary	Core, section, interval (cm)	Depth CSF (m)	Core, section, interval (cm)	Depth CSF (m)
		320-U1336A-		320-U1336B-	
I	Nannofossil ooze with minor but varying amounts of clay, radiolarians, and foraminifers; two thin intervals of diatom nannofossil ooze.	8H-7, 5	73.05	9H-5, 84	75.14
II	Nannofossil ooze, minor chert near base, vivid redox coloring from pale yellow to greenish gray, very low magnetic susceptibility values.	22H-4, 20	189.5	20H-7, 58	173.98†
III*	Nannofossil chalk and chert.	35X-CC, 38	299.6		

Notes: Intervals/depths are given for basal boundary of each unit. * = unit extends through at least given interval and depth, but boundary was not cored, † = end of Hole U1336B.

Table T3. Calcareous nannofossil datums, Site U1336. (See table note.)

Core, section, interval (cm)		Marker species	Age (Ma)	Depth CSF (m)			
Top	Bottom			Top	Bottom	Midpoint	±
320-U1336A-	320-U1336A-						
—	1H-1, 110	T *Coronocyclus nitescens*	12.12		1.10	1.10	
—	1H-1, 110	T *Calcidiscus premacintyrei*	12.45		1.10	1.10	
2H-4, 80	2H-6, 80	Tc *Cyclicargolithus floridanus*	13.33	13.30	16.30	14.80	1.50
2H-CC	3H-2, 90	T *Sphenolithus heteromorphus*	13.53	17.68	19.90	18.79	1.11
4H-2, 90	4H-4, 90	Tc *Discoaster deflandrei*	15.66	29.40	32.40	30.90	1.50
5H-4, 64	5H-6, 35	B *Discoaster petaliformis*	15.70	41.64	44.35	43.00	1.36
7H-2, 50	7H-3, 52	Bc *Sphenolithus heteromorphus*	17.71	57.50	59.02	58.26	0.76
7H-2, 50	7H-3, 52	Tc *Sphenolithus belemnos*	17.95	57.50	59.02	58.26	0.76
7H-2, 50	7H-3, 52	T *Triquetrorhabdulus carinatus*	18.28	57.50	59.02	58.26	0.76
8H-CC	9H-1, 55	B *Sphenolithus belemnos*	19.03	74.38	75.05	74.72	0.34
13H-6, 60	13H-CC	Tc *Triquetrorhabdulus carinatus*	22.09	120.60	122.58	121.59	0.99
15H-CC	16H-2, 90	B *Sphenolithus disbelemnos*	22.80	133.38	135.40	134.39	1.01
		Oligocene/Miocene boundary					
17H-2, 90	17H-4, 90	T *Sphenolithus delphix*	23.1	144.40	147.40	145.90	1.50
17H-6, 90	17H-CC	B *Sphenolithus delphix*	23.2	150.40	151.84	151.12	0.72
20H-5, 100	20H-CC	T *Sphenolithus ciperoensis*	24.4	177.50	180.13	178.82	1.32
20H-5, 100	20H-CC	X *T. longus*/*T. carinatus*	24.7	177.50	180.13	178.82	1.32
19H-5, 70	19H-6, 70	Tc *Cyclicargolithus abisectus*	24.7	167.70	169.20	168.45	0.75
24X-1, 112	24X-3, 73	T *Sphenolithus distentus*	26.8	203.52	206.13	204.83	1.30
24X-3, 112	24X-5, 53	T *Sphenolithus predistentus*	26.9	206.13	208.93	207.53	1.40
24X-5, 53	24X-CC	B *Sphenolithus ciperoensis*	27.1	208.93	209.62	209.28	0.34
29X-3, 40	29X-CC	B *Sphenolithus distentus*	30.0	253.80	254.52	254.16	0.36
34X-CC	35X-1, 34	T *Reticulofenestra umbilicus*	32.0	294.07	298.64	296.36	2.29
321-U1336B-	321-U1336B-						
1H-CC	2H-CC	T *Coronocyclus nitescens*	12.12	1.68	11.88	6.78	5.10
1H-CC	2H-CC	T *Calcidiscus premacintyrei*	12.45	1.68	11.88	6.78	5.10
2H-CC	3H-CC	Tc *Cyclicargolithus floridanus*	13.33	11.63	21.16	16.40	4.77
2H-CC	3H-CC	T *Sphenolithus heteromorphus*	13.53	11.63	21.16	16.40	4.77
4H-CC	5H-CC	Tc *Discoaster deflandrei*	15.66	30.54	40.30	35.42	4.88
6H-CC	7H-CC	Bc *Sphenolithus heteromorphus*	17.71	49.87	58.68	54.28	4.41
6H-CC	7H-CC	T *Sphenolithus belemnos*	17.95	49.87	58.68	54.28	4.41
6H-CC	7H-CC	T *Triquetrorhabdulus carinatus*	18.28	49.87	58.68	54.28	4.41
9H-CC	10H-CC	B *Sphenolithus belemnos*	19.03	77.72	87.80	82.76	5.04
14H-1, 149	14H-2, 149	Tc *Triquetrorhabdulus carinatus*	22.09	117.29	118.79	118.04	0.75
15H-1, 10	15H-2, 10	B *Sphenolithus disbelemnos*	22.80	125.40	126.90	126.15	0.75
		Oligocene/Miocene boundary					
16H-CC	17H-1, 150	T *Sphenolithus delphix*	23.1	136.81	138.30	137.56	0.75
17H-3,149	17H-4, 148	B *Sphenolithus delphix*	23.2	141.29	142.78	142.04	0.75

Note: T = top, Tc = top common, B = bottom, Bc = bottom common, X = abundance crossover.

Table T4. Radiolarian datums, Site U1336. (See table notes.)

Geologic age	Zone	Marker species	Age (Ma)	Core, section, interval (cm)		Depth CSF (m)			
				Top	Bottom	Top	Bottom	Midpoint	±
	RN6			320-U1336A-	320-U1336A-				
		B *D. petterssoni*	12.11	1H-4, 104–106	1H-CC	5.54	8.19	6.87	1.33
	RN5	B *C. japonica*	12.41	1H-4, 104–106	1H-CC	5.54	8.19	6.87	1.33
		B *L. neotera*	12.95	1H-CC	2H-2, 105–107	8.19	10.55	9.37	1.18
		T *C. robusta*	13.348	2H-CC	3H-2, 105–107	17.68	20.05	18.87	1.19
		T *S. armata*	13.5	2H-CC	3H-2, 105–107	17.68	20.05	18.87	1.19
		T *A. octopylus*	13.88	3H-2, 105–107	3H-4, 105–107	20.05	23.05	21.55	1.50
		T *C. costata*	14.229	3H-4, 105–107	3H-CC	23.05	27.47	25.26	2.21
		T *D. dentata*	14.666	4H-2, 105–107	4H-4, 105–107	27.47	32.55	30.01	2.54
		T *L. stauropora*	14.826	4H-2, 105–107	4H-4, 105–107	27.47	32.55	30.01	2.54
		D. dentata > *D. alata*	14.78	4H-2, 105–107	4H-4, 105–107	27.47	32.55	30.01	2.54
middle Miocene	RN4	B *D. alata*	15.08	4H-CC	5H-2, 105–107	36.20	39.05	37.63	1.43
		B *L. parkerae*	15.03	4H-CC	5H-2, 105–107	36.20	39.05	37.63	1.43
		T *C. cingulata*	15.13	5H-4, 105–107	5H-CC	42.05	46.41	44.23	2.18
		T *L. elongata*	15.15	6H-2, 105–107	6H-4, 105–107	48.55	48.57	48.56	0.01
		B *L. renzae*	16.77	6H-2, 105–107	6H-4, 105–107	48.55	48.57	48.56	0.01
		B *C. costata*	17.49	6H-4, 105–107	6H-CC	48.57	55.14	51.86	3.29
	RN3	B *D. dentata*	17.72	6H-CC	7H-2, 104–106	55.14	58.04	56.59	1.45
		B *L. stauropora*	17.72	6H-CC	7H-2, 104–106	55.14	58.04	56.59	1.45
		T *D. scambos*	18.53	7H-4, 104–106	7H-CC	61.05	65.60	63.33	2.28
		B *S. wolffii*	18.57	8H-2, 105–107	8H-4, 105–107	67.55	70.55	69.05	1.50
	RN2	B *D. forcipata*	18.61	8H-2, 105–107	8H-4, 105–107	67.55	70.55	69.05	1.50
		T *D. simplex*	18.69	8H-CC	9H-2, 105–107	74.38	77.05	75.72	1.34
		T *D. praeforcipata*	19.77	9CC	10H-2, 105–107	84.60	86.56	85.58	0.98
		B *D. simplex*	20.34	10H-4, 105–107	10H-CC	89.55	93.78	91.67	2.12
early Miocene		B *S. delmontensis*	20.68	11H-2, 105–107	11H-4, 105–107	96.05	99.05	97.55	1.50
		T *L. pegetrum*	20.89	11H-4, 105–107	11H-CC	99.05	103.48	101.27	2.22
		T *T. annosa*	21.38	12H-2, 105–107	12H-4, 105–107	105.55	108.55	107.05	1.50
	RN1	B *C. virginis*	21.39	11H-CC	12H-2, 105–107	103.48	105.55	104.52	1.04
		T *E. mitodes*	21.95	13H-4, 104–106	13H-CC	118.04	122.58	120.31	2.27
		B *C. serrata*	22.04	15H-2, 105–104	15H-4, 105–107	126.05	129.05	127.55	1.50
		B *C. cornuta*	22.26	15H-4, 105–107	15H-CC	129.05	133.38	131.22	2.16
		B *C. tetrapera*	22.35	15H-4, 105–107	15H-CC	129.05	133.38	131.22	2.16
	RP22	T *A. gracilis*	22.62	16H-2, 105–107	16H-4, 105–107	133.55	138.55	136.05	2.50
		B *E. diaphanes*	22.95	16H-CC	17H-2, 105–107	141.99	144.55	143.27	1.28
		T *D. cyclacantha*	22.98	16H-CC	17H-2, 105–107	141.99	144.55	143.27	1.28
		B *D. cyclacantha*	23.29	17H-2, 105–107	17H-4, 105–107	144.55	147.55	146.05	1.50
late Oligocene		T *D. papilio*	23.31	17H-4, 105–107	17H-CC	147.55	151.84	149.70	2.15
		T *L. longicornuta*	24.12	18H-2, 105–107	18H-4, 105–107	154.04	157.05	155.55	1.51
		T *L. apodora*	24.50	—	—			0.00	0.00
		B *L. elongata*	25.05	—	—			0.00	0.00

Notes: B = bottom, T = top. — = not encountered.

Table T5. Preservation and relative abundance of radiolarians, Hole U1336A. This table is available in an **oversized format.**

Table T6. Preservation and relative abundance of radiolarians, Hole U1336B. (**See table notes.**)

Core, section, interval (cm)	Radiolarian zone	Abundance	Preservation	Mixing	*Acrocubus octopylus*	*Artophormis gracilis*	*Botryostrobus miralestensis*	*Calocycletta caepa*	*Calocycletta costata*	*Calocycletta robusta*	*Calocycletta serrata*	*Calocycletta virginis*	*Carpocanopsis cingulata*	*Cyrtocapsella cornuta*	*Cyrtocapsella tetrapera*	*Diartus petterssoni*	*Didymocyrtis bassanii*	*Didymocyrtis laticonus*	*Didymocyrtis prismatica*	*Didymocyrtis tubaria*	*Didymocyrtis violina*	*Dorcadospyris alata*	*Dorcadospyris ateuchus*	*Dorcadospyris cyclacantha*	*Dorcadospyris dentata*	*Dorcadospyris forcipata*	*Dorcadospyris papilio*	*Dorcadospyris praeforcipata*	*Dorcadospyris riedeli*	*Dorcadospyris scambos*	*Eucyrtidium diaphanes*	*Liriospyris parkerae*	*Liriospyris stauropora*	*Lithopera neotera*	*Lithopera renzae*	*Lychnocanoma elongata*	*Lychnodictyum audax*	*Phormostichoartus fistula*	*Stichocorys delmontensis*	*Stichocorys wolffii*	*Theocyrtis amnosa*
320-U1336B-																																							
1H-CC	RN6	C	G				F	F							F	F		C				R									R					F	C			
2H-CC	RN5	C	G				F	R						R				F				R								R			F	R				C		
3H-CC		C	G				F			C				R	R							R									F						C		
4H-CC		C	G				R		F	C				R	R							R									F						C		
5H-CC	RN4	C	G				F		F	F		R		R	R						R				F	R					R					R	C		
6H-CC		C	G						R	F		F		R					R		F				F	R				R		R				R	F		
7H-CC	RN3	C	G				R			F		R	R	R	F				R		R					R									R		R	F	R	
8H-CC		C	G				R			F		R	R	R					R	R						R									R	R	R	F		
9H-CC	RN2	C	G							F		R	R	F	R		R		R		R					R			R						F		R	F		
10H-CC		C	M							F		R			R				R	R									R	R					F			F		
11H-CC		C	M							F				R	F		R		R										R						F			F		
12H-CC		C	M							F				R	R		R		R																R					
13H-CC		C	M				R			F				R	F				R										R	R					F					
14H-CC	RN1	C	M							R				R	R																				F					R
15H-CC	RP22	C	M							F							R		R																F					F
16H-CC	RP22?	R	M							R									R																R		R			
17H-CC	RP22	C	M							F							R		R				R	R					R						F					F
18H-CC		C	M							F									R				R						R						F					F
19H-CC		C	M			R				F									R				R				R	R	R						F					F
20H-CC		C	M		R	R				F									R				R					R							R					F

Notes: Abundance: C = common, F = frequent, R = rare. Preservation: G = good, M = moderate. Mixing: blank = no mixing of older specimens detected.

Table T7. Distribution of diatoms, Site U1336. (See table notes.)

Core, section	Preservation	Abundance	*Cestodiscus peplum*	*Cestodiscus pulchellus*	*Cestodiscus trochus*	*Coscinodiscus lewisianus* var. *spiralis*	*Crucidenticula nicobarica*	*Ethmodiscus* (fragments)	*Hemidiscus cuneiformis*	*Rhaphidiscus marylandicus*	*Rocella vigilans*	*Rosiella paleaceae*	*Synedra jouseana/miocenica*	*Thalassionema nitzschioides* var. *parva*	*Thalassionema robusta*	*Thalassiothrix yabei*
320-U1336B-																
1H-CC	M	F	?	R			R	R					F			R
2H-CC	P	R					R				?	R			?	
3H-CC	P–M	R							R							
4H-CC		B														
5H-CC	P	R		R				R								
6H-CC	P	R			?										?	
7H-CC	P–M	R		R		?				?				R		
8H-CC		B														
9H-CC		B														
10H-CC		B														
11H-CC		B														
12H-CC		B														
13H-CC		B														
14H-CC		B														
15H-CC		B														
16H-CC		B														
17H-CC		B														
18H-CC		B														
19H-CC		B														
20H-CC		B														

Notes: All samples are of middle Miocene age. Preservation: M = moderate, P = poor. Abundance: F = few, R = rare, B = barren, ? = uncertainty.

Table T8. Planktonic foraminifer datums, Site U1336. (See table note.)

Core, section, interval (cm)		Marker species	Age (Ma)	Depth CSF (m)			
Top	Bottom			Top	Bottom	Midpoint	±
320-U1336A-	320-U1336A-						
—	1H-3, 38–40	T *Globorotalia (Fohsella) fohsi* s.l.	11.79	0.00	3.38	1.69	1.69
1H-3, 38–40	1H-CC	B *Globorotalia (Fohsella) fohsi robusta*	13.13	3.38	8.19	5.79	2.41
2H-CC	3H-2, 38–40	B *Globorotalia (Fohsella) fohsi* s.l.	13.41	17.68	19.38	18.53	0.85
3H-2, 38–40	3H-5, 38–40	B *Globorotalia (Fohsella) "praefohsi"*	13.77	19.38	23.88	21.63	2.25
3H-2, 38–40	3H-5, 38–40	T *Clavatorella bermudezi*	13.82	19.38	23.88	21.63	2.25
3H-5, 38–40	3H-CC	T *Globorotalia (Fohsella) peripheroronda*	13.80	23.88	27.47	25.68	1.80
3H-CC	4H-3, 38–40	B *Globorotalia (Fohsella) peripheroacuta*	14.24	27.47	30.38	28.93	1.46
3H-5, 38–40	3H-CC	B *Orbulina* spp.	14.74	23.88	27.47	25.68	1.80
3H-CC	4H-3, 38–40	B *Clavatorella bermudezi*	14.89	27.47	30.38	28.93	1.46
5H-CC	6H-2, 38–40	B *Praeorbulina glomerosa*	16.27	46.41	47.88	47.15	0.73
5H-CC	6H-2, 38–40	B *Praeorbulina sicana*	16.97	46.41	47.88	47.15	0.73
8H-2, 38–40	8H-4, 38-40	T *Globoquadrina binaiensis*	19.09	66.88	69.88	68.38	1.50
10H-CC	11H-2, 30–32	T *Paragloborotalia kugleri*	21.12	93.78	95.30	94.54	0.76
10H-CC	11H-2, 30–32	T *Paragloborotalia pseudokugleri*	21.31	93.78	95.30	94.54	0.76
15H-2, 38–40	15H-4, 38–40	B *Globoquadrina dehiscens*	22.44	125.38	128.38	126.88	1.50
		Oligocene/Miocene boundary					
16H-CC	17H-2, 38–40	B *Paragloborotalia kugleri*	23.0	141.99	143.88	142.94	0.94
19H-CC	20H-2, 38–40	B *Paragloborotalia pseudokugleri*	25.2	170.60	172.38	171.49	0.89
23X-CC	24X-2, 41–43	T *Paragloborotalia opima*	26.9	202.15	207.30	204.73	2.58
25X-2, 45–47	25X-CC	Tc *Chiloguembelina cubensis*	28.0	213.95	216.91	215.43	1.48
27X-CC	28X-2, 20–22	B *Globigerina angulisuturalis*	29.2	237.38	242.50	239.94	2.56
29X-2, 24–26	29X-CC	T *Subbotina angiporoides*	29.8	242.50	252.14	247.32	4.82
29X-CC	30X-2, 38–40	T *Turborotalia ampliapertura*	30.3	254.52	261.88	258.20	3.68
29X-CC	30X-2, 38–40	B *Paragloborotalia opima*	30.8	254.52	261.88	258.20	3.68
321-U1336B-	321-U1336B-						
1H-CC	2H-CC	B *Globorotalia (Fohsella) fohsi robusta*	13.13	1.73	11.85	6.79	5.06
2H-CC	3H-CC	B *Globorotalia (Fohsella) fohsi* s.l.	13.41	11.88	21.13	16.51	4.63
2H-CC	3H-CC	B *Globorotalia (Fohsella) "praefohsi"*	13.77	11.88	21.13	16.51	4.63
2H-CC	3H-CC	T *Clavatorella bermudezi*	13.82	11.88	21.13	16.51	4.63
3H-CC	4H-CC	B *Globorotalia (Fohsella) peripheroacuta*	14.24	21.16	30.54	25.85	4.69
3H-CC	4H-CC	B *Orbulina* spp.	14.74	21.16	30.54	25.85	4.69
3H-CC	4H-CC	B *Clavatorella bermudezi*	14.89	21.16	30.54	25.85	4.69
4H-CC	5H-CC	B *Praeorbulina glomerosa*	16.27	30.57	40.27	35.42	4.85
5H-CC	6H-CC	B *Praeorbulina sicana*	16.97	40.30	49.87	45.09	4.79
7H-CC	8H-CC	T *Catapsydrax dissimilis*	17.54	58.68	68.45	63.57	4.89
8H-CC	9H-CC	T *Globoquadrina binaiensis*	19.09	68.50	77.72	73.11	4.61
11H-CC	12H-CC	T *Paragloborotalia kugleri*	21.12	97.25	106.54	101.90	4.65
13H-CC	14H-CC	T *Paragloborotalia pseudokugleri*	21.31	116.41	125.84	121.13	4.72
14H-CC	15H-CC	B *Globoquadrina dehiscens*	22.44	125.84	134.83	130.34	4.50
16H-1, 52–54	17H-3, 80–82	T *Globigerina ciperoensis*	22.90	134.83	140.60	137.72	2.88
		Oligocene/Miocene boundary					
16H-1, 52–54	17H-3, 80–82	B *Paragloborotalia kugleri*	23.0	134.83	140.60	137.72	2.88

Note: T = top, B = bottom, Tc = top common occurrence.

Table T9. Distribution of planktonic foraminifers, Hole U1336A. This table is available in an **oversized format.**

Table T10. Distribution of planktonic foraminifers, Hole U1336B. (**See table notes.**) (**Continued on next page.**)

Core, section, interval (cm)	Preservation	Abundance (%)	Zone/Subzone	*Catapsydrax dissimilis*	*Catapsydrax parvulus*	*Catapsydrax unicavus*	*Clavatorella bermudezi*	*Dentoglobigerina altispira*	*Dentoglobigerina altispira globosa*	*Dentoglobigerina baroemoensis*	*Dentoglobigerina larmeui*	*Dentoglobigerina tripartita s.s.*	*Globigerina angustiumbilicata*	*Globigerina bulloides*	*Globigerina ciperoensis*	*Globigerina falconensis*	*Globigerina praebulloides*	*Globigerina winkleri*	*Globigerinita glutinata*	*Globigerinoides altiaperturus*	*Globigerinoides bisphericus*	*Globigerinoides obliquus*	*Globigerinoides primordius*	*Globigerinoides quadrilobatus*	*Globigerinoides sacculifer*	*Globigerinoides subquadratus*	*Globigerinoides trilobus*	*Globoquadrina binaiensis*	*Globoquadrina dehiscens*	*Globoquadrina sellii*	*Globoquadrina venezuelana*	*Globorotalia (Fohsella) fohsi*	*Globorotalia (Forsella) fohsi lobata*	*Globorotalia (Fohsella) fohsi robusta*	*Globorotalia (Fohsella) peripheroacuta*	*Globorotalia (Fohsella) peripheroronda*	*Globorotalia (Fohsella) "praefohsi"*	*Globorotalia (Menardella) menardii*	*Globorotalia (Menardella) praemenardii*	*Globorotalia praescitula*	*Globorotaloides suteri*	*Globoturborotalita druryi*	*Orbulina suturalis*	*Orbulina universa*	*Paragloborotalia bella*	*Paragloborotalia continuosa*	*Paragloborotalia kugleri*	*Paragloborotalia mayeri*
320-U1336B-																																															
1H-CC	M	42	N12					D	F	A						R													F		A	P	P	P						R			P		P	
2H-CC	M	87	N12					D		A				R		F								P	P	R			R		R	P	P		R				P			P		A	
3H-CC	M	99	N10				R	D		A									P			R		P	P	P	R		P		F			P			R	P	P		R	R			R	
4H-CC	M	87	M5b					D		F							P					R		R		F	R		R		D				P		P	P				P		R	
5H-CC	M	92	M5b			R		D	R	A							R					R		R		R			R		A								P					F	
6H-CC	P	24	M4					D	R	R	A										P		R			R	R		R		F													F	
7H-CC	M	40	M4			R		D	R	R	A	F														P			F		A													P	
8H-CC	M	84	M2-M3	R				D	A	R	A	R	R																F		A								P					F	
9H-CC	M	96	M2-M3	R		R		R	D	R	A	A	R				R						R					P		P	A								P	P			F	
10H-CC	M	89	M2-M3	R				A	R		A	A																			A								P					F	
11H-CC	M	95	M2-M3	F	R			F			D	A	R							P			P					P		P	A								P					P	
12H-CC	P	95	M1b	R		F					A	R	A				R										R				A								R			P	A		
13H-CC	P	78	M1b	R		R		A		R	A	F	F														R	P	R	P	A								R			P	F		
14H-CC	P	80	M1b			A					A	A																	A		A											P	R		
15H-CC	P	43	M1a	R		D			P		R	F																		R	D											P	P		
16H-1, 52–54	P	32	M1a			F					R	A			F													R			A											P	F		
16H-CC	P	24	M1b?			A			P	R	A	F															R	P	P	R	D			—				—			P				
17H-3, 80–82	VP	6	O6									P																			P											P		P	
17H-CC	p	65	O6			A					A	A																		R	D											P			
18H-CC	P	77	O6	R		D					R	R																			D											R		A	
19H-CC	P	78	O6	R		D					A	F			P																A													R	
20H-CC	P	67	O6			A					A				R			R													D											R			P	

Notes: Preservation: M = moderate, P = poor, VP = very poor. Abundance: D = dominant, A = abundant, F = few, R = rare, P = present, — = flow-in.

Table T10 (continued).

Core, section, interval (cm)	Preservation	Abundance (%)	Zone/Subzone	*Paragloborotalia nana*	*Paragloborotalia pseudocontinuosa*	*Paraglobrotalia pseudokugleri*	*Paragloborotalia semivera*	*Paragloborotalia siakensis*	*Praeobulina glomerosa*	*Praeorbulina curva*	*Praeorbulina sicana*	*Sphaeroidinellopsis seminulina*	*Sphaeroidnellopsis disjuncta*
320-U1336B-													
1H-CC	M	42	N12					P				P	
2H-CC	M	87	N12					R				R	
3H-CC	M	99	N10										
4H-CC	M	87	M5b						P	R	R		
5H-CC	M	92	M5b					R		P	R		
6H-CC	P	24	M4										R
7H-CC	M	40	M4										
8H-CC	M	84	M2-M3				P						
9H-CC	M	96	M2-M3				P						
10H-CC	M	89	M2-M3				P	F					
11H-CC	M	95	M2-M3				P	F					
12H-CC	P	95	M1b				R						
13H-CC	P	78	M1b			P	R	R					
14H-CC	P	80	M1b		P	P	R	P					
15H-CC	P	43	M1a		P	P	P						
16H-1, 52–54	P	32	M1a		F	P	F	P					
16H-CC	P	24	M1b?		p	R		R					
17H-3, 80–82	VP	6	O6	P	P	P							
17H-CC	p	65	O6		P		R	P					
18H-CC	P	77	O6		F	R		A					
19H-CC	P	78	O6			R	F	P					
20H-CC	P	67	O6				A	P					

Table T11. Distribution of benthic foraminifers, Hole U1336A. (See table notes.) (Continued on next page.)

Core, section, interval (cm)	Depth CSF (m)	Preservation	*Alabamminella weddelensis*	*Amphicoryna* sp.	*Anomalinoides globulosus*	*Anomalinoides* sp. A	*Astrononion echolsi*	*Astrononion* sp. indet.	*Bigenerina* sp.	*Brizalina pusilla*	*Bulimina alazanensis*	*Buliminella parvula*	*Cassidulina* sp. A	*Chrysalogonium crassitestum*	*Chrysalogonium* sp. indet.	*Cibicidoides eocaenus*	*Cibicidoides grimsdalei*	*Cibicidoides havanensis*	*Cibicidoides micrus*	*Cibicidoides mundulus*	*Cibicidoides wuellerstorfi*	*Cibicidoides* sp. A	*Cibicidoides* sp. C	*Cibicidoides* sp. indet.	*Cystammina pauciloculata*	*Dentalina* spp.	*Eggerella bradyi*	*Ehrenbergina hystrix*	*Evolvocassidulina* cf. *howei*	*Favocassidulina favus*	*Favocassidulina spinifer*	*Favocassidulina subfavus*	*Fursenkoina bradyi*	*Glandulina* sp.	*Globocassidulina subglobosa*	*Gyroidinoides soldanii*	*Gyroidinoides* sp. A	*Gyroidinoides* sp. B	*Gyroidinoides* sp. C	*Gyroidinoides* sp. D	*Gyroidinoides* sp. indet.	*Haplophragmoides* sp. indet.	*Heronallenia* sp.	*Karreriella chapapotensis*	*Laticarinina pauperata*	*Lenticulina* spp.	*Martinotiella communis*
320-U1336A-																																													
1H-CC, 21–26	8.22	M										R								F						R							R	R	R			R		R				
2H-CC, 15–20	17.71	G				F														F			R				R						R					R		F				
3H-CC, 24–29	27.50	G					R			R							R	R		A		R		R		R	R				F			F				R		R				
4H-CC, 17–22	36.23	G				R							R					R		R													R	R			R			R				
5H-CC, 21–26	46.44	G				F														R																R			R			R			
6H-CC, 14–19	55.17	G					R		R				R				R			F						R							A	R	R	R		R			R			
7H-CC, 27–32	65.59	G				R	R	R		R							R			F						R					R		F	R		R	R	R						
8H-CC, 14–19	74.41	G								R										F		R				R	R		R			R	A	R	R	R					R			
9H-CC, 21–26	84.61	G				R				R										F		R											F	R							R	F	R		
10H-CC, 20–25	93.81	G				R	F						R					R									R	R				F		F	R	R	R		F	R				
11H-CC, 18–23	103.51	G															R			F													F		R	R			R			R		
12H-CC, 17–22	112.46	G															F			F													F		R	R	F						R	
13H-CC, 26–31	122.61	G				R		R												F		R							R				R		R	F		F	R		R	F		
14H-CC, 0–5	123.53	G				F	R	R					F							F				R		R							F		F		R				R		R	
15H-CC, 22–27	133.41	G																	R					F									F		R		F	F						
16H-CC, 22–27	142.02	G				R						R	R			R	R					F				R					R		A		F		R	R	R		R			
17H-CC, 21–26	151.87	G		R		F		R					R				R			R				R									A			F	R	R	R		R			
18H-CC, 26–31	161.56	G					R					R	R				R			A		R					R						F	R	R			R			R			
19H-CC, 23–28	170.63	G			R		R						F				R	R		R		R		R									A		R	R	F							
20H-CC, 0–5	180.16	M				R	R						R							R		R											A	R	A	R		R			R			
21X-CC, 20–25	184.81	M				F	R					R									R	R	R									R		R	R	R		R			R	R		
22X-CC, 13–18	192.75	M	R			R												R		R	R		R									D		R	R	R	R			R			
23X-CC, 25–30	202.18	M				R	A	R					R							R		R	R									A		F		R		R					
24X-CC, 35–40	209.65	M					R						F		R					R												A												
25X-CC, 41–46	216.94	M												R						F												F			F		R	F				R		
26X-CC, 33–38	237.81	M					R													F												A	R	R			R	R					
27X-CC, 25–30	243.81	M					R						R							R				R								R				R	R	R					
28X-CC, 47–52	254.55	M				R	F					R								R													F	R	R		R						
29X-CC, 48–53	264.41	M				R	F			R		R								A		R										A	F	R		R	A	F			R		
30X-CC, 55–60	264.48	M				F				D										R			R									F	F		R		F						
31X-CC, 33–38	274.59	M				R							R				R	R		F			R	R								A	R	R	R	R	R	F			R		
32X-CC, 38–43	283.32	P				R		F									R	R		A			F	F								F		F		R	F		R				
33X-CC, 70–75	291.27	P				R											F	R		A												R			R		R	R						
34X-CC, 27–32	294.10	M																		P	P												P												
35X-CC, 37–40	299.61	M				R	R	R										R		A			R						R			A	F	R	R		R	F					

Notes: Bathymetry is lower bathyal to abyssal zones. Preservation: G = good, M = moderate, P = poor. Abundance: D = dominant, A = abundant, F = few, R = rare, P = present. * = genus and species indeterminate.

Table T11 (continued).

Core, section, interval (cm)	Depth CSF (m)	Presevation	*Myllostomella* spp.	*Nodosaria* spp.	*Nonion affine*	*Nonion havanensis*	*Nuttallides umbonifer*	*Nuttallides* sp.	*Oridorsalis umbonatus*	*Orthomorphina* spp.	*Paracassidulina* sp.	*Planulina costata*	*Planulina renzi*	*Pleurostomella* spp.	*Pseudoparrella exigua*	*Pseudopleurostomella* spp.	*Pullenia bulloides*	*Pullenia osloensis*	*Pullenia quinqueloba*	*Pullenia salisburyi*	*Pullenia subcarinata*	*Pullenia* sp. A	*Pullenia* sp. indet.	*Pyrulina* spp.	*Quadrimorphina?* sp.	*Quinqueloculina* sp.	*Siphonodosaria antillea*	*Siphonodosaria spinata*	*Siphonodosaria* sp. indet.	*Sphaeroidina bulloides*	*Spiroloculina* sp.	*Spiroplectammina spectabilis*	*Textularia* spp.	*Triloculina* sp.	*Trochammina?* sp.	*Turrilina robertsi*	Tube-shaped agglutinated forms	Unilocular species	*Uvigerina peregrina bradyiana*	*Vulvulina spinosa*	Agglutinated foraminifers*	Calcareous hyaline foraminifers*
320-U1336A-																																										
1H-CC, 21–26	8.22	M					A		R					R	R		R					F	R			R		R	R		R					F				R
2H-CC, 15–20	17.71	G							R								R									R						R								F
3H-CC, 24–29	27.50	G							F				R				R	R		R		R		R		R	R		R		R					F		R		F
4H-CC, 17–22	36.23	G					R		F				R	R								R				R										R					R
5H-CC, 21–26	46.44	G					R							F										R		R										F		R		F
6H-CC, 14–19	55.17	G					R		A			R	R	R	R			R				R		R				R	R		R					F	R	R	R	R
7H-CC, 27–32	65.59	G					R		A					F	R		R							F		R		R	R	R						F				F
8H-CC, 14–19	74.41	G				R	R		A					R			A	R								R		R	R	R			R			F				R
9H-CC, 21–26	84.61	G			R				A					R		R	R									R	R	R								R		R		
10H-CC, 20–25	93.81	G					R		F	R				R	R		F					R							A												
11H-CC, 18–23	103.51	G	R	R			R		A					F			R					R		F			R	R	F								F				R
12H-CC, 17–22	112.46	G							F	R							R									R	R	R		R						R	R			F
13H-CC, 26–31	122.61	G						R	R					F										R				R				R				F				F
14H-CC, 0–5	123.53	G					R		F					F			R					R			R		R	R	R							F				F
15H-CC, 22–27	133.41	G					F		F				R	R			F							F				F						R		R				F
16H-CC, 22–27	142.02	G					R		R					F			R					R		R		R	R	R	R			R				F		R		R
17H-CC, 21–26	151.87	G				R			F							R	F			F	R			R				R								R				F
18H-CC, 26–31	161.56	G				F			A				R	R								R		R					R	R							R				R
19H-CC, 23–28	170.63	G				R			F					R	R				F			R		R			R		R								R		R		F
20H-CC, 0–5	180.16	M				R	R		F	R			R	F			R					R							R	R							A	R			R
21X-CC, 20–25	184.81	M				R	R		F								R		R							R			F							A	R			A
22X-CC, 13–18	192.75	M				R			A					R								R	R				R		R							R				R
23X-CC, 25–30	202.18	M					F		F						R									R					R							F		R		F
24X-CC, 35–40	209.65	M					R		A								R										R									R				F
25X-CC, 41–46	216.94	M					R		A					R										R												R				R
26X-CC, 33–38	237.81	M							F		R								R					R					R		R					R				R
27X-CC, 25–30	243.81	M							R								R	R	R					R					R		R							R		R
28X-CC, 47–52	254.55	M				R			A					F		R	R																			R				
29X-CC, 48–53	264.41	M					R		R					R			R	F					R						R											
30X-CC, 55–60	264.48	M				R			A															R			R									R				R
31X-CC, 33–38	274.59	M			R				A					R			R			R			R	R					R	R					R		R			
32X-CC, 38–43	283.32	P				R			A					R			R												R											
33X-CC, 70–75	291.27	P							A														R																	F
34X-CC, 27–32	294.10	M							P					P												P														
35X-CC, 37–40	299.61	M				R			A					R			R																							

Table T12. Distribution of benthic foraminifers, Hole U1336B. (See table notes.) (Continued on next page.)

Core, section	Top depth CSF (m)	Presevation	Benthic/Planktonic foraminifers (%)	*Ammodiscus* sp.	*Anomalinoides globulosus*	*Astacolus* spp.	*Buliminella parvula*	*Cassidulina* spp.	*Chrysalogonium crassitestum*	*Chrysalogonium* spp.	*Cibicidoides barnetti*	*Cibicidoides bradyi*	*Cibicidoides grimsdalei*	*Cibicidoides havanensis*	*Cibicidoides mundulus*	*Cibicidoides wuellerstorfi*	*Cibicidoides robertsonianus*	*Cibicidoides* spp.	*Dentalina* spp.	*Eggerella bradyi*	*Favocassidulina favus*	*Ehrenbergina histrix*	*Favocassidulina spinifer*	*Favocassidulina subfavus*	*Fissurina formosa*	*Fissurina* spp.	*Gaudryina* spp.	*Glandulina* sp.	*Globulina* spp.	*Globocassidulina subglobosa*	*Gyroidinoides soldanii*	*Gyroidinoides orbicularis*	*Gyroidinoides* spp.	*Karreriella bradyi*	*Laticarinina pauperata*	*Lenticulina* spp.	*Martinotiella communis*	*Melonis barleeanum*	*Myllostomella* spp.	*Nodosaria* spp.	*Nonion havanensis*	*Nuttallides umbonifer*	*Nuttallides* sp.
320-U1336B-																																											
1H-CC	1.68	M	1/99							F			R		A				R										R			F			A		R					F		
2H-CC	11.85	M	1/99		R		R			F		R		R	A	R		R	F	F				R	F			R	F	R		R		R		F					R		
3H-CC	21.13	M	1/99				R	R				R	R		A				R											F	R	F		R	R							R		
4H-CC	30.54	M	1/99		R			R					F	F	R			R	R	R			R	R		F			R		R	F				R		F		R	R		
5H-CC	40.27	M	1/99			R				F			F	F	R		R		R							F		R			F	R	F		A		R				R		
6H-CC	49.87	P	25/75		R	R				R			F	R	F		F			R		R							A	F						F			R	R		
7H-CC	58.63	M	2/98		R					R			F	F	F		R	R	F	F		R				R			A	R	R	F		F		R				R		
8H-CC	68.45	M	2/98	R								R		F	F			R	R			F				F			A		F			R		R			F			
9H-CC	77.72	M	1/99		R							R	F	R	A		R	R		F			R			R			A			R		F								
10H-CC	87.75	M	2/98										A	A	R			F	F			R					R		A	R		R		R								
11H-CC	97.20	M	1/99												R		R	R								F			A	R	F	F										
12H-CC	106.54	M	1/99							R					A			R		R									R	R		A						R				
13H-CC	116.36	M	1/99		F								F		F			F	F					R				R		F	F		F		F		R					
14H-CC	125.84	M	2/98				F			F				F	R			F	F		R					F			A	R	F	R		F				R	R	R		
15H-CC	134.78	M	1/99		R								F	A	R			F				F	R	R		F										F				R	R		
16H-CC	136.81	M	1/99						R	F	F		A	F	F		F	R	F	R									F	F				F						F		
17H-CC	145.61	M	6/94							R			R	F	F			R	R					R		R	F		F	F	F	R		F					R		
18H-CC	155.00	M	5/95				F	R		F	R		R	R	F		R	R	F	F							F		A	F	R	F				R				F		F
19H-CC	164.69	M	7/93				R			R	R	R	F	F	F		F	R	F	F							R		F					R			R			R	R		
20H-CC	173.98	M	10/90		R				R	F			R	F	F			R									R		A	R				F	R	R				F	R		

Notes: Bathymetry is lower bathyal to abyssal zones. Preservation: M = moderate, P = poor. Abundance: A = abundant, F = few, R = rare. * = genus and species indeterminate.

Table T12 (continued).

Core, section	Top depth CSF (m)	Presevation	Benthic/Planktonic foraminifers (%)	*Oridorsalis umbonatus*	*Orthomorphina* spp.	*Planulina costata*	*Planulina renzi*	*Pleurostomella brevis*	*Pleurostomella* spp.	*Polymorphina* spp.	*Pseudoparrella exigua*	*Pullenia bulloides*	*Pullenia quinqueloba*	*Pyrgo* spp.	*Pyrulina* spp.	*Quinqueloculina* spp.	*Recurvoides* spp.	*Rectuvigerina striata*	*Reticulophragmium* sp.	*Siphonodosaria abyssorum*	*Siphonodosaria hispidula*	*Siphonodosaria* spp.	*Spiroloculina* spp.	*Spiroplectella earlandi*	*Triloculina* sp.	Tube-shaped agglutinated forms	Unilocular species	*Uvigerina* spp.	*Uvigerina peregrina*	*Vulvulina spinosa*	Agglutinated foraminifers*	Calcareous hyaline foraminifers*
320-U1336B-																																
1H-CC	1.68	M	1/99	R			R	R				R	R	R	R	R											F					F
2H-CC	11.85	M	1/99	F									R	F	F	R	R			F	F		R				F					F
3H-CC	21.13	M	1/99	R					R			R			R					R			R				F					F
4H-CC	30.54	M	1/99	R		R	R		R				R	R						F	R	R	R							F		F
5H-CC	40.27	M	1/99	F					R					R	F	R			R	A	F					F						F
6H-CC	49.87	P	25/75	F					R																	F						A
7H-CC	58.63	M	2/98	A			F				R				R					F	F	F					R					F
8H-CC	68.45	M	2/98	F			R		F						F							F				R		R		R	R	F
9H-CC	77.72	M	1/99	F			R								R						F	F										F
10H-CC	87.75	M	2/98	R					R												R	R										F
11H-CC	97.20	M	1/99	R																	R	F		F								F
12H-CC	106.54	M	1/99	A																R								R				R
13H-CC	116.36	M	1/99	A					R	R			R	R	R						F	R			R							F
14H-CC	125.84	M	2/98	F					F						R					F	F	F										F
15H-CC	134.78	M	1/99	F			F	R	F				F							R		F										F
16H-CC	136.81	M	1/99	A					F				R								R	R		R						R		R
17H-CC	145.61	M	6/94	A					F			R	R		R					R	F	F								F		F
18H-CC	155.00	M	5/95	F	R		F		R			R	R			R		R				A								F		F
19H-CC	164.69	M	7/93	A	F															F	R	F									R	F
20H-CC	173.98	M	10/90	A					F											F	R	A		R					R		R	

Table T13. Coring-disturbed intervals and gaps, Site U1336. (See table notes.)

Core, section, interval (cm)	Type of disturbance
320-U1336A-	
1H-1, 0–31	Minor
2H-1, 0–76	Top of core
3H-1, 0–127	Top of core
4H-1, 0–142	Top of core
5H-1, 0–12	Top of core
6H-1, 0–34	Top of core
10H-1, 0–64	Top of core
11H-1, 0–6	Top of core
12H-1, 0–84	Top of core
12H-7, 8–70	Distorted liner
13H-1, 0–111	Top of core
14H-1, 0–150	Slurry
15H-1, 0–30	Top of core
16H-1, 0–82	Top of core
16H-3, 100–150	Slight
16H-4, 94–150	Drilling biscuits
16H-5, 0–5	Drilling biscuits
16H-5, 5–150	Flow-in
16H-6, 0–127	Flow-in
17H-1, 0–12	Top of core
19H-1, 0–25	Top of core
21H-1, 0–42	Top of core
22X-35X, all sections	Drilling biscuits
320-U1336B-	
2H-1, 0–60	Top of core
2H-1, 85–87	Void
4H-1, 0–25	Top of core
5H-1, 0–5	Top of core
6H-1, 0–50	Top of core
7H-1, 0–55	Top of core
8H-1, 0–60	Top of core
9H-1, 0–130	Top of core
10H-1, 0–10	Top of core
11H-1, 0–20	Top of core
12H-1, 0–20	Top of core
13H-1, 0–10	Top of core
14H-1, 0–10	Top of core
14H-4, 122–150	Flow-in
14H-5, 0–150	Flow-in
14H-6, 0–150	Flow-in
14H-7, 0–end	Flow-in
15H-1, 0–30	Top of core
16H-1, 0–15	Top of core
16H-2, 0–150	Disturbed
17H-1, 0–15	Top of core
18H-1, 0–20	Top of core
19H-1, 0–10	Top of core
20H-1, 0–10	Top of core
20H-7, 20–end	Deformed liner

Notes: When interval listed is 0–150 cm, entire section is included even if true section length is <150 cm. Top of core = myriad forms of voids, disturbance, and debris from uphole that affect top portion of most cores. For that reason, probably the top 20 cm or so of all cores should be avoided.

Table T14. Principal component analysis results, Hole U1336A. (See table notes.)

Core, section, interval (cm)	Depth CSF (m)	PCA					
		Declination					
		Azimuthally unoriented (°)	Geographical coordinates 0°–360°	Inclination (°)	MAD (°)	Range (mT)	NRM (A/m)
320-U1336A-							
1H-2, 85	2.35	319.2	325.7	5.9	3.5	10–35	6.58E–04
2H-2, 85	10.35	200.7	164.8	–5.2	15.9	20–50	6.99E–04
3H-2, 85	19.85	301.7	13.0	24.2	10.3	5–25	6.05E–04
4H-2, 85	29.35	NA		NA	NA	NA	9.41E–05
5H-2, 85	38.85	312.1	168.1	3.8	33.5	5–60	3.77E–04
6H-2, 85	48.35	117.3	7.3	4.8	5.5	10–30	1.03E–03
7H-2, 85	57.85	11.1	156.1	–1.6	5.8	20–50	1.79E–03
8H-2, 85	67.35	316.3	355.3	21.0	17.3	25–60	6.78E–04
9H-2, 85	76.85	108.6	312.6	17.8	41.2	10–60	4.69E–04
10H-2, 85	86.35	NA		NA	NA	NA	2.20E–04
11H-2, 85	95.85	NA		NA	NA	NA	6.62E–05
12H-2, 85	105.35	NA		NA	NA	NA	9.97E–05
13H-2, 85	114.85	NA		NA	NA	NA	1.59E–04
15H-2, 85	125.85	176.1	8.1	19.2	11.1	5–25	7.47E–05
16H-2, 85	135.35	NA		NA	NA	NA	1.00E–04
17H-2, 85	144.35	NA		NA	NA	NA	2.44E–04
18H-2, 85	153.85	NA		NA	NA	NA	1.82E–04
19H-2, 85	163.35	18.4	94.4	–37.8	24.1	5–30	2.39E–04
20H-2, 85	172.85	NA		NA	NA	NA	2.23E–04
21H-2, 85	182.35	203.9	348.9	59.9	11.8	5–25	2.29E–04

Notes: PCA = principal component analysis, MAD = maximum angular deviation, NRM = natural remanent magnetization after 20 mT demagnetization. NA = not applicable.

Table T15. Interpretation of polarity stratigraphy, Site U1336.

Chron	Age (Ma)	Hole U1336A			Hole U1336B		
		Core, section, interval (cm)	Depth CSF (m)	Depth CCSF-A (m)	Core, section, interval (cm)	Depth CSF (m)	Depth CCSF-A (m)
C1n	0.000						
C5r.3r/C5An.1n	12.014	1H-1, 52	0.50	0.76	1H-1, 82	0.83	0.83
C5An.1n/C5An.1r	12.116	1H-1, 145	1.43	1.69			
C5An.1r/C5An.2n	12.207	1H-2, 67	2.14	2.40			
C5An.2n/C5Ar.1r	12.415	1H-4, 70	5.20	5.46	2H-3, 25	5.05	5.58
C5Ar.1r/C5Ar.1n	12.730				2H-5, 105	8.85	9.38
C5Ar.1n/C5Ar.2r	12.765				2H-5, 142	9.22	9.75
C5Ar.2r/C5Ar.2n	12.820	2H-1, 102	9.02	10.53	2H-6, 68	9.97	10.50
C5Ar.2n/C5Ar.3r	12.878	2H-1, 132	9.34	10.85	2H-6, 115	10.47	11.00
C5Ar.3r/C5AAn	13.015	2H-2, 140	10.89	12.40			
C5AAn/C5AAr	13.183	2H-3, 137	12.37	13.88	3H-1, 115	11.44	14.00
C5AAr/C5ABn	13.369	2H-5, 15	14.15	15.66	3H-2, 35	13.14	15.70
C5ABn/C5ABr	13.605				3H-4, 107	16.88	19.44
C5ABr/C5ACn	13.734	3H-2, 35	19.35	21.18	3H-5, 140	18.69	21.25
C5ADn/C5ADr	14.581				4H-5, 5	26.82	31.00
C5ADr/C5Bn.1n	14.784	4H-2, 75	29.25	32.05	4H-5, 135	28.12	32.30
C5Bn.1n/C5Bn.1r	14.877	4H-3, 20	30.15	32.95	4H-6, 52	28.82	33.00
C5Bn.1r/C5Bn.2n	15.032	4H-4, 42	31.95	34.75			
C5Bn.2n/C5Br	15.160	4H-5, 55	33.55	36.35	5H-1, 50	30.80	36.38
C5Br/C5Cn.1n	15.974	5H-6, 102	45.02	48.30	6H-1, 105	40.85	48.38
C5Cn.1n/C5Cn.1r	16.268				6H-4, 20	44.47	52.00
C5Cn.1r/C5Cn.2n	16.303	6H-1, 35	46.36	53.00	6H-4, 127	45.57	53.10
C5Cn.2n/C5Cn.2r	16.472	6H-1, 100	47.01	53.65	6H-5, 35	46.15	53.68
C5Cn.2r/C5Cn.3n	16.543	6H-2, 30	47.80	54.44	6H-5, 107	46.87	54.40
C5Cn.3n/C5Cr	16.721	6H-2, 110	48.61	55.25	6H-6, 37	47.67	55.20
C5Cr/C5Dn	17.235	6H-5, 82	52.82	59.46	7H-1, 150	50.81	59.50
C5Dn/C5Dr	17.533				7H-3, 137	53.68	62.37
C5Dr/C5Dr-1n	17.717				7H-5, 50	55.81	64.50
C5Dr-1n/C5Dr	17.740	7H-2, 5	57.06	65.10	7H-5, 102	56.31	65.00
C5Dr/C5En	18.056	7H-3, 105	59.56	67.60			
C5En/C5Er	18.524	7H-6, 140	64.40	72.44	8H-4, 42	63.72	72.60
C5Er/C6n	18.748	8H-1, 92	65.91	75.00	8H-5, 120	66.00	74.88

Table T16. Interstitial water data from squeezed whole-round samples, Hole U1336B. (See table notes.)

Core, section, interval (cm)	Depth CSF (m)	pH	Alkalinity (mM)	Cl^- (mM)	Na^+ (mM)	SO_4^{2-} (mM)	HPO_4^- (μM)	H_4SiO_4 (μM)	Mn^{2+} (μM)	Fe^{2+} (μM)	Ca^{2+} (mM)	Mg^{2+} (mM)	B (μM)	Sr^{2+} (μM)	Ba^{2+} (μM)	Li^+ (μM)	K^+ (mM)
320-U1336B-																	
2H-2, 145–150	4.75	7.71	2.39	556	ND	26.2	1.65	329	BDL	BDL	10.1	50.0	422.5	83.7	BDL	23.88	ND
2H-5, 145–150	9.25	7.96	2.71	557	ND	25.9	4.77	325	BDL	BDL	10.6	49.0	439.5	93.8	BDL	23.22	ND
3H-2, 145–150	14.25	7.73	2.66	561	ND	26.9	0.91	426	BDL	BDL	11.6	49.9	455.0	109.5	BDL	23.16	ND
3H-5, 145–150	18.75	7.75	2.69	559	488	26.0	0.43	514	BDL	BDL	11.7	48.1	461.2	115.6	BDL	22.93	11.4
4H-2, 145–150	23.75	7.78	2.72	563	492	25.4	0.44	471	0.18	BDL	12.7	46.7	454.9	121.9	BDL	21.54	10.7
4H-5, 145–150	28.25	7.74	2.84	566	491	26.8	0.39	564	1.11	BDL	13.7	48.1	452.1	134.6	BDL	22.33	11.9
5H-2, 145–150	33.25	7.76	2.79	568	496	25.1	0.42	488	2.91	BDL	13.8	45.9	433.4	142.9	0.51	21.29	10.3
5H-5, 145–150	37.75	7.69	2.82	570	496	25.7	0.43	541	4.66	BDL	14.4	46.7	446.8	145.8	BDL	20.18	10.8
6H-2, 145–150	42.75	7.62	2.75	567	495	24.9	0.42	536	5.53	BDL	14.5	44.9	438.2	154.5	BDL	19.81	10.4
6H-5, 145–150	47.25	7.61	2.60	567	491	27.3	0.40	594	5.38	BDL	15.8	47.6	436.8	157.6	BDL	19.40	11.2
7H-3, 145–150	53.75	7.70	2.70	567	492	25.5	0.25	574	6.23	BDL	15.8	45.6	423.5	165.3	BDL	18.88	10.5
8H-3, 140–150	63.20	7.76	2.63	565	493	24.6	0.29	607	6.29	BDL	16.0	43.5	430.5	176.9	BDL	17.50	9.9
9H-3, 140–150	72.70	7.45	2.63	565	490	24.7	0.32	633	5.82	BDL	16.9	43.7	419.6	186.1	BDL	16.98	9.8
10H-4, 140–150	83.70	7.59	2.67	566	488	26.0	0.29	673	4.37	BDL	18.5	45.1	418.0	201.0	BDL	16.46	10.1
11H-4, 140–150	93.20	7.61	2.73	567	493	24.0	0.27	687	3.17	BDL	18.3	41.8	406.5	211.4	BDL	16.54	9.3
12H-4, 140–150	102.70	7.59	2.30	568	490	25.0	0.30	724	2.74	4.36	19.4	43.3	427.9	220.5	BDL	15.49	10.0
13H-4, 140–150	112.20	7.78	2.66	567	492	24.0	0.35	730	2.34	8.60	19.5	41.1	430.2	231.1	BDL	14.29	9.4
14H-4, 140–150	121.70	7.45	2.29	568	492	24.1	BDL	695	2.12	9.92	20.1	40.8	417.0	236.5	BDL	14.06	9.3
15H-4, 140–150	131.20	7.44	1.73	566	494	23.9	BDL	671	1.61	18.43	26.4	32.5	404.8	342.2	BDL	8.91	8.6
18H-4, 140–150	151.30	7.08	1.34	569	497	23.1	BDL	818	1.75	14.88	28.4	29.8	402.8	390.2	BDL	7.88	8.2
19H-3, 140–150	159.30	7.52	1.24	571	499	22.7	BDL	853	1.77	11.74	28.7	29.2	404.5	404.2	BDL	8.13	8.2
20H-3, 140–150	168.80	7.24	1.01	569	498	22.2	BDL	800	1.76	17.08	28.9	28.4	396.7	417.8	BDL	8.84	7.9

Notes: ND = not determined. BDL = below detection limit (HPO_4^- = 0.2 μM, Mn^{2+} = 0.1 μM, Fe^{2+} = 0.6 μM, B = 4 μM, Sr^{2+} = 0.8 μM, Ba^{2+} = 0.5 μM, Li^+ = 1.8 μM) calculated as three times the standard deviation of multiple measures of a blank. H_4SiO_4 values measured by different techniques during Expeditions 320 and 321 disagree significantly, especially for low values. Therefore, caution should be used concerning the H_4SiO_4 data and comparison between the different expeditions.

Table T17. Carbon concentrations, Site U1336. (See table notes.) (Continued on next page.)

Core, section, interval (cm)	Depth (m)		Carbon (wt%)			
	CSF	CCSF-A	$CaCO_3$	IC	TC	TOC
320-U1336A-						
1H-1, 65–66	0.65	0.91	76.5	9.2	ND	ND
1H-2, 65–66	2.15	2.41	78.7	9.4	ND	ND
1H-3, 65–66	3.65	3.91	92.2	11.1	ND	ND
1H-4, 65–66	5.15	5.41	89.9	10.8	ND	ND
1H-5, 65–66	6.65	6.91	89.8	10.8	ND	ND
1H-6, 25–26	7.75	8.01	84.0	10.1	ND	ND
2H-1, 65–65	8.65	10.16	80.6	9.7	ND	ND
2H-2, 65–66	10.15	11.66	86.9	10.4	ND	ND
2H-3, 65–66	11.65	13.16	78.4	9.4	ND	ND
2H-4, 65–66	13.15	14.66	83.8	10.1	ND	ND
2H-5, 65–66	14.65	16.16	87.5	10.5	ND	ND
2H-6, 65–66	16.15	17.66	87.6	10.5	ND	ND
2H-7, 25–26	17.25	18.76	88.0	10.6	ND	ND
3H-2, 65–66	19.65	21.48	81.3	9.8	ND	ND
3H-3, 65–66	21.15	22.98	92.0	11.0	ND	ND
3H-4, 65–66	22.65	24.48	67.7	8.1	ND	ND
3H-5, 65–66	24.15	25.98	83.6	10.0	ND	ND
3H-6, 65–66	25.65	27.48	75.4	9.1	ND	ND
3H-7, 45–46	26.95	28.78	82.0	9.8	ND	ND
4H-2, 65–66	29.15	31.95	78.1	9.4	ND	ND
4H-3, 65–66	30.65	33.45	89.2	10.7	ND	ND
4H-4, 65–66	32.15	34.95	82.2	9.9	ND	ND
4H-5, 65–66	33.65	36.45	72.3	8.7	ND	ND
4H-6, 45–46	34.95	37.75	89.3	10.7	ND	ND
4H-7, 20–21	35.51	38.31	71.8	8.6	ND	ND
5H-1, 65–66	37.15	40.43	84.9	10.2	ND	ND
5H-2, 65–66	38.65	41.93	85.9	10.3	ND	ND
5H-3, 65–66	40.15	43.43	83.0	10.0	ND	ND
5H-4, 65–66	41.65	44.93	81.9	9.8	ND	ND
5H-5, 65–66	43.15	46.43	81.7	9.8	ND	ND
5H-6, 65–66	44.65	47.93	84.2	10.1	ND	ND
5H-7, 40–41	45.90	49.18	85.8	10.3	ND	ND
6H-1, 65–66	46.65	53.29	80.3	9.6	ND	ND
6H-2, 65–66	48.15	54.79	48.1	5.8	ND	ND
6H-3, 65–66	49.65	56.29	71.4	8.6	ND	ND
6H-4, 65–66	51.15	57.79	67.1	8.1	ND	ND
6H-5, 65–66	52.65	59.29	76.7	9.2	ND	ND
6H-6, 65–66	54.15	60.79	75.2	9.0	ND	ND
7H-1, 64–65	56.14	64.18	85.5	10.3	ND	ND
7H-2, 64–65	57.64	65.68	79.5	9.5	ND	ND
7H-3, 64–65	59.14	67.18	84.0	10.1	ND	ND
7H-4, 64–65	60.64	68.68	71.5	8.6	ND	ND
7H-5, 64–65	62.14	70.18	80.7	9.7	ND	ND
7H-6, 64–65	63.64	71.68	84.9	10.2	ND	ND
7H-7, 49–50	64.99	73.03	84.4	10.1	ND	ND
8H-1, 65–66	65.65	74.74	84.7	10.2	ND	ND
8H-2, 65–66	67.15	76.24	85.3	10.2	ND	ND
8H-3, 65–66	68.65	77.74	79.6	9.6	ND	ND
8H-4, 65–66	70.15	79.24	85.1	10.2	ND	ND
8H-5, 65–66	71.65	80.74	88.2	10.6	ND	ND
8H-6, 20–21	72.70	81.79	86.6	10.4	ND	ND
8H-7, 65–66	73.65	82.74	86.6	10.4	ND	ND
9H-1, 65–66	75.15	84.92	90.9	10.9	ND	ND
9H-2, 62–63	76.62	86.39	90.0	10.8	ND	ND
9H-3, 65–66	78.15	87.92	87.8	10.5	ND	ND
9H-4, 65–66	79.65	89.42	88.3	10.6	ND	ND
9H-5, 65–66	81.15	90.92	86.5	10.4	ND	ND
9H-6, 65–66	82.65	92.42	89.0	10.7	ND	ND
9H-7, 65–66	84.15	93.92	88.0	10.6	ND	ND
10H-1, 89–90	84.89	94.60	83.7	10.0	ND	ND
10H-2, 65–66	86.15	95.86	86.8	10.4	ND	ND
10H-3, 65–66	87.65	97.36	81.2	9.7	ND	ND
10H-4, 65–66	89.15	98.86	90.1	10.8	ND	ND
10H-5, 65–66	90.65	100.36	86.6	10.4	ND	ND
10H-6, 65–66	92.15	101.86	84.5	10.1	ND	ND
10H-7, 50–51	93.20	102.91	88.1	10.6	ND	ND
11H-1, 65–66	94.15	105.94	91.1	10.9	ND	ND
11H-2, 65–66	95.65	107.44	91.0	10.9	ND	ND
11H-3, 65–66	97.15	108.94	85.3	10.2	ND	ND
11H-4, 65–66	98.65	110.44	87.8	10.5	ND	ND
11H-5, 65–66	100.15	111.94	88.5	10.6	ND	ND
11H-6, 65–66	101.65	113.44	89.1	10.7	ND	ND
11H-7, 45–46	102.95	114.74	90.1	10.8	ND	ND
12H-2, 65–66	105.15	118.03	89.0	10.7	ND	ND
12H-3, 65–66	106.65	119.53	91.3	11.0	ND	ND
12H-4, 65–66	108.15	121.03	90.6	10.9	ND	ND
12H-5, 65–66	109.65	122.53	88.2	10.6	ND	ND
12H-6, 55–56	111.05	123.93	90.7	10.9	ND	ND
12H-7, 45–46	111.95	124.83	92.0	11.0	ND	ND
13H-2, 65–66	114.65	128.87	90.3	10.8	ND	ND
13H-3, 65–66	116.15	130.37	88.5	10.6	ND	ND
13H-4, 65–66	117.65	131.87	89.9	10.8	ND	ND
13H-5, 65–66	119.15	133.37	87.2	10.5	ND	ND
13H-6, 65–66	120.65	134.87	79.7	9.6	ND	ND
13H-7, 35–36	121.85	136.07	91.6	11.0	ND	ND
15H-1, 65–66	124.15	140.38	89.5	10.7	ND	ND
15H-2, 65–66	125.65	141.88	87.3	10.5	ND	ND
15H-3, 65–66	127.15	143.38	89.0	10.7	ND	ND
15H-4, 65–66	128.65	144.88	88.0	10.6	ND	ND
15H-5, 65–66	130.15	146.38	91.0	10.9	ND	ND
15H-6, 65–66	131.65	147.88	83.7	10.0	ND	ND
15H-7, 40–41	132.90	149.13	88.3	10.6	ND	ND
16H-1, 121–122	134.21	155.71	87.8	10.5	ND	ND
16H-2, 65–66	135.15	156.65	89.7	10.8	ND	ND
16H-3, 65–65	136.65	158.15	83.2	10.0	ND	ND
16H-4, 65–65	138.15	159.65	88.9	10.7	ND	ND
16H-5, 110–111	140.10	161.60	90.3	10.8	ND	ND
16H-6, 65–65	141.15	162.65	90.0	10.8	ND	ND
17H-1, 65–66	142.65	166.06	89.0	10.7	ND	ND
17H-2, 65–66	144.15	167.56	90.2	10.8	ND	ND
17H-3, 65–66	145.65	169.06	80.9	9.7	ND	ND
17H-4, 65–66	147.15	170.56	89.0	10.7	ND	ND
17H-5, 65–66	148.65	172.06	86.6	10.4	ND	ND
17H-6, 65–66	150.15	173.56	87.2	10.5	ND	ND
17H-7, 40–41	151.40	174.81	85.4	10.2	ND	ND
18H-1, 65–66	152.15	175.56	76.8	9.2	ND	ND
18H-2, 65–66	153.65	177.06	82.9	9.9	ND	ND
18H-3, 65–66	155.15	178.56	86.5	10.4	ND	ND
18H-4, 65–66	156.65	180.06	88.5	10.6	ND	ND
18H-5, 65–66	158.15	181.56	89.7	10.8	ND	ND
18H-6, 65–66	159.65	183.06	83.7	10.0	ND	ND
18H-7, 50–51	161.00	184.41	83.9	10.1	ND	ND
19H-1, 65–66	161.65	185.06	87.1	10.5	ND	ND
19H-2, 65–66	163.15	186.56	86.4	10.4	ND	ND
19H-3, 65–66	164.65	188.06	88.8	10.7	ND	ND
19H-4, 65–66	166.15	189.56	88.7	10.6	ND	ND
19H-5, 65–66	167.65	191.06	84.7	10.2	ND	ND
19H-6, 65–66	169.15	192.56	88.2	10.6	ND	ND
19H-7, 20–21	170.20	193.61	89.1	10.7	ND	ND
20H-1, 64–65	171.14	194.55	88.2	10.6	ND	ND
20H-2, 64–65	172.64	196.05	87.4	10.5	ND	ND
20H-3, 64–65	174.14	197.55	86.5	10.4	ND	ND
20H-4, 64–65	175.64	199.05	88.3	10.6	ND	ND
20H-5, 64–65	177.14	200.55	90.7	10.9	ND	ND
20H-6, 64–65	178.64	202.05	90.2	10.8	ND	ND
21H-1, 65–66	180.65	204.06	90.8	10.9	ND	ND
21H-2, 65–66	182.15	205.56	88.7	10.6	ND	ND
21H-3, 65–66	183.65	207.06	90.5	10.9	ND	ND
21H-4, 25–26	184.25	207.66	93.0	11.2	ND	ND
22X-1, 65–66	185.45	208.86	89.7	10.8	ND	ND
22X-2, 65–66	186.95	210.36	91.2	11.0	ND	ND
22X-3, 60–61	188.40	211.81	89.0	10.7	ND	ND
22X-4, 65–66	189.95	213.36	91.1	10.9	ND	ND
22X-5, 65–66	191.45	214.86	90.9	10.9	ND	ND
22X-6, 4–5	192.14	215.55	92.4	11.1	ND	ND

Table T17 (continued).

Core, section, interval (cm)	Depth (m)		Carbon (wt%)			
	CSF	CCSF-A	$CaCO_3$	IC	TC	TOC
23X-1, 58–59	194.98	218.39	92.2	11.1	ND	ND
23X-2, 59–60	196.49	219.90	91.1	10.9	ND	ND
23X-3, 59–60	197.99	221.40	91.2	10.9	ND	ND
23X-4, 58–60	199.48	222.89	91.2	11.0	ND	ND
23X-5, 60–61	201.00	224.41	90.2	10.8	ND	ND
24X-1, 62–63	203.02	226.43	93.1	11.2	ND	ND
24X-2, 54–55	204.44	227.85	92.1	11.1	ND	ND
24X-3, 72–73	206.12	229.53	94.3	11.3	ND	ND
24X-4, 56–57	207.46	230.87	92.4	11.1	ND	ND
24X-5, 54–55	208.94	232.35	91.0	10.9	ND	ND
25X-1, 60–61	212.60	236.01	91.8	11.0	ND	ND
25X-2, 60–61	214.10	237.51	90.7	10.9	ND	ND
25X-3, 60–61	215.60	239.01	87.5	10.5	ND	ND
26X-1, 62–63	222.22	245.63	91.8	11.0	ND	ND
26X-2, 61–62	223.71	247.12	92.5	11.1	ND	ND
26X-3, 60–61	225.20	248.61	92.0	11.0	ND	ND
26X-4, 72–73	226.82	250.23	93.0	11.2	ND	ND
26X-5, 68–69	228.28	251.69	91.8	11.0	ND	ND
26X-6, 64–65	229.74	253.15	89.1	10.7	ND	ND
27X-1, 59–60	231.79	255.20	92.2	11.1	ND	ND
27X-2, 61–62	233.31	256.72	92.2	11.1	ND	ND
27X-3, 59–60	234.79	258.20	92.7	11.1	ND	ND
27X-4, 58–59	236.28	259.69	92.6	11.1	ND	ND
27X-5, 18–19	237.18	260.59	92.6	11.1	ND	ND
28X-1, 42–43	241.22	264.63	91.7	11.0	ND	ND
28X-2, 30–31	242.60	266.01	93.0	11.2	ND	ND
29X-1, 54–55	250.94	274.35	92.5	11.1	ND	ND
29X-2, 66–67	252.56	275.97	93.2	11.2	ND	ND
29X-3, 57–58	253.97	277.38	92.5	11.1	ND	ND
30X-1, 62–63	260.62	284.03	91.7	11.0	ND	ND
30X-2, 64–65	262.14	285.55	92.8	11.1	ND	ND
30X-3, 45–46	263.45	286.86	92.0	11.0	ND	ND
31X-1, 55–55	270.15	293.56	92.7	11.1	ND	ND
31X-2, 60–61	271.70	295.11	92.0	11.0	ND	ND
31X-3, 42–43	273.02	296.43	93.1	11.2	ND	ND
32X-1, 62–63	279.82	303.23	92.1	11.1	ND	ND
32X-2, 54–55	281.24	304.65	91.3	11.0	ND	ND
32X-3, 32–33	282.52	305.93	89.4	10.7	ND	ND
33X-2, 47–48	289.42	312.83	89.3	10.7	ND	ND
35X-1, 74–75	299.04	322.45	90.0	10.8	ND	ND

Core, section, interval (cm)	Depth (m)		Carbon (wt%)			
	CSF	CCSF-A	$CaCO_3$	IC	TC	TOC
320-U1336B-						
1H-1, 71–72	0.71	0.71	78.6	9.4	9.49	0.18
2H-2, 72–73	4.02	4.55	94.4	11.3	11.33	0.07
2H-6, 72–73	10.02	10.55	74.6	9.0	ND	ND
3H-2, 72–73	13.52	16.08	91.1	10.9	10.93	0.08
3H-6, 72–73	19.52	22.08	86.0	10.3	ND	ND
4H-2, 72–73	23.02	27.20	89.5	10.7	10.70	0.08
4H-6, 72–73	29.02	33.20	90.7	10.9	ND	ND
5H-2, 72–73	32.52	38.10	84.6	10.2	10.16	0.08
5H-6, 72–73	38.52	44.10	79.8	9.6	ND	ND
6H-2, 72–73	42.02	49.55	88.6	10.6	10.63	0.05
6H-6, 72–73	48.02	55.55	80.6	9.7	ND	ND
7H-2, 72–73	51.52	60.21	85.4	10.3	10.22	0.10
7H-4, 72–73	54.52	63.21	89.2	10.7	ND	ND
7H-6, 72–73	57.52	66.21	82.4	9.9	ND	ND
8H-2, 72–73	61.02	69.90	77.7	9.3	9.36	0.05
8H-6, 72–73	67.02	75.90	82.7	9.9	ND	ND
9H-2, 72–73	70.52	79.33	86.7	10.4	10.35	0.06
9H-6, 72–73	76.52	85.33	92.6	11.1	ND	ND
10H-2, 72–73	80.02	90.21	90.5	10.9	10.83	0.05
10H-6, 72–73	86.02	96.21	86.5	10.4	ND	ND
11H-2, 71–72	89.51	100.20	91.9	11.0	10.99	0.05
11H-6, 83–84	95.63	106.32	93.8	11.3	ND	ND
12H-2, 71–72	99.01	111.52	88.0	10.6	10.55	0.05
12H-6, 71–72	105.01	117.52	94.0	11.3	ND	ND
13H-2, 71–72	108.51	122.77	94.0	11.3	11.21	0.14
13H-6, 71–72	114.51	128.77	94.2	11.3	ND	ND
14H-2, 72–73	118.02	135.00	87.1	10.5	10.42	0.30
14H-4, 70–71	121.00	137.98	95.9	11.5	ND	ND
15H-2, 72–73	127.52	145.31	92.9	11.2	11.09	0.17
15H-6, 72–73	133.52	151.31	93.4	11.2	ND	ND
16H-1, 42–43	135.22	153.01	94.1	11.3	11.24	0.15
17H-2, 72–73	139.02	156.81	92.0	11.0	10.98	0.07
17H-6, 34–35	144.14	161.93	91.1	10.9	ND	ND
18H-2, 71–72	147.61	165.40	90.4	10.9	10.79	0.07
18H-6, 71–72	153.61	171.40	84.8	10.2	ND	ND
19H-2, 71–72	157.11	174.90	84.9	10.2	10.23	0.06
19H-6, 71–72	163.11	180.90	90.6	10.9	ND	ND
20H-2, 71–72	166.61	184.40	89.5	10.8	10.74	0.06
20H-6, 71–72	172.61	190.40	92.8	11.1	ND	ND

Notes: IC = inorganic carbon, TC = total carbon, TOC = total organic carbon determined by acidification method. ND = not determined.

Table T18. Inorganic geochemistry of solid samples, Hole U1336B. (See table notes.)

Core, section, interval (cm)	Depth (m)		Major element oxide (wt%)										Trace element (ppm)		
	CSF	CCSF-A	SiO_2	Al_2O_3	Fe_2O_3 T	MnO	MgO	CaO	Na_2O	K_2O	TiO_2	P_2O_5	Ba	Sr	Zr
320-U1336B-															
1H-1, 71–72	0.71	0.71	8.93	1.495	1.248	0.312	0.768	43.5	1.833	0.302	0.0300	0.389	2143	1190	29.22
2H-6, 72–73	10.02	10.55	11.78	1.601	1.783	0.202	0.847	41.6	1.735	0.320	0.0359	0.308	2466	1220	31.62
3H-6, 72–73	19.52	22.08	5.81	0.814	1.109	0.160	0.587	46.7	1.279	0.176	BDL	0.175	1475	1246	19.81
4H-6, 72–73	29.02	33.20	3.74	0.221	0.454	0.101	0.397	49.2	0.917	0.059	BDL	0.114	839	1072	8.50
5H-6, 72–73	38.52	44.10	9.88	0.941	1.322	0.192	0.647	43.8	1.515	0.206	0.0063	0.191	1996	980	19.10
6H-6, 72–73	48.02	55.55	9.97	0.974	1.076	0.131	0.548	43.5	1.382	0.223	0.0089	0.169	1546	1092	15.98
7H-6, 72–73	57.52	66.21	8.85	0.772	1.312	0.193	0.583	45.0	1.332	0.172	BDL	0.201	1951	1146	15.70
9H-6, 72–73	76.52	85.33	2.94	0.000	0.257	0.088	0.317	49.6	0.861	0.011	BDL	0.102	565	1018	6.30
10H-6, 72–73	86.02	96.21	6.63	0.458	0.869	0.104	0.494	47.2	1.115	0.092	BDL	0.167	1567	1168	10.40
11H-6, 83–84	95.63	106.32	2.68	0.023	0.156	0.089	0.253	50.9	0.655	0.016	BDL	0.108	708	1052	6.67
12H-6, 71–72	105.01	117.52	2.14	0.031	0.131	0.081	0.241	50.1	0.717	0.022	BDL	0.105	692	1148	2.88
13H-6, 71–72	114.51	128.77	2.29	0.044	0.153	0.088	0.225	51.1	0.582	0.014	BDL	0.125	787	1094	5.33
14H-4, 70–71	121.00	137.98	1.12	0.013	0.012	0.075	0.189	52.1	0.323	0.000	BDL	0.114	824	904	2.88
15H-6, 72–73	133.52	151.31	2.73	0.098	0.181	0.093	0.207	49.5	0.604	0.023	BDL	0.101	915	1066	7.12
16H-1, 42–43	135.22	153.01	1.79	0.142	0.147	0.075	0.198	49.9	0.553	0.038	BDL	0.139	1365	997	6.89
17H-6, 34–35	144.14	161.93	4.57	0.228	0.427	0.070	0.239	49.7	0.632	0.046	BDL	0.120	1366	1152	8.50
18H-6, 71–72	153.61	171.40	8.94	0.474	0.615	0.077	0.300	44.7	0.818	0.093	BDL	0.152	2138	1152	11.59
19H-6, 71–72	163.11	180.90	4.89	0.222	0.344	0.073	0.222	48.2	0.613	0.042	BDL	0.126	1398	1147	7.64
20H-6, 71–72	172.61	190.40	3.46	0.169	0.334	0.072	0.209	49.1	0.541	0.029	BDL	0.095	1384	1168	8.07

Notes: BDL = below detection limit (Al_2O_3 = 0.003 wt%, K_2O = 0.007 wt%, TiO_2 = 0.0014 wt%). Values for Sr and Ba are well above the calibration range (Sr < 700 ppm, Ba < 570 ppm). H_4SiO_4 values measured by different techniques during Expeditions 320 and 321 disagree significantly, especially for low values. Therefore, caution should be used concerning the H_4SiO_4 data and comparison between the different expeditions. See "Geochemistry" in the "Methods" chapter for uncertainty estimates and assessment of accuracy.

Table T19. Moisture and density measurements, Site U1336. (Continued on next page.)

Core, section, interval (cm)	Depth CSF (m)	Water content (wt%)	Density (g/cm³) Wet bulk	Dry bulk	Grain	Porosity (%)
320-U1336A-						
1H-1, 75–76	0.75	59.0	1.40	0.58	3.00	80.8
1H-2, 75–76	2.25	48.5	1.54	0.80	2.95	73.1
1H-3, 75–76	3.75	38.4	1.70	1.05	2.89	63.8
1H-4, 75–76	5.25	39.6	1.68	1.02	2.91	65.1
1H-5, 75–76	6.75	40.0	1.67	1.00	2.88	65.2
1H-6, 35–36	7.85	46.7	1.56	0.83	2.86	71.0
2H-1, 75–76	8.75	50.5	1.51	0.75	2.90	74.3
2H-2, 75–76	10.25	44.5	1.59	0.88	2.87	69.2
2H-3, 75–76	11.75	50.6	1.50	0.74	2.87	74.1
2H-4, 75–76	13.25	45.9	1.55	0.84	2.77	69.6
2H-5, 75–76	14.75	43.9	1.58	0.89	2.76	67.8
2H-6, 75–76	16.25	44.2	1.57	0.88	2.73	67.9
2H-7, 35–36	17.35	43.4	1.62	0.92	2.94	68.7
3H-2, 75–76	19.75	46.5	1.56	0.83	2.86	70.8
3H-3, 75–76	21.25	52.7	1.48	0.70	2.91	76.0
3H-4, 75–76	22.75	52.1	1.48	0.71	2.88	75.4
3H-5, 75–76	24.25	44.2	1.58	0.88	2.78	68.2
3H-6, 75–76	25.75	48.7	1.51	0.78	2.77	71.9
3H-7, 55–56	27.05	46.1	1.57	0.85	2.89	70.7
4H-2, 75–76	29.25	48.8	1.56	0.80	3.08	74.1
4H-3, 75–76	30.75	39.6	1.65	1.00	2.76	63.8
4H-4, 75–76	32.25	45.0	1.58	0.87	2.87	69.6
4H-5, 75–76	33.75	54.0	1.45	0.67	2.83	76.4
4H-6, 55–56	35.05	42.1	1.62	0.94	2.81	66.6
4H-7, 30–31	35.61	49.6	1.50	0.76	2.79	72.8
5H-1, 75–76	37.25	48.9	1.50	0.77	2.72	71.8
5H-2, 75–76	38.75	47.4	1.54	0.81	2.81	71.2
5H-3, 75–76	40.25	49.6	1.50	0.76	2.79	72.8
5H-4, 75–76	41.75	48.3	1.52	0.78	2.76	71.6
5H-5, 75–76	43.25	50.0	1.49	0.74	2.73	72.7
5H-6, 75–76	44.75	48.3	1.53	0.79	2.87	72.4
5H-7, 50–51	46.00	47.4	1.55	0.82	2.90	71.9
6H-1, 75–76	46.75	46.5	1.54	0.83	2.77	70.1
6H-2, 75–76	48.25	58.5	1.38	0.57	2.72	78.9
6H-3, 75–76	49.75	50.6	1.49	0.74	2.79	73.6
6H-4, 75–76	51.25	48.6	1.52	0.78	2.81	72.2
6H-5, 75–76	52.75	50.6	1.51	0.75	2.94	74.6
6H-6, 75–76	54.25	45.4	1.56	0.85	2.74	69.0
7H-1, 75–76	56.25	46.3	1.56	0.84	2.85	70.6
7H-2, 75–76	57.75	48.7	1.51	0.78	2.78	72.0
7H-3, 75–76	59.25	44.9	1.57	0.87	2.80	69.0
7H-4, 75–76	60.75	45.0	1.56	0.86	2.73	68.6
7H-5, 75–76	62.25	45.3	1.57	0.86	2.82	69.5
7H-6, 75–76	63.75	44.3	1.59	0.89	2.85	68.8
7H-7, 60–61	65.10	44.7	1.59	0.88	2.86	69.3
8H-1, 75–76	65.75	48.1	1.53	0.80	2.83	71.9
8H-2, 75–76	67.25	43.8	1.60	0.90	2.84	68.4
8H-3, 75–76	68.75	45.4	1.56	0.85	2.75	69.1
8H-4, 75–76	70.25	41.4	1.64	0.96	2.83	66.1
8H-5, 75–76	71.75	42.1	1.61	0.93	2.75	66.1
8H-6, 30–31	72.80	39.9	1.65	0.99	2.77	64.3
8H-7, 75–76	73.75	42.5	1.62	0.93	2.82	67.1
9H-1, 75–76	75.25	40.3	1.65	0.98	2.79	64.7
9H-2, 72–73	76.72	42.3	1.62	0.93	2.80	66.7
9H-3, 75–76	78.25	42.4	1.61	0.93	2.80	66.8
9H-4, 75–76	79.75	42.3	1.62	0.94	2.83	67.0
9H-5, 75–76	81.25	49.8	1.41	0.71	2.26	68.7
9H-6, 75–76	82.75	41.3	1.64	0.97	2.87	66.4
9H-7, 75–76	84.25	41.9	1.60	0.93	2.71	65.6
10H-1, 75–76	84.75	46.6	1.50	0.80	2.53	68.4
10H-2, 75–76	86.25	42.1	1.63	0.94	2.85	66.9
10H-3, 75–76	87.75	42.7	1.61	0.92	2.79	67.0
10H-4, 75–76	89.25	39.8	1.64	0.99	2.72	63.7
10H-5, 75–76	90.75	42.4	1.63	0.94	2.90	67.6
10H-6, 75–76	92.25	43.5	1.58	0.89	2.72	67.2
10H-7, 60–61	93.30	40.7	1.66	0.98	2.88	65.9
11H-1, 75–76	94.25	34.8	1.74	1.13	2.77	59.1
11H-2, 75–76	95.75	36.9	1.70	1.07	2.77	61.2
11H-3, 75–76	97.25	40.3	1.64	0.98	2.75	64.5
11H-4, 75–76	98.75	39.3	1.68	1.02	2.85	64.3
11H-5, 75–76	100.25	42.3	1.61	0.93	2.77	66.5
11H-6, 75–76	101.75	38.9	1.67	1.02	2.77	63.2
11H-7, 55–56	103.05	37.2	1.69	1.06	2.76	61.4
12H-2, 75–76	105.25	37.5	1.70	1.06	2.81	62.2
12H-3, 75–76	106.75	38.1	1.67	1.04	2.75	62.3
12H-4, 75–76	108.25	38.2	1.69	1.05	2.85	63.2
12H-5, 75–76	109.75	35.4	1.73	1.12	2.78	59.7
12H-6, 65–66	111.15	35.3	1.70	1.10	2.67	58.7
12H-7, 55–56	112.05	37.0	1.72	1.08	2.86	62.1
13H-2, 75–76	114.75	37.5	1.69	1.06	2.79	62.1
13H-3, 75–76	116.25	39.2	1.65	1.00	2.72	63.2
13H-4, 75–76	117.75	35.7	1.74	1.12	2.84	60.6
13H-5, 75–76	119.25	38.7	1.68	1.03	2.85	63.7
13H-6, 75–76	120.75	41.4	1.62	0.95	2.77	65.6
13H-7, 45–46	121.95	35.6	1.73	1.12	2.81	60.2
15H-1, 75–76	124.25	33.7	1.78	1.18	2.86	58.7
15H-2, 75–76	125.75	16.4	2.57	2.15	3.65	41.2
15H-3, 75–76	127.25	38.2	1.71	1.06	2.90	63.6
15H-4, 75–76	128.75	34.3	1.77	1.16	2.87	59.4
15H-5, 75–76	130.25	36.4	1.75	1.12	2.96	62.3
15H-6, 75–76	131.75	32.1	1.81	1.23	2.82	56.6
15H-7, 50–51	133.00	37.6	1.71	1.07	2.85	62.6
16H-1, 130–131	134.30	36.8	1.69	1.07	2.72	60.8
16H-2, 75–76	135.25	35.8	1.73	1.11	2.81	60.5
16H-3, 75–76	136.75	38.1	1.68	1.04	2.78	62.6
16H-4, 75–76	138.25	38.0	1.69	1.05	2.83	62.9
16H-5, 120–121	140.20	35.6	1.75	1.13	2.89	60.9
16H-6, 75–76	141.25	36.1	1.72	1.10	2.81	60.8
17H-1, 75–76	142.75	38.1	1.69	1.04	2.80	62.8
17H-2, 75–76	144.25	34.2	1.77	1.16	2.83	59.0
17H-3, 75–76	145.75	36.8	1.70	1.08	2.78	61.3
17H-4, 75–76	147.25	36.9	1.72	1.09	2.86	62.1
17H-5, 75–76	148.75	34.9	1.77	1.15	2.89	60.1
17H-6, 75–76	150.25	37.6	1.71	1.07	2.86	62.7
17H-7, 50–51	151.50	36.8	1.70	1.08	2.78	61.2
18H-1, 75–76	152.25	39.2	1.66	1.01	2.77	63.6
18H-2, 75–76	153.75	36.3	1.71	1.09	2.75	60.5
18H-3, 75–76	155.25	36.8	1.70	1.08	2.77	61.1
18H-4, 75–76	156.75	34.9	1.74	1.13	2.77	59.3
18H-5, 75–76	158.25	35.6	1.71	1.10	2.72	59.5
18H-6, 75–76	159.75	34.4	1.76	1.15	2.82	59.0
18H-7, 60–61	161.10	34.9	1.76	1.14	2.85	59.9
19H-1, 75–76	161.75	33.8	1.78	1.18	2.85	58.7
19H-2, 75–76	163.25	36.9	1.70	1.07	2.78	61.4
19H-3, 75–76	164.75	37.2	1.70	1.07	2.81	62.0
19H-4, 75–76	166.25	35.0	1.73	1.12	2.74	59.0
19H-5, 75–76	167.75	33.9	1.75	1.16	2.76	58.1
19H-6, 75–76	169.25	33.5	1.77	1.18	2.80	57.9
19H-7, 30–31	170.30	34.2	1.75	1.15	2.76	58.4
20H-1, 75–76	171.25	34.1	1.76	1.16	2.79	58.4
20H-3, 75–76	174.25	36.6	1.71	1.09	2.81	61.3
20H-4, 75–76	175.75	32.8	1.81	1.22	2.90	58.1
20H-5, 75–76	177.25	31.8	1.84	1.25	2.92	57.0
20H-6, 75–76	178.75	33.0	1.77	1.19	2.76	57.0
21H-1, 75–76	180.75	31.0	1.81	1.25	2.77	54.8
21H-2, 75–76	182.25	28.3	1.87	1.34	2.76	51.5
21H-3, 75–76	183.75	29.6	1.86	1.31	2.84	53.8
21H-4, 34–35	184.34	29.0	1.84	1.30	2.72	52.1
22X-1, 72–73	185.52	31.3	1.92	1.32	3.20	58.8
22X-3, 88–89	188.68	28.2	2.10	1.51	3.56	57.8
22X-4, 59–60	189.89	30.7	1.83	1.27	2.82	54.9
22X-5, 78–79	191.58	30.3	1.84	1.28	2.82	54.4
23X-1, 78–79	195.18	29.9	1.86	1.31	2.87	54.5
23X-2, 78–79	196.68	27.9	1.90	1.37	2.84	51.8
23X-3, 75–76	198.15	28.5	2.04	1.46	3.36	56.6

Table T19 (continued).

Core, section, interval (cm)	Depth CSF (m)	Water content (wt%)	Density (g/cm³) Wet bulk	Dry bulk	Grain	Porosity (%)
23X-4, 72–73	199.62	29.3	1.86	1.31	2.81	53.2
320-U1336B-						
1H-1, 74–76	0.75	53.4	1.44	0.67	2.72	75.3
2H-2, 74–76	4.05	37.8	1.67	1.04	2.70	61.6
2H-4, 74–76	7.05	39.9	1.64	0.99	2.75	64.0
2H-6, 74–76	10.05	47.3	1.48	0.78	2.45	68.3
3H-2, 74–76	13.55	43.2	1.58	0.90	2.70	66.7
3H-4, 74–76	16.55	44.3	1.57	0.87	2.72	67.9
3H-6, 74–76	19.55	45.6	1.53	0.83	2.61	68.2
4H-2, 74–76	23.05	42.3	1.60	0.92	2.70	66.0
4H-4, 74–76	26.05	38.1	1.67	1.03	2.72	62.1
4H-6, 74–76	29.05	40.1	1.68	1.01	2.94	65.8
5H-2, 74–76	32.55	49.0	1.51	0.77	2.77	72.2
5H-4, 74–76	35.55	49.4	1.49	0.75	2.66	71.7
5H-6, 74–76	38.55	52.9	1.46	0.69	2.80	75.5
6H-2, 74–76	42.05	47.3	1.53	0.81	2.77	70.8
6H-4, 74–76	45.05	47.3	1.52	0.80	2.68	70.1
6H-6, 74–76	48.05	41.7	1.70	0.99	3.20	69.0
7H-2, 74–76	51.55	44.6	1.57	0.87	2.77	68.5
7H-4, 74–76	54.55	44.1	1.56	0.87	2.68	67.4
7H-6, 74–76	57.55	45.9	1.54	0.83	2.67	68.9
8H-2, 74–76	61.05	47.9	1.51	0.79	2.68	70.6
8H-4, 74–76	64.05	43.8	1.57	0.88	2.68	67.1
8H-6, 74–76	67.05	44.7	1.55	0.86	2.67	67.8
9H-2, 68–70	70.49	42.6	1.60	0.92	2.77	66.8
9H-4, 74–76	73.55	39.9	1.63	0.98	2.68	63.5
9H-6, 74–76	76.55	40.3	1.63	0.97	2.69	64.0
10H-1, 74–76	78.55	41.1	1.63	0.96	2.77	65.4
10H-4, 74–76	83.05	43.0	1.58	0.90	2.67	66.3
10H-6, 74–76	86.05	42.7	1.59	0.91	2.70	66.2
11H-2, 74–76	89.55	48.3	1.46	0.76	2.44	69.0
11H-4, 74–76	92.55	40.3	1.62	0.97	2.69	63.9
11H-6, 79–81	95.6	43.0	1.53	0.87	2.45	64.4
12H-2, 74–76	99.05	43.3	1.59	0.90	2.77	67.3
12H-4, 74–76	102.05	36.3	1.69	1.08	2.69	59.9
12H-6, 74–76	105.05	38.1	1.66	1.03	2.71	62.0
13H-2, 74–76	108.55	42.5	1.60	0.92	2.75	66.5
13H-4, 74–76	111.55	30.9	1.87	1.29	2.99	56.6
13H-6, 74–76	114.55	34.6	1.72	1.13	2.70	58.3
14H-2, 74–76	118.05	42.5	1.59	0.91	2.67	65.9
14H-4, 72–74	121.03	27.2	1.88	1.37	2.73	49.9
15H-2, 74–76	127.55	33.0	1.78	1.19	2.78	57.3
15H-4, 74–76	130.55	39.5	1.64	0.99	2.68	63.1
15H-6, 74–76	133.55	30.7	1.80	1.25	2.70	53.9
16H-1, 44–46	135.25	34.2	1.75	1.15	2.78	58.5
17H-2, 74–76	139.05	36.9	1.70	1.08	2.79	61.5
17H-4, 74–76	142.05	33.1	1.75	1.17	2.70	56.6
17H-6, 36–38	144.17	35.1	1.72	1.11	2.70	58.8
18H-2, 74–76	147.65	36.7	1.70	1.08	2.77	61.2
18H-4, 74–76	150.65	39.5	1.63	0.99	2.67	63.0
18H-6, 74–76	153.65	38.1	1.65	1.02	2.66	61.6
19H-2, 74–76	157.15	36.4	1.70	1.08	2.74	60.5
19H-4, 74–76	160.15	33.2	1.75	1.17	2.69	56.7
19H-6, 74–76	163.15	34.3	1.73	1.13	2.70	57.9
20H-2, 74–76	166.65	32.4	1.78	1.20	2.76	56.4
20H-4, 74–76	169.65	33.6	1.74	1.16	2.70	57.1
20H-6, 74–76	172.65	33.6	1.67	1.11	2.46	54.9

Table T20. Split-core *P*-wave velocity measurements, Site U1336. (**Continued on next page.**)

Core, section	Depth CSF (m)	Velocity (m/s) *x*-axis	*y*-axis	*z*-axis
320-U1336A-				
1H-1	1.30	1519		
1H-1	1.39		1493	1488
1H-3	4.33	1547		
1H-3	4.41		1522	1514
1H-4	5.83	1535		
1H-4	5.91		1506	1502
1H-5	7.31	1535		
1H-5	7.41		1503	1501
2H-1	9.34			1452
2H-1	9.45	1532		
2H-2	10.74	1551		
2H-2	10.93			1831
2H-3	12.31	1521		
2H-3	12.40		1504	1502
2H-4	13.81	1540		
2H-4	13.91		1506	1494
2H-5	15.37		1500	1494
2H-5	15.46	1540		
2H-6	16.81	1529		
2H-6	16.90			1445
3H-2	20.16	1527		
3H-3	21.80	1545		
3H-3	21.90		1507	1503
3H-4	23.39		1513	1503
3H-4	23.47	1546		
3H-5	24.86		1510	1508
3H-5	24.95	1534		
3H-6	26.38			1497
4H-2	29.84	1520		
4H-2	29.93		1509	1502
4H-3	31.37			1499
4H-3	31.45	1530		
4H-4	32.88		1505	1499
4H-4	32.96	1527		
4H-5	34.32	1537		
4H-5	34.41		1515	1515
4H-6	35.23		1400	1506
4H-6	35.30	1542		
5H-1	37.85			1443
5H-1	37.95	1510		
5H-2	39.35		1509	1502
5H-2	39.45	1531		
5H-3	40.85			1502
5H-3	40.96	1512		
5H-4	42.36			1493
5H-4	42.45	1516		
5H-5	43.86		1509	1503
5H-5	43.95	1527		
5H-6	45.35			1506
5H-6	45.45	1525		
6H-1	47.45	1513		
6H-2	48.87			1501
6H-2	48.95	1520		
6H-3	50.45	1525		
6H-4	51.86			1506
6H-4	51.95	1522		
6H-5	53.37		1514	1499
6H-5	53.45	1506		
6H-6	54.85			1507
6H-6	54.95	1516		
7H-1	56.95	1507		
7H-2	58.35		1519	
7H-2	58.44	1526		
7H-3	59.95	1554		
7H-4	61.38			1504
7H-4	61.45	1522		
7H-5	62.91			1503
7H-5	62.98	1532		
7H-6	64.37			1506
7H-6	64.45	1526		
8H-1	66.37			1507
8H-1	66.45	1511		
8H-2	67.87			1511
8H-2	67.95	1527		
8H-3	69.38			1511
8H-3	69.45	1523		
8H-4	70.90		1529	1518
8H-4	70.96	1535		
8H-5	72.36			1515
8H-5	72.44	1536		
9H-1	75.96	1516		
9H-2	77.37			1518
9H-2	77.45	1548		
9H-3	78.95	1566		
9H-4	80.37			1468
9H-4	80.45	1538		

Table T20 (continued).

Core, section	Depth CSF (m)	Velocity (m/s)		
		x-axis	*y*-axis	*z*-axis
9H-5	81.95	1545		
9H-6	83.34			1516
9H-6	83.45	1514		
10H-1	85.45	1530		
10H-2	86.85		1407	
10H-2	86.94	1528		
10H-3	88.44	1554		
10H-4	89.95	1543		
10H-5	91.46	1546		
11H-1	94.82	1548		
11H-1	94.91		1431	
11H-2	96.46	1557		
11H-3	97.96	1551		
11H-4	99.31	1515		
11H-4	99.40		1536	
11H-5	100.82	1523		
11H-5	100.91		1529	1529
11H-6	102.31	1553		
11H-6	102.40		1558	
12H-2	105.94	1541		
12H-3	107.37		1553	1530
12H-3	107.45	1522		
12H-4	108.87			1534
12H-4	108.95	1549		
12H-5	110.36		1541	1532
12H-5	110.45	1551		
12H-6	111.38		1564	1486
12H-6	111.46	1548		
13H-2	115.44	1557		
13H-3	116.87		1425	
13H-3	116.95	1546		
13H-5	119.86		1403	
13H-5	119.94	1537		
13H-6	121.36		1414	1524
13H-6	121.44	1529		
13H-7	122.20		1546	1540
13H-7	122.27	1549		
15H-2	126.35			1479
15H-2	126.44	1529		
15H-3	127.88		1433	
15H-3	127.96	1561		
15H-4	129.36		1448	1552
15H-4	129.45	1565		
15H-5	130.83	1543		
15H-5	130.93			1530
15H-6	132.22		1440	
15H-6	132.37		1549	
15H-6	132.45	1544		
16H-2	135.87		1464	
16H-3	137.34			1540
16H-3	137.44	1539		
16H-5	140.36		1544	1539
16H-6	141.63		1535	1531
17H-1	143.31			1483
17H-2	144.87		1563	
17H-2	144.95	1561		
17H-3	146.37		1553	
17H-3	146.45	1585		
17H-4	147.86		1343	1540
17H-4	148.09	1494		
17H-5	149.36			1542
17H-5	149.44	1558		
17H-6	150.87			1488
17H-6	151.11	1538		
18H-1	152.94	1547		
18H-2	154.45	1555		
18H-3	155.95	1544		
18H-4	157.45	1547		
18H-5	158.95	1541		
18H-6	160.45	1553		
19H-1	162.45	1531		
19H-2	163.94	1566		
19H-3	165.45	1552		
19H-4	166.95	1528		
19H-5	168.45	1566		
19H-6	169.95	1560		
20H-1	171.94	1549		
20H-2	173.45	1518		
20H-3	174.95	1544		
20H-4	176.45	1560		
20H-5	177.95	1616		
21H-1	181.66	1586		
21H-2	182.91	1583		
22X-1	186.24	1698		
22X-2	187.75	1608		
22X-3	189.24	1683		
22X-4	190.66	1814		
22X-5	191.68	1651		
23X-1	195.85	1648		
23X-2	197.36	1902		
23X-3	198.85	1802		
23X-4	200.33	1834		
23X-5	201.70	1890		
24X-1	203.73	1858		
24X-2	205.32	1891		
24X-3	206.74	1906		
24X-4	207.47	2016		
24X-4	207.47	7377		
25X-1	213.14	2015		
25X-2	214.61	1853		
25X-3	215.85	1896		
26X-1	222.93	1959		
26X-2	224.33	2069		
26X-3	225.97	1830		
26X-4	227.51	1963		
26X-5	228.93	1984		
26X-6	230.08	1999		
27X-1	232.57	2046		
27X-2	234.00	2181		
27X-3	235.30	2121		
27X-4	236.89	2007		
28X-1	242.27	1988		
28X-2	243.08	1847		
29X-1	251.73	2021		
29X-2	253.20	2068		
29X-3	253.65	2184		
30X-1	261.41	2137		
30X-2	262.67	2037		
30X-3	263.30	2058		
32X-1	280.53	2103		
32X-2	281.98	2066		
32X-3	282.34	2174		
33X-2	289.35	2255		
33X-2	289.35	10391		
320-U1336B-				
1H-1	0.80	1533		
2H-2	4.20		1507	1515
2H-2	4.10	1576		
2H-4	7.20			1501
2H-4	7.10	1558		
2H-6	10.20			1492
2H-6	10.10	1524		
3H-2	13.70		1513	1498
3H-2	13.60	1585		
3H-4	16.73			1504
3H-4	16.60	1583		
3H-6	19.70			1497
3H-6	19.60	1551		
4H-2	23.20			1499
4H-2	23.10	1557		
4H-4	26.20		1509	1498
4H-4	26.10	1583		
4H-6	29.20		1511	1513
4H-6	29.10	1570		
5H-2	32.70			1499
5H-2	32.60	1582		
5H-4	35.60	1573		
5H-6	38.60	1588		
6H-2	42.20		1494	1496
6H-2	42.10	1562		
6H-4	45.20		1501	1502
6H-4	45.30	1568		
6H-6	47.90		1501	1497
6H-6	47.81	1549		
7H-2	51.63		1494	
7H-2	51.71	1570		
7H-4	54.69		1400	1514
7H-4	54.60	1555		
7H-6	57.61	1555		
8H-2	61.23		1495	1494
8H-2	61.12	1538		
8H-4	64.10	1564		
8H-6	66.94	1549		
9H-2	70.70	1624		
9H-4	73.81	1550		
9H-6	76.60	1592		
10H-2	80.10	1574		
10H-4	83.10	1562		
10H-6	86.10	1549		
11H-2	89.60	1620		
11H-4	92.60	1570		
11H-6	95.80			1499
11H-6	95.70	1598		
12H-2	99.10	1560		
12H-4	102.10	1585		
12H-6	105.20		1413	
12H-6	105.10	1593		
13H-2	108.60	1578		
13H-4	111.69	1596		
13H-6	114.60	1591		
14H-4	120.99	1652		
15H-2	127.60	1559		
15H-4	130.60	1549		
15H-6	133.48	1576		
17H-2	139.20			1540
17H-2	139.10	1592		
17H-4	142.20		1466	
17H-4	142.10	1573		
17H-6	144.21	1605		
18H-2	147.70	1539		
18H-4	150.70	1556		
18H-6	153.71	1550		
19H-2	157.20	1571		
19H-4	160.20	1595		
19H-6	163.20	1630		
20H-2	166.70	1622		
20H-4	169.70	1606		
20H-6	172.70	1608		

Table T21. Thermal conductivity, Site U1336.

Core, section, interval (cm)	Depth CSF (m)	Thermal conductivity (W/[m·K])
320-U1336A-		
1H-3, 115	4.15	1.210
2H-3, 115	12.15	1.106
3H-3, 115	21.65	1.114
4H-3, 115	31.15	0.911
5H-3, 115	40.65	1.073
6H-3, 115	50.15	0.994
7H-3, 115	59.65	1.061
8H-3, 115	69.15	1.110
9H-3, 115	78.65	1.132
10H-3, 115	88.15	1.100
11H-3, 115	97.65	1.186
12H-3, 115	107.15	1.256
13H-3, 115	116.65	1.209
15H-3, 115	127.65	1.228
16H-3, 115	137.15	1.228
17H-3, 115	146.15	1.209
18H-3, 115	155.65	1.202
19H-3, 115	165.13	1.286
20H-3, 115	174.65	1.314
21H-2, 115	182.65	1.375
22X-3, 115	188.95	1.209
320-U1336B-		
2H-4, 75	7.05	1.335
3H-4, 75	16.55	1.136
4H-4, 75	26.05	1.281
5H-4, 75	35.55	0.986
6H-4, 75	45.05	1.051
7H-4, 75	54.55	1.163
8H-4, 75	64.05	1.106
9H-4, 75	73.55	1.366
10H-4, 75	83.05	1.211
11H-4, 75	92.55	1.008
12H-4, 75	102.05	1.311
13H-4, 75	111.55	1.708
14H-4, 75	121.05	1.084
15H-4, 75	130.55	1.332
17H-4, 75	142.05	1.335
18H-4, 75	150.65	1.164
19H-4, 75	160.15	1.309
20H-4, 75	169.65	1.360

Table T22. Shipboard core top, composite, and corrected composite depths, Site U1336.

Core	Depth CSF (m)	Offset (m)	Top depth (m) CCSF-A	Top depth (m) CCSF-B
320-U1336A-				
1H	0.00	0.26	0.26	0.23
2H	8.00	1.51	9.51	8.41
3H	17.50	1.83	19.33	17.11
4H	27.00	2.80	29.80	26.37
5H	36.50	3.28	39.78	35.21
6H	46.00	6.64	52.64	46.58
7H	55.50	8.04	63.54	56.23
8H	65.00	9.09	74.09	65.56
9H	74.50	9.77	84.27	74.58
10H	84.00	9.71	93.71	82.93
11H	93.50	11.79	105.29	93.18
12H	103.00	12.88	115.88	102.55
13H	112.50	14.22	126.72	112.14
14H	122.00	15.73	137.73	121.89
15H	123.50	16.23	139.73	123.66
16H	133.00	21.50	154.50	136.72
17H	142.00	23.41	165.41	146.38
18H	151.50	23.41	174.91	154.79
19H	161.00	23.41	184.41	163.19
20H	170.50	23.41	193.91	171.60
21H	180.00	23.41	203.41	180.01
22X	184.80	23.41	208.21	184.26
23X	194.40	23.41	217.81	192.75
24X	202.40	23.41	225.81	199.83
25X	212.00	23.41	235.41	208.33
26X	221.60	23.41	245.01	216.82
27X	231.20	23.41	254.61	225.32
28X	240.80	23.41	264.21	233.81
29X	250.40	23.41	273.81	242.31
30X	260.00	23.41	283.41	250.81
31X	269.60	23.41	293.01	259.30
32X	279.20	23.41	302.61	267.80
33X	288.80	23.41	312.21	276.29
34X	293.80	23.41	317.21	280.72
35X	298.30	23.41	321.71	284.70
320-U1336B-				
1H	0.00	0.00	0.00	0.00
2H	1.80	0.53	2.33	2.06
3H	11.30	2.56	13.86	12.27
4H	20.80	4.18	24.98	22.11
5H	30.30	5.58	35.88	31.75
6H	39.80	7.53	47.33	41.89
7H	49.30	8.69	57.99	51.32
8H	58.80	8.88	67.68	59.90
9H	68.30	8.81	77.11	68.24
10H	77.80	10.19	87.99	77.86
11H	87.30	10.69	97.99	86.72
12H	96.80	12.51	109.31	96.73
13H	106.30	14.26	120.56	106.69
14H	115.80	16.98	132.78	117.50
15H	125.30	17.79	143.09	126.62
16H	134.80	17.79	152.59	135.03
17H	136.80	17.79	154.59	136.80
18H	145.40	17.79	163.19	144.41
19H	154.90	17.79	172.69	152.82
20H	164.40	17.79	182.19	161.23

Table T23. Splice tie points, Site U1336.

Hole, core, section, interval (cm)	Depth CSF	Depth CCSF-A		Hole, core, section, interval (cm)	Depth CSF	Depth CCSF-A
320-				320-		
U1336B-1H-1, 55	0.55	0.55	Tie to	U1336A-1H-1, 29	0.29	0.55
U1336A-1H-5, 78	6.78	7.04	Tie to	U1336B-2H-4, 21	6.51	7.04
U1336B-2H-7, 26	11.06	11.59	Tie to	U1336A-2H-2, 58	10.08	11.59
U1336A-2H-6, 109	16.59	18.09	Tie to	U1336B-3H-3, 123	15.53	18.09
U1336B-3H-7, 5	20.35	22.91	Tie to	U1336A-3H-3, 58	21.08	22.91
U1336A-3H-6, 54	25.54	27.38	Tie to	U1336B-4H-2, 90	23.20	27.38
U1336B-4H-6, 137	29.67	33.85	Tie to	U1336A-4H-3, 105	31.05	33.85
U1336A-4H-7, 11	35.42	38.22	Tie to	U1336B-5H-2, 84	32.64	38.22
U1336B-5H-6, 126	39.06	44.64	Tie to	U1336A-5H-4, 36	41.36	44.64
U1336A-5H-6, 135	45.35	48.63	Tie to	U1336B-6H-1, 130	41.10	48.63
U1336B-6H-6, 148	48.78	56.31	Tie to	U1336A-6H-3, 67	49.67	56.31
U1336A-6H-6, 131	54.81	61.45	Tie to	U1336B-7H-3, 46	52.76	61.45
U1336B-7H-7, 14	58.14	66.83	Tie to	U1336A-7H-3, 29	58.79	66.83
U1336A-7H-7, 43	64.93	72.97	Tie to	U1336B-8H-4, 79	64.09	72.97
U1336B-8H-6, 9	66.39	75.27	Tie to	U1336A-8H-1, 119	66.19	75.27
U1336A-8H-7, 56	73.56	82.64	Tie to	U1336B-9H-4, 103	73.83	82.64
U1336B-9H-7, 6	77.06	85.88	Tie to	U1336A-9H-2, 11	76.11	85.88
U1336A-9H-4, 104	80.04	89.81	Tie to	U1336B-10H-2, 33	79.63	89.81
U1336B-10H-6, 125	86.55	96.74	Tie to	U1336A-10H-2, 153	87.03	96.74
U1336A-10H-6, 94	92.44	102.14	Tie to	U1336B-11H-3, 115	91.45	102.14
U1336B-11H-6, 82	95.62	106.31	Tie to	U1336A-11H-1, 102	94.52	106.31
U1336A-11H-4, 54	98.54	110.34	Tie to	U1336B-12H-1, 103	97.83	110.34
U1336B-12H-6, 112	105.42	117.93	Tie to	U1336A-12H-2, 55	105.05	117.93
U1336A-12H-4, 121	108.71	121.59	Tie to	U1336B-13H-1, 103	107.33	121.59
U1336B-13H-6, 90	114.70	128.97	Tie to	U1336A-13H-2, 75	114.75	128.97
U1336A-13H-6, 62	120.62	134.84	Tie to	U1336B-14H-2, 56	117.86	134.84
U1336B-14H-7, 66	125.46	142.44	Append to	U1336B-15H-1, 0	125.30	143.09
U1336B-15H-2, 67	127.47	145.25	Tie to	U1336A-15H-4, 102	129.02	145.25
U1336A-15H-7, 61	133.11	149.35	Append to	U1336A-16H-1, 5	133.05	154.55
U1336A-16H-3, 121	137.21	158.71	Tie to	U1336B-17H-3, 112	140.92	158.71
U1336B-17H-7, 79	145.29	163.07	Append to	U1336B-18H-1, 0	145.40	163.19
U1336B-18H-7, 15	154.55	172.33	Tie to	U1336A-17H-5, 92	148.92	172.33
U1336A-17H-7, 58	151.58	174.99	Append			

Table T24. Magnetostratigraphic and biostratigraphic datums, Site U1336. (See table note.) (Continued on next page.)

Event	Age (Ma)	Depth CCSF-A (m)	Error (m)
Polarity chron			
C5r.3r/C5An.1n	12.014	0.55	
C5An.1n/C5An.1r	12.116	1.45	
C5An.1r/C5An.2n	12.207	2.19	
C5An.2n/C5Ar.1r	12.415	5.19	
C5Ar.1r/C5Ar.1n	12.730	7.99	
C5Ar.1n/C5Ar.2r	12.765	8.46	
C5Ar.2r/C5Ar.2n	12.820	9.00	
C5Ar.2n/C5Ar.3r	12.878	9.38	
C5Ar.3r/C5AAn	13.015	10.90	
C5AAn/C5AAr	13.183	12.36	
C5AAr/C5ABn	13.369	14.18	
C5ABr/C5ACn	13.734	19.38	
C5ADn/C5ADr	14.581	30.21	
C5ADr/C5Bn.1n	14.784	32.05	
C5Bn.1n/C5Bn.1r	14.877	33.56	
C5Bn.1r/C5Bn.2n	15.032	34.84	
C5Bn.2n/C5Br	15.160	35.16	
C5Br/C5Cn.1n	15.974	45.01	
C5Cn.1n/C5Cn.1r	16.268	46.13	
C5Cn.1r/C5Cn.2n	16.303	46.13	
C5Cn.2n/C5Cn.2r	16.472	46.99	
C5Cn.2r/C5Cn.3n	16.543	47.79	
C5Cn.3n/C5Cr	16.721	48.60	
C5Cr/C5Dn	17.235	52.83	
C5Dn/C5Dr	17.533	56.99	
C5Dr/C5En	18.056	59.58	
C5En/C5Er	18.524	64.39	
C5Er/C6n	18.748	65.83	
Nannofossils			
T *Coronocyclus nitescens*	12.12	1.36	
T *Calcidiscus premacintyrei*	12.45	1.36	
Tc *Cyclicargolithus floridanus*	13.33	16.31	1.50
T *Sphenolithus heteromorphus*	13.53	20.46	1.27
Tc *Discoaster deflandrei*	15.66	33.70	1.50
B *Discoaster petaliformis*	15.70	46.28	1.36
Bc *Sphenolithus heteromorphus*	17.71	66.30	0.76
Tc *Sphenolithus belemnos*	17.95	66.30	0.76
T *Triquetrorhabdulus carinatus*	18.28	66.30	0.76
B *Sphenolithus belemnos*	19.03	84.14	0.68
Tc *Triquetrorhabdulus carinatus*	22.09	135.81	0.99
B *Sphenolithus disbelemnos*	22.8	153.25	3.64
T *Sphenolithus delphix*	23.1	169.31	1.50
B *Sphenolithus delphix*	23.2	174.53	0.72
T *Sphenolithus ciperoensis*	24.4	202.23	1.32
X *T. longus*/*T. carinatus*	24.7	202.23	1.32
Tc *Cyclicargolithus abisectus*	24.7	191.86	0.75
T *Sphenolithus distentus*	26.8	228.24	1.31
T *Sphenolithus predistentus*	26.9	230.94	1.40
B *Sphenolithus ciperoensis*	27.1	232.69	0.34
B *Sphenolithus distentus*	30.0	277.57	0.36
T *Reticulofenestra umbilicus*	32.0	319.77	2.29
Radiolarians			
B *Diartus petterssoni*	12.11	7.12	1.33
B *Cyrtocapsella japonica*	12.41	7.12	1.33
B *Lithopera neotera*	12.95	10.25	1.80
T *Calocycletta robusta*	13.35	20.53	1.35
T *Stichocorys armata*	13.50	20.53	1.35
T *Acrocubus octopyle*	13.88	23.38	1.50
T *Calocycletta costata*	14.23	27.09	2.21
T *Dorcadospyris dentata*	14.66	32.81	2.54
T *Liriospyris stauropora*	14.83	32.81	2.54
D. dentata > *D. alata*	14.78	32.81	2.54
B *Dorcadospyris alata*	15.08	40.67	1.67
B *Liriospyris parkerae*	15.03	40.67	1.67
T *Carpocanopsis cingulata*	15.13	47.51	2.18

Table T24 (continued).

Event	Age (Ma)	Depth CCSF-A (m)	Error (m)
T *Lychnocanoma elongata*	15.15	55.20	0.01
B *Lithopera renzae*	16.77	55.20	0.01
B *Calocycletta costata*	17.49	58.49	3.29
B *Dorcadospyris dentata*	17.72	63.93	2.15
B *Liriospyris stauropora*	17.72	63.93	2.15
T *Dorcadospyris scambos*	18.53	71.37	2.28
B *Stichocorys wolffii*	18.57	78.14	1.50
B *Dorcadospyris forcipata*	18.61	78.14	1.50
T *Dorcadospyris simplex* s.s.	18.69	85.14	1.68
T *Dorcadospyris praeforcipata*	19.77	95.32	0.95
B *Dorcadospyris simplex* s.s.	20.34	101.37	2.12
B *Stichocorys delmontensis*	20.68	109.34	1.50
T *Lophocyrtis pegetrum*	20.89	113.06	2.22
T *Theocyrtis annosa*	21.38	119.93	1.50
B *Calocycletta virginis*	21.39	116.85	1.58
T *Eucyrtidium mitodes*	21.95	134.53	2.27
B *Calocycletta serrata*	22.04	143.78	1.50
B *Cyrtocapsella cornuta*	22.26	147.45	2.16
B *Cyrtocapsella tetrapera*	22.35	147.45	2.16
T *Artophormis gracilis*	22.62	157.55	2.50
B *Eucyrtidium diaphanes*	22.95	165.72	2.24
T *Dorcadospyris cyclacantha*	22.98	165.72	2.24
B *Dorcadospyris cyclacantha*	23.29	169.46	1.50
T *Dorcadospyris papilio*	23.31	173.11	2.14
T *Liriospyris longicornuta*	24.12	178.96	1.51
Foraminifers			
T *Globorotalia (Fohsella) fohsi* s.l.	11.79	1.95	1.69
B *Globorotalia (Fohsella) fohsi robusta*	13.13	6.04	2.41
B *Globorotalia (Fohsella) fohsi* s.l.	13.41	20.36	0.85
B *Globorotalia (Fohsella) "praefohsi"*	13.77	23.46	2.25
T *Clavatorella bermudezi*	13.82	23.46	2.25
T *Globorotalia (Fohsella) peripheroronda*	13.80	27.51	1.80
B *Globorotalia (Fohsella) peripheroacuta*	14.24	31.73	1.46
B *Orbulina* spp.	14.74	27.51	1.80
B *Clavatorella bermudezi*	14.89	31.73	1.46
T *Praeorbulina glomerosa*	14.8	31.73	1.46
T *Praeorbulina circularis*	14.58	34.68	1.50
B *Praeorbulina glomerosa*	16.27	53.78	0.73
B *Praeorbulina sicana*	16.97	53.78	0.73
T *Globoquadrina binaiensis*	19.09	77.47	1.50
T *Paragloborotalia kugleri*	21.12	106.33	0.76
T *Paragloborotalia pseudokugleri*	21.31	106.33	0.76
B *Globoquadrina dehiscens*	22.44	143.11	1.50
B *Paragloborotalia kugleri*	23.00	166.35	0.94
B *Paragloborotalia pseudokugleri*	25.2	194.90	0.89
T *Paragloborotalia opima*	26.9	228.14	2.58
Tc *Chiloguembelina cubensis*	28.00	238.84	1.48
B *Globigerina angulisuturalis*	29.2	263.35	2.56
T *Subbotina angiporoides*	29.8	270.73	4.82
T *Turborotalia ampliapertura*	30.3	281.61	3.68
B *Paragloborotalia opima*	30.8	281.61	3.68

Note: T = top, Tc = top common, B = bottom, Bc = bottom common, X = abundance crossover.